MARTIN MARIETTA ENERGY SYSYEMS LIBRARIES

3 4456 0325131 7

ORNL/TM-11742

ornl

OAK RIDGE
NATIONAL
LABORATORY

MARTIN MARIETTA

^{56}Fe Resonance Parameters for Neutron Energies up to 850 keV

C. M. Perey
F. G. Perey
J. A. Harvey
N. W. Hill
N. M. Larson

OAK RIDGE NATIONAL LABORATORY
CENTRAL RESEARCH LIBRARY
CIRCULATION SECTION
4500N ROOM 175
LIBRARY LOAN COPY
DO NOT TRANSFER TO ANOTHER PERSON
If you wish someone else to see this report, send in name with report and the library will arrange a loan.

OPERATED BY
MARTIN MARIETTA ENERGY SYSTEMS, INC.
FOR THE UNITED STATES
DEPARTMENT OF ENERGY

This report has been reproduced directly from the best available copy.

Available to DOE and DOE contractors from the Office of Scientific and Technical Information, P.O. Box 62, Oak Ridge, TN 37831, prices available from (615) 576-8401, FTS 626-8401.

Available to the public from the National Technical Information Service, U.S. Department of Commerce, 5285 Port Royal Rd., Springfield, VA 22161.

This report was prepared as an account of work sponsored by an agency of the United States Government. Neither the United States Government nor any agency thereof, nor any of their employees, makes any warranty, express or implied, or assumes any legal liability or responsibility for the accuracy, completeness, or usefulness of any information, apparatus, product, or process disclosed, or represents that its use would not infringe privately owned rights. Reference herein to any specific commercial product, process, or service by trade name, trademark, manufacturer, or otherwise, does not necessarily constitute or imply its endorsement, recommendation, or favoring by the United States Government or any agency thereof. The views and opinions of authors expressed herein do not necessarily state or reflect those of the United States Government or any agency thereof.

ORNL/TM-11742

Engineering Physics and Mathematics Division

^{56}Fe RESONANCE PARAMETERS FOR NEUTRON ENERGIES UP TO 850 keV

C. M. Perey, F. G. Perey, J. A. Harvey,
N. W. Hill, N. M. Larson

DATE PUBLISHED — December 1990

Prepared for the
Office of Energy Research
Division of Nuclear Physics

Prepared by the
OAK RIDGE NATIONAL LABORATORY
Oak Ridge, Tennessee 37831
operated by
MARTIN MARIETTA ENERGY SYSTEMS, INC.
for the
U.S. DEPARTMENT OF ENERGY
under contract DE-AC05-84OR21400

MARTIN MARIETTA ENERGY SYSYEMS LIBRARIES

3 4456 0325131 7

CONTENTS

ACKNOWLEDGMENTS ix
ABSTRACT xi
1. INTRODUCTION 1
2. DATA ACQUISITION AND DATA PROCESSING 2
2.1 TRANSMISSION MEASUREMENTS 2
2.1.1 Data Acquisition 2
2.1.2 Data Reduction 3
2.2 DIFFERENTIAL ELASTIC SCATTERING MEASUREMENT . . 3
2.2.1 Data Acquisition 3
2.2.2 Data Reduction 5
3. DATA ANALYSIS 6
3.1 TRANSMISSION DATA ANALYSIS 6
3.2 DIFFERENTIAL ELASTIC SCATTERING DATA ANALYSIS . . 9
4. RESULTS 37
4.1 CAPTURE KERNELS AND RADIATION WIDTHS 37
4.2 DISCUSSION OF THE UNCERTAINTIES 39
4.3 SPIN AND PARITY ASSIGNMENTS 39
4.4 THERMAL CROSS SECTIONS 40
5. COMPARISON WITH RESULTS FROM PREVIOUS ANALYSES . . 41
5.1 COMPARISON WITH GEEL RESULTS 41
5.2 COMPARISON WITH PREVIOUS ORELA RESULTS 43
5.2.1 Transmission 43
5.2.2 Differential Elastic Scattering 45
5.3 COMPARISON WITH KARLSRUHE RESULTS 45
6. DISCUSSION AND EXTRACTION OF AVERAGE PARAMETERS . 46
6.1 REDUCED NEUTRON WIDTH DISTRIBUTION 46
6.1.1 $\ell = 0$ Resonances 46
6.1.2 $\ell > 0$ Resonances 46
6.2 S-WAVE LEVEL SPACINGS 48
6.3 LEVEL DENSITIES 51
6.4 STRENGTH FUNCTION 53
6.4.1 $\ell = 0$ Resonances 53
6.4.2 $\ell > 0$ Resonances 57

6.5 AVERAGE RADIATION WIDTHS 59
6.5.1 $\ell = 0$ Resonances 59
6.5.2 $\ell > 0$ Resonances 59
6.6 CORRELATION BETWEEN Γ_n^0 AND Γ_γ FOR S-WAVE RESONANCES 60
7. CONCLUSIONS 61
REFERENCES 63

LIST OF TABLES

Table		Page
1	Summary of Data Analyzed	2
2	Resonance parameters for ^{56}Fe + n from 1 to 850 keV.	11
3	Resonance parameters of the large s-wave resonances for the minor iron isotopes and for the ^{55}Mn impurity, used in the analysis of the natural iron transmission data from 5 to 120 keV.	19
4	Comparison of resonance energies and neutron widths, times the statistical weight g, for $\ell > 0$ resonances observed in our transmission data and in the 200-m Geel transmission data, between 40 and 240 keV.	31
5	Comparison of resonance energies and neutron widths, times the statistical weight g, for $\ell > 0$ resonances observed in our transmission data and in Geel and Karlsruhe data, between 500 and 600 keV.	34
6	Parameters for s-wave resonances from Table 2 compared with results of Geel analyses.	42
7	Parameters for s-wave resonances from Table 2 compared with earlier results. Uncertainties are given in parentheses. The notation is such that 1.409 (1) means 1.409 ± 0.001.	44
8	Resonance parameter statistics for s-wave resonances compared with results of three earlier analyses and with recommended values of Mughabghab et al.	50
9	Average radiation widths, $< \Gamma_\gamma >$, and their standard deviations, from this work and from two earlier publications. N represents the number of resonances used to calculate the average radiation width.	60

LIST OF FIGURES

Fig.		Page
1	Data below 2 keV used in the SAMMY fitting process	8
2	Top: Natural iron theoretical total cross section calculated with combined parameters of Tables 2 and 3, compared with the total cross-section data from 5 to 45 keV. For the minor iron isotopes and the ^{55}Mn impurity only the total cross section of the large resonances were calculated. Bottom: The four ^{56}Fe narrow resonances from the upper plot were enlarged to show in detail the comparison of the calculated cross section with the data	21
3	Top: Same as Fig. 2 (top) except from 45 to 65 keV. Bottom: Four of the five ^{56}Fe narrow resonances from the upper plot were enlarged to show in detail comparison of the calculated cross section with the data	22
4	Top: Same as Fig. 2 (top) except from 65 to 90 keV. Bottom: The three ^{56}Fe narrow resonances from the upper plot were enlarged to show in detail comparison of the calculated cross section with the data	23
5	Top: Same as Fig. 2 (top) except from 90 to 115 keV. Bottom: The two groups of ^{56}Fe narrow resonances around 92.8 and 96.4 keV, and the narrow resonance at 103.1 keV, were enlarged from the upper plot to show in detail comparison of the calculated cross section with the data	24
6	^{56}Fe theoretical cross section calculated with parameters of Table 2, compared with the total cross-section data from 120 to 175 keV . .	25
7	Same as Fig. 6 except from 175 to 230 keV	26
8	Same as Fig. 6 except from 230 to 305 keV	27
9	Same as Fig. 6 except from 305 to 400 keV	28
10	Same as Fig. 6 except from 400 to 600 keV	29

Fig.		Page
11	Same as Fig. 6 except from 600 to 850 keV	30
12	Theoretical differential elastic-scattering cross sections calculated with the ℓ and J values assigned in this work (thick line) and with those assigned in Ref. COR85 (thin line) compared with data for three scattering angles	33
13	In the upper plot the theoretical total cross section, calculated with parameters in Table 2, is compared with the data. Parentheses are used to indicate uncertain ℓ and J assignments. These assignments were made using the differential elastic-scattering data shown in the three lower plots	35
14	This figure is the same as Fig. 13 except that the ℓ and J assignments of four $\ell > 0$ resonances were set to the values assigned in Ref. COR83 (see Table 5). The assignments for the other resonances, not specified here, were kept the same as in Fig. 13. The ORELA transmission data were fitted using this new set of assignments and the total cross section calculated with the resulting parameters is compared with the data in the upper plot. The theoretical differential elastic-scattering cross sections are compared with the data, at three different angles, in the lower part of the figure. The agreement with the differential elastic-scattering data is now clearly unsatisfactory, especially at 90° and 160o scattering angles, for three of the four resonances . . .	36
15	(a) Distribution of normalized reduced neutron widths for the 33 observed s-wave resonances in Table 2. The smooth curve is the Porter-Thomas distribution normalized to the area under the histogram corresponding to values of $\Gamma_n^0/ < \Gamma_n^0 >$ larger than 0.1. (b) Distribution of nearest level spacings for the 33 observed s-wave resonances. The smooth curves is the Wigner distribution normalized to the area under the histogram	47
16	Distributions of normalized reduced neutron widths for $\ell = 1$ and $\ell = 2$ resonances. All assigned $\ell = 1$ and $\ell = 2$ resonances were used to generate the histograms. The smooth curves are Porter-Thomas distributions normalized to the areas under the histograms corresponding to values of $\Gamma_n^\ell/ < \Gamma_n^\ell >$ larger than 0.2	49

Fig. Page

17 Cumulative number of s-wave levels, and p- and d-wave levels as a function of incident neutron energy. Circles represent the number of observed levels. Lines represent the numbers of levels predicted by the Fermi-gas model (Gilbert and Cameron formula). Full lines are obtained assuming four missing s-wave levels and dashed lines assuming eight missing s-wave levels 52

18 Cumulative number of s-wave resonances as a function of incident neutron energy. The histogram represents the number of observed resonances. The full line is the fit to the data using the Δ_3 statistics test of Dyson and Metha. The dashed line is the fit to the data using the Fermi-gas model. Thirty-three s-wave resonances, as observed between 0 and 850 keV, were used in both calculations 54

19 Sum of reduced neutron widths for s-wave resonances as function of incident neutron energy. The strength function for the entire range of the analysis is given by the slope of the full line. The slope of the dashed line gives the strength function below 360 keV 55

20 Lorentz-weighted s-wave strength function for reduced neutron widths averaged with $I = 50$ keV between 0 and 850 keV. $SINT$ is the contribution of the 33 observed s-wave resonances inside the 0- to 850-keV region. S_{EXT} is the contribution of the seven fictitious resonances outside the range of the analysis. S_{TOTAL} is the sum of S_{INT} and S_{EXT} 57

21 Sum of reduced neutron widths for $\ell = 1$ and $\ell = 2$ resonances as a function of incident neutron energy. Only resonances with definite ℓ-assignment were used to generate the histograms. Slopes of the straight lines are the strength functions S_1 and S_2 58

ACKNOWLEDGMENTS

The authors thank E. M. Cornelis, L. Mewissen and F. Poortmans for sending us, before publication, the results of their ^{56}Fe transmission data analysis below 240 keV, L. C. Leal for providing the code to perform the Dyson-Metha Δ_3 statistics test, and the reviewers of this report, D. C. Larson and C. Y. Fu for many useful discussions and constructive suggestions. We also thank R. E. Chrien, from Brookhaven National Laboratory, for the loan of the ^{56}Fe sample used for the measurements. We are grateful to S. R. Damewood for her invaluable technical know-how in the typing and presentation of this report. This research was sponsored by the Office of Energy Research, Division of Nuclear Physics, U. S. Department of Energy, under Contract No. DE-AC05-84OR21400 with Martin Marietta Energy Systems, Inc.

ABSTRACT

High-resolution neutron measurements for ^{56}Fe-enriched iron targets were made at the Oak Ridge Electron Linear Accelerator (ORELA) in transmission below 20 MeV and in differential elastic scattering below 5 MeV. Transmission measurements were also performed with a natural iron target below 160 keV. The transmission data were analyzed from 5 to 850 keV with the multilevel R-matrix code SAMMY which uses Bayes' theorem for the fitting process. This code provides energies and neutron widths of the resonances inside the 5- to 850-keV energy region, as well as possible parameterization for resonances external to the analyzed region to describe the smooth cross section from a few eV to 850 keV. The resulting set of resonance parameters yields the accepted values for the thermal total and capture cross sections.

The differential elastic-scattering data at several scattering angles were compared to theoretical calculations from 40 to 850 keV using the R-matrix code RFUNC based on the Blatt-Biedenharn formalism. Various combinations of spin and parity were tried to predict cross sections for the well defined $\ell > 0$ resonances; comparison of these predictions with the data allowed us to determine the most likely spin and parity assignments for these resonances.

The results of a capture data analysis by Corvi et al. (COR84), from 2 to 350 keV, were combined with our results to obtain the radiation widths of the resonances below 350 keV observed in transmission, capture, and differential elastic-scattering experiments.

The distribution of the reduced widths of the 33 s-wave resonances is consistent with a Porter-Thomas distribution and the distribution of the nearest neighbor spacings agrees with a Wigner distribution. The average s-wave level spacing is equal to 25.4 ± 2.2 keV. The Porter-Thomas distribution and the Fermi-gas model suggest that several s-wave levels may have been missed but the Dyson-Metha Δ_3 statistics test fails to confirm this possibility. The distributions of the reduced neutron widths for the $\ell = 1$ and $\ell = 2$ resonances were also consistent with Porter-Thomas distributions.

Even though modulations are observed in the staircase plot of the reduced s-wave level widths, and in the plot of the Lorentz-weighted strength function, these modulations do not provide a clear indication of the presence of doorway states because of the small number of s-wave resonances. The s-wave strength function is equal to $(2.3 \pm 0.6) \times 10^{-4}$.

The mean values and standard deviations of the distributions of the radiation widths are 0.92 ± 0.41 eV for the s-wave resonances, 0.45 ± 0.23 eV for the p-wave and 0.75 ± 0.27 eV for the d-wave resonances. The correlation coefficient between the s-wave reduced neutron widths and radiation widths using the parameters of the 10 s-wave resonances below 300 keV is equal to 0.29 ± 0.15: a markedly smaller value than the ones found for other nuclides in this mass region.

1. INTRODUCTION

The cross sections of structural materials in the iron region are important in reactor applications because of the stainless steels that are used. The ENDF/B-V evaluation of the ^{56}Fe resonance parameters (PER80), based on previous Oak Ridge Electron Linear Accelerator (ORELA) measurements (PAN75, ALL76, and KIN76), covered the energy region below 400 keV. In this report the resonance analysis is extended to 850 keV. The neutron widths and the spin and parity assignments of resonances are based on new ORELA 200-m transmission and differential elastic-scattering measurements. The results of the ^{56}Fe capture analysis up to 350 keV by Corvi et al. (COR84) were combined with the results of our analysis to determine the radiation widths of the resonances from 2 to 350 keV.

As found in the analysis of the ^{58}Ni transmission data up to 813 keV (PER88), the ^{56}Fe transmission data were properly fitted up to 850 keV by using a different channel radius for the p-wave channel than for the s- and d-wave channels.

The experimental procedures used in the transmission and differential elastic measurements are described in Sect. 2 with discussions of the various background and deadtime corrections. Details on the analysis of the transmission data from 5 to 850 keV and on the use of some low energy data in the fitting process to insure that the final resonance parameters would produce acceptable thermal scattering cross sections are reported in Sect. 3.1. In Sect. 3.2 the usefulness of the elastic-scattering data in the determination of the spin and parity of some $\ell > 0$ resonances is illustrated for two energy regions.

The results of our analysis combined with those of the capture data analysis of Corvi et al. (COR84) are presented in Sect. 4. Our resonance parameters are compared with those reported in earlier publications in Sect. 5 and the behavior of the average resonance parameters are discussed in Sect. 6.

2. DATA ACQUISITION AND DATA PROCESSING

2.1 TRANSMISSION MEASUREMENTS

2.1.1 Data Acquisition

Two transmission measurements were made by the time-of-flight technique using neutron pulses from the ORELA water-moderated tantalum target. One measurement used unmoderated neutrons directly from the target and the other measurement used moderated neutrons. The two measurements were made at the 200-m flight path with two different samples (see Table 1) and different detectors.

Table 1. Summary of Data Analyzed

Sample	Energy range (keV)	Flight path (m)	Burst width (ns)	Average sample thickness (at/b)
Analyzed transmission data				
Natural Fe	5 to 120	201.583 ± 0.005	7	0.2144 ± 0.0005
^{56}Fe	120 to 850	201.575 ± 0.005	4.5	0.2227 ± 0.0005
Analyzed differential elastic scattering data				
^{56}Fe	40 to 850	200.191 ± 0.014	6	0.0677 ± 0.0020
Geel capture data and analysis (COR84)				
^{56}Fe	1 to 350	58.	4.4	0.015

The measurement with moderated neutrons was made on a natural iron sample weighing 4236.5 g with a thickness of 0.2144 ± 0.0005 at/b. The electron beam burst was 7 ns wide, producing a beam power of 10 kW at 800 Hz. Transmission data from 2 to 163 keV were obtained using a 1-cm-thick, 9- by 9-cm NE-110 scintillator epoxy-coupled to two 12.5-cm-diameter RCA 8854 photomultipliers (PM). This bare (non-coated) scintillator is mounted in a 0.025-mm-thick, 17.8-cm-diameter Mylar reflecting cylinder. Each PM is biased below the single photoelectron level and a coincidence is required between the outputs of the two PMs to eliminate counts due to PM noise and reduce the effects of after-pulsing. The detector has an efficiency of $\approx$40% at 15 keV. Details on this detector can be found in Ref. HAR88. In addition to the shadow bar (2.5 cm each of uranium, thorium and tantalum) shadowing the tantalum part of the target, three filters were inserted in the neutron beam at 5 m: a 0.3 g/cm^2 ^{10}B filter to reduce overlap neutrons and a 0.73-cm-thick uranium filter plus a 1.27-cm-thick lead filter to reduce the intensity of the gamma flash from the target.

The transmission measurement on a ^{56}Fe sample (2.380-cm diameter) was made with an "effective" sample enrichment of 99.92% ^{56}Fe achieved by the use of a 0.025-cm-thick foil of natural iron in the open beam to compensate for the ^{54}Fe in the 92.997 g of iron enriched to 99.87% in ^{56}Fe. The sample thickness of ^{56}Fe was 0.2227 ± 0.0005 at/b. Unmoderated neutrons from the tantalum target were used. The electron beam burst was 4.5-ns wide producing a beam power of 6 kW at 800 Hz. The measurements covered the energy region from ≈100 keV to 20 MeV. A 2.5-cm-thick, 5.2- by 8.9-cm NE-110 scintillator also mounted between two RCA 8854 photomultipliers was used as the detector. Two filters were inserted in the beam at 5 m: a 0.3 g/cm^2 ^{10}B filter and a 4.4-cm-thick uranium filter.

For both transmission measurements the neutron beam was collimated so that all neutrons passed only through the scintillator. The detectors were gated off during the gamma flash and the succeeding ≈35 μs for the natural iron sample measurement, and ≈3 μs for the ^{56}Fe sample measurement, to eliminate possible extraneous events due to phototube afterpulsing.

Data were acquired using an EG&G time digitizer and stored in one of the ORELA Data Acquisition Computers (BET69).

2.1.2 Data Reduction

The data were first corrected for the deadtime (1104 ns) of the digitizer and then corrected for the backgrounds.

During the transmission measurements using water-moderated neutrons two sources of background were monitored: (1) a background arising from 2.2-MeV gamma rays produced by neutron capture in the water moderator of the target; (2) a time and beam independent room background. To aid in the determination of these backgrounds and to optimize the signal-to-background ratio, four separate pulse-height spectra were recorded. At low energies (below 5 keV) the background is mainly (90%) due to a constant time independent background. At high energies it is mostly due to 2.2-MeV gamma rays from the moderator (≈70% at 100 keV). For these operating conditions, the signal to background ratio for the open beam is greater than 1000 above 20 keV, 100 at 5 keV and 30 at 2.8 keV. See Ref. LAR83 for more details on corrections for these backgrounds.

The transmission data using unmoderated neutrons were corrected only for a time-independent background (determined at long times) since there was little neutron capture in the narrow water-cooling channels in the tantalum target. This constant background for the open beam is less than 0.3% above 180 keV.

2.2 DIFFERENTIAL ELASTIC SCATTERING MEASUREMENT

2.2.1 Data Acquisition

The scattering measurement was also done with the time-of-flight technique using neutron pulses from the ORELA water-moderated tantalum target. The 200-m flight path was used (see Table 1) and the filters and collimators allowed both unmoderated and moderated neutrons to reach the sample.

4 *DATA ACQUISITION AND DATA PROCESSING*

The scattering measurement was made using 123.4 g of iron enriched to 99.87% in ^{56}Fe. The sample was a hollow cylinder 6.35-cm high with a 3.0-cm outside diameter and a wall thickness of 0.282 ± 0.005 cm. The cylinder was suspended at the center of a 183-cm-diameter scattering chamber which was evacuated and isolated from the flight-path beam tube by means of a 0.025-cm Mylar entrance window.

The scattering data were obtained with a 0.3 g/cm^2 ^{10}B filter to eliminate low-energy neutrons associated with the previous burst and with two other filters to reduce the intensity of the gamma flash from the target: one made of uranium, 0.73-cm thick, covered the whole beam; the other composed of three 2.5-cm-thick layers of uranium, thorium and tantalum shadowed only the tantalum part of the target.

The electron beam burst width was 6 ns producing a beam power of 10 kW at 800 Hz. The measurement covered the energy region from approximately 10 keV to 5 MeV.

Six neutron detectors were located 19.1 cm from the center of the chamber at angles of 39°, 55°, 90°, 120°, 140°, and 160° from the direction of the incident neutron beam. Each neutron detector consisted of a 7.62-cm-long by 4.32-cm-diameter cylinder of NE-110 which was viewed at each end by RCA 8850 photomultiplier tubes. Additional details of the experimental arrangement for these scattering measurements can be found in reference HOR86.

The threshold for each phototube was set below the single photoelectron level, and a fast coincidence between the two tubes of each detector was required to define an event. The summed anode signals were split into two pulse-height windows and an 45,000 channel time-of-flight (TOF) spectrum was taken for each window. The lower window was from threshold to about 14 photoelectrons, which corresponds to 160 keV proton energy for this detector. The upper window was for summed pulses greater than 14 photoelectrons. The two TOF spectra for a detector had equal counts at about 300 keV neutron energy. The relative efficiencies vs energy of the six detectors were determined from series of measurements using a carbon scatterer.

The fast outputs of the six detectors were multiplexed to provide the stop signal and to set a four-bit tag generator of an EG&G clock. The system was designed so that each detector could record a maximum of only one event from each accelerator burst (i.e., 800 s^{-1}). The data had to be corrected for deadtime which was caused predominantly by detection of the gamma flash scattered by the sample. A second EG&G time digitizer was modified so as to provide a seven-bit tag generator, and this was operated in parallel with the other time digitizer but with considerably fewer TOF channels. This allowed direct measurement of the gamma-flash events recorded by each detector, i.e., singly or in any multiple coincidence.

Data were also taken with one of the detectors placed in the direct beam to measure the product of the flux and the detector efficiency as a function of neutron energy.

2.2.2 Data Reduction

All spectra were normalized by means of a neutron monitor detector. After correcting for deadtime and a constant room background, the scattering spectra were divided by the spectrum from the in-beam detector to remove the energy dependence of the incident flux and detector efficiency. The data were not corrected for multiple scattering in the sample but were corrected for geometrical factors to deduce a relative differential scattering cross section with an uncertainty of $\approx$5%.

3. DATA ANALYSIS

3.1 TRANSMISSION DATA ANALYSIS

The transmission data were analyzed with the multilevel R-matrix Reich-Moore (REI58) formalism code SAMMY (LAR80-90). SAMMY is a constrained least-squares code which uses Bayes' theorem for the fitting process. By using Bayes' equations, various data sets can be analyzed sequentially to yield a result equivalent to the simultaneous analysis of these data sets.

The iron data analysis documented in this report is similar to previously published analyses of ^{58}Ni (PER88) and ^{60}Ni (PER83) nuclei; these publications should be consulted for more details. Complete documentation on Bayes' theorem, and on the formalism used in the code SAMMY with details on the code itself and specific examples, are given in Ref. LAR80-90.

Two main data sets were analyzed between 5 and 850 keV. From 5 to 120 keV the transmission data analyzed were those obtained with the natural iron sample, and from 120 to 850 kev with the enriched ^{56}Fe sample. As noted earlier, both experiments used the 200-m flight path. The main characteristics of the experiments are given in Table 1. Details of the experimental setups and of the various corrections applied during the data reduction process were reported in Sect. 2.1.

The transmission data from the original data files were averaged whenever it was possible to do so without compromising any information. The number of data points was reduced on average by a factor of 30 for the natural iron data below 120 keV and by a factor of 3 above 120 keV for the ^{56}Fe data. This reduced number of data points allowed us to submit each of the data sets in a single run of the code SAMMY.

The narrow, isolated resonances of the minor iron isotopes which would not affect the determination of the ^{56}Fe resonance parameters were removed from the natural iron data file (however the narrow resonance at 53.57 keV in ^{54}Fe was not eliminated since it was unresolved from the ^{56}Fe resonance at 53.56 keV). The parameters of the wide resonances which contribute to the smooth cross section were included in the parameter file and adjusted along with the ^{56}Fe isotope resonance parameters to optimize the fit to the transmission data.

Due to the low inelastic-scattering threshold (14.4 keV) of the ^{57}Fe isotope, the inelastic-scattering contribution to the transmission data is significant and cannot be ignored. It was simulated by assigning very large values to the radiation widths of the wide ^{57}Fe s-wave resonances as recommended by M. C. Moxon in his natural iron analysis from 0.3 to 50 keV (MOX88).

Also present in the natural iron sample is a small ^{55}Mn impurity ($\approx$0.13%) which contributes slightly to the smooth cross section of our data. Therefore, the parameters recommended for the large s-wave resonances for this isotope in Ref. MUG81 were included in our parameter file, along with the parameters of the large resonances of the minor iron isotopes (54, 57 and 58).

The initial input resonance parameter file included, below 120 keV, resonance parameters for all previously reported resonances in natural iron (except for the

narrow resonances of the minor iron isotopes), the parameters of the large s-wave resonances of the ^{55}Mn impurity and, above 120 keV, only the resonance parameters of the ^{56}Fe isotope. Uncertainties were assigned to the adjusted parameters. The resonances external to the energy region analyzed are represented by fictitious resonances outside the energy range of this analysis.

All resonances showing the characteristic interference pattern of s-waves were assigned as s-waves. The ^{56}Fe differential elastic scattering data were used to confirm the s-wave assignments and to assign the spin and parity of $\ell > 0$ resonances whose neutron widths were large enough for them to be observed in this experiment (see Sect. 3.2). We also assigned spins and parities to the narrow resonances even though most of the assignments are, at best, uncertain and often arbitrary.

A Gaussian resolution function was used in the transmission data analysis with the code SAMMY. This Gaussian resolution is a function of the electron burst width, Δt, and of the spread of the flight-path length distribution, ΔL. Because of the relatively small energy range of the natural iron data analysis ΔL could be kept constant at the value of 45 mm determined by fitting narrow resonances. With this value of ΔL the effective Gaussian resolution (full width half maximum, FWHM) calculated for these data is 1.5 eV at the incident neutron energy of 5 keV, increasing to 54 eV at 120 keV.

In the case of the ^{56}Fe data it became evident in the course of the analysis that the resolution width calculated with a constant value for the spread of the flight-path length distribution would not allow a good fit to the transmission data over the complete energy range. The energy dependence of ΔL was investigated by F. G. Perey and S. N. Cramer (PER90). Their Monte-Carlo calculations of the flight-path length distribution for the ORELA tantalum target indicate that ΔL decreases linearly with energy in the range 100 keV to 1 MeV. Consequently a linear energy dependence for ΔL was included in the code SAMMY:

$$\Delta L = aE + b$$

The parameters a and b used in the analysis of the ^{56}Fe data, obtained from the Monte-Carlo calculations, are:

$$a = -2.2 \times 10^{-8} \quad \text{m/eV}$$

$$\text{and } b = 5.95 \times 10^{-2} \quad \text{m.}$$

These values yield a ΔL of 56.9 mm at 120 keV and 40.8 mm at 850 keV. The corresponding effective Gaussian resolution widths are equal to 52.7 eV and 537 eV.

In the analysis of ^{58}Ni (PER88) it was found that a single channel radius was inadequate to describe the transmission data when the analysis was extended above 200 keV. A good fit to the data was achieved with the radius for the p-wave 30% smaller than the radius for the s- and d-wave resonances. For the present analysis two radii were also used; the final values obtained with the code SAMMY are 5.437 fm for the s- and d-waves resonances and 4.896 fm for the p-waves. Although the two radii differ by only 10% for the ^{56}Fe data the χ^2 per degree of freedom is 23% smaller than when a single radius is used.

During the process of fitting the transmission data with the code SAMMY, a normalization factor and a background correction, both energy independent, were allowed to be adjusted for each data set. Background corrections were determined to be negligible for both data sets. No normalization correction was necessary for the natural iron transmission data, but a 1.0225 ± 0.0005 normalization factor was needed for the ^{56}Fe transmission data. The reason for such a large renormalization of the data is presently unknown.

In order to insure that the resonance parameters based upon the analysis of the 200-m data would produce acceptable thermal scattering cross sections, data in four small energy intervals between 20 eV and 2 keV were also used in the fitting process. These data were based upon transmission measurements made with a ^{6}Li-glass detector at 17 and 80-m flight paths. The data used in this low-energy region and the theoretical cross section generated from the final resonance parameters, given in Tables 2 and 3, are shown in Fig. 1 (excluding the 1.15-keV resonance). The thermal total cross section generated from the ^{56}Fe parameters of Table 2 is equal to 14.64 b, which is in good agreement with the value of 15.05 ± 0.50 b recommended in Ref. MUG81 for the sum of the thermal neutron scattering and capture cross sections.

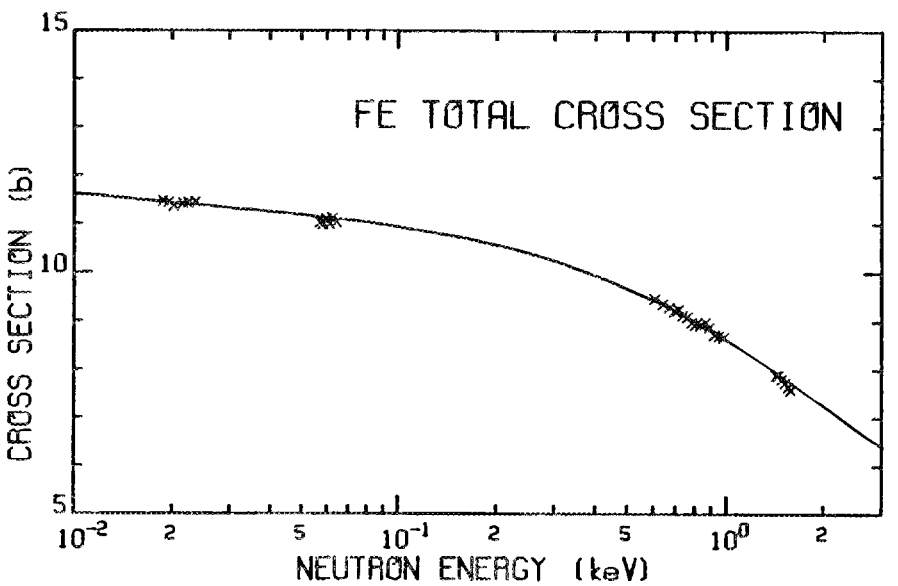

Fig. 1. Data below 2 keV used in the SAMMY fitting process. The smooth line is the plot of the theoretical cross section calculated with combined parameters of Tables 2 and 3, excluding the 1.15-keV resonance.

The fit to the natural iron data (from which the narrow isolated resonances of the minor iron isotopes were removed) obtained with the combined parameters of Tables 2 and 3 are shown in Figs. 2 through 5. The large resonances of the non-^{56}Fe isotopes and of the ^{55}Mn impurity which contribute to the smooth cross section are identified in the upper plots. The lower plots show details of the narrow ^{56}Fe resonances from the upper plots. In Figs. 6 through 11 the ^{56}Fe data, from 120 to 850 keV, are compared with the theoretical cross sections calculated with the parameters of Table 2 obtained with the code SAMMY.

3.2 DIFFERENTIAL ELASTIC SCATTERING DATA ANALYSIS

The differential elastic-scattering measurements were used as the principal tool to determine the spin and parity of the $\ell > 0$ resonances. The main characteristics of the experiment are given in Table 1. Details of the experimental setup and of the various corrections applied during the data reduction process were reported in Sect. 2.2. The theoretical calculations of the cross section at six scattering angles were compared to the experimental data. Various combinations of spins and parities were tested; the combination which yielded the best agreement with the data was adopted.

The theoretical cross sections were calculated as a function of the incident neutron energy with the R-matrix code RFUNC (PER89), which is based on the Blatt-Biedenharn formalism (BLA52). Doppler broadening and experimental resolution are taken into account. The Gaussian resolution width in this experiment is 30 eV at a neutron incident energy of 50 keV and 815 ev at 850 keV: $\approx$50% larger than for the transmission data. The code includes approximate corrections for attenuation and multiple scattering in the sample. The same channel radii determined in the transmission data analysis are used in the code RFUNC.

To illustrate how the differential elastic-scattering data allows us to determine the spin and parity of resonances seen clearly in this experiment we consider first the region from 40 to 240 keV. The resonance parameters are reported in Table 2 and the parameters of the $\ell > 0$ resonances are compared with those of Ref. COR85 in Table 4. Whereas we can assign definite spin and parity to 21 of the 43 observed resonances in this 200 keV energy region, Cornelis et al., with transmission data alone using a 200-m flight path, could assign the spin and parity only to the largest resonance in this energy region, at 122.8 keV, and we disagree with their assignment.

In Fig. 12 are plotted the differential elastic-scattering data and theoretical calculations for three of the six scattering angles in a small energy region which includes the large resonance at 122.8 keV, and two smaller ones. The transmission data for the resonance at 122.8 keV is fitted just as well if the assignment is $p_{1/2}$ or $p_{3/2}$; however, these assignments yield differential elastic-scattering cross sections that are quite different. The thin line, which corresponds to a $p_{1/2}$ assignment, does not agree with the data at any of the three scattering angles whereas the thick line, generated from a $p_{3/2}$ assignment, is in good agreement with the data at 39° and 160° scattering angles. Even though the theoretical curves do not agree well with the data at 90° a $p_{3/2}$ assignment is still clearly favored over a $p_{1/2}$ assignment.

The next resonance at 124.2 keV illustrates the point that definite spin and parity assignments can be made for narrow resonances, here only 10 eV wide, if they are isolated. The comparison of the differential elastic-scattering data for

the d-wave resonance at 125.2 keV with the data for the two p-wave resonances, in Fig. 12, illustrates how p- and d-wave resonances are differentiated: the 39° scattering angle does not provide useful information since the asymmetric shape of the resonances are similar for both ℓ-values; at 90° the shapes are different: the $\ell = 1$ resonances have a symmetric shape about the resonance energy whereas the $\ell = 2$ resonances have an asymmetric shape; at 160° asymmetric patterns are again observed for both ℓ-values but they are reversed for a p- and a d-wave.

We now consider the 550 to 600 keV energy region. The resonance parameters from this work and from the 400-m transmission data (from 240 to 850 keV) of Cornelis et al. (COR83) are compared, for this energy region, in the lower half of Table 5. Excluding the resonance at 558.8 keV, which is fitted as a doublet in our analysis but as a singlet in Ref. COR83, only two of our ℓ and J assignments agree with the ones given by Cornelis et al. and we clearly disagree with four of their assignments.

In Fig. 13 the total cross section and differential elastic-scattering data from ORELA are compared with the theoretical calculations obtained from the parameters of Table 2. Figure 14 differs from Fig. 13 only in the assignments of the ℓ and J values for the four resonances on which we disagree with Cornelis et al. and in some values of the neutron widths since a new fit to the transmission data was performed using these four assignments from Ref. COR83. Only these four assignments and the s-wave associated with the first $d_{3/2}$ resonance, are identified on Fig. 14.

When the resonance at 561.4 keV (on top of an s-wave resonance) is fitted as a $p_{3/2}$ resonance in Fig. 13, and then as a $d_{3/2}$ resonance in Fig. 14, the fit to the transmission data is just slightly worsened but the agreement with the differential elastic-scattering data is lost. This demonstrates that even in the case of a large resonance, and especially if it interferes with another large one, the analysis of the transmission data alone cannot be depended upon to provide determination of spins and parities. The usefulness of the differential scattering data in assigning spins and parities is demonstrated again for the smaller but isolated resonance at 590.4 keV.

For many p-wave resonances one can make a definite J-assignment because the differential elastic-scattering cross section for a $p_{1/2}$ and a $p_{3/2}$ resonance are quite different. However, this sensitivity is less for $d_{3/2}$ and $d_{5/2}$ resonances. For example, the fit to the total cross section for the two d-wave resonances, at 569.4 and 579.9 keV, is just as good in Fig. 14 as it is in Fig. 13, and the agreement with the differential elastic-scattering data is markedly worse in Fig. 14 only at the 160° scattering angle.

Table 2. Resonance parameters for ^{56}Fe + n from 1 to 850 keV.

The transmission and differential elastic scattering data analyses were performed with the following channel radii:

$R = 5.437 \pm 0.002$ fm for the $\ell = 0$ and $\ell = 2$ resonances,

$R = 4.896 \pm 0.003$ fm for the $\ell = 1$ and $\ell = 3$ resonances.

The three negative energy resonances and the six resonances above 851 keV describe the smooth cross section in the analyzed region and are an integral part of the parameter file. Uncertainties are given in parentheses. The notation is such that −473. (19) means −473. ± 19.

	E_0 (keV)	Γ_n (eV)	$g\Gamma_n\Gamma_\gamma/\Gamma^a$ (eV)	Γ_γ (eV)	ℓ^b	J^b	Notes
*1	−473. (19)	308.E+3 (12)		1.0	0	0.5	1
*2	−24. (2)	2.71E+3 (17)		1.0	0	0.5	1
*3	−2.44 (5)	193. (7)		0.86	0	0.5	1
4	1.15	61.7E−3 (9)	55.7E−3 (8)	0.574 (40)	1	0.5	2
5	2.35	0.21E−3	0.42E−3 (8)	0.75	[2	1.5]	3
6	12.45	2.8E−3	2.8E−3 (7)	0.45	[1	0.5]	3
7	17.75	14.8E−3	14.4E−3 (16)	0.45	[1	0.5]	3
8	20.17	4.2E−3	8.3E−3 (18)	0.75	[2	1.5]	3
9	22.801 (4)	0.214 (12)	0.191 (19)	1.8 (10)	[1	0.5]	4
*10	27.791 (2)	1409.3 (11)	0.86 (13)	0.86 (13)	0	0.5	
11	34.234 (1)	0.35 (2)	0.61 (6)	2.4 (12)	[1	1.5]	4
12	36.725 (1)	0.57 (3)	0.271 (15)	0.52 (6)	[1	0.5]	
13	38.418 (1)	0.238 (13)	0.36 (2)	0.74 (21)	[1	1.5]	
14	46.0535 (2)	5.14 (8)	0.54 (3)	0.29 (2)	1	1.5	
15	52.1397 (2)	17.29 (13)	0.77 (4)	0.39 (2)	1	1.5	
16	53.561 (1)	1.12 (5)	0.38 (2)	0.58 (5)	[1	0.5]	
17	53.68	0.037	0.034 (8)	0.45	[1	0.5]	3
18	59.2318 (2)	4.81 (8)	0.82 (5)	0.45 (3)	1	1.5	
19	63.474 (1)	0.80 (3)	0.65 (4)	0.55 (6)	[1	1.5]	
20	72.988 (1)	0.28 (2)	0.77 (8)	3.1 (22)	[2	2.5]	4
*21	74.029 (1)	611.5 (8)	0.59 (8)	0.59 (8)	0	0.5	
22	77.082 (1)	3.52 (12)	0.28 (2)	0.31 (2)	1	0.5	
23	80.8419 (2)	11.78 (11)	2.07 (11)	0.73 (4)	2	2.5	
*24	83.628 (1)	1215.1 (13)	0.54 (8)	0.54 (8)	0	0.5	
25	90.3379 (4)	22.0 (3)	0.83 (5)	0.42 (3)	1	[1.5]	
26	92.708 (1)	1.80 (8)	1.06 (6)	0.75 (6)	2	[1.5]	
27	92.928 (2)	0.76 (11)	0.56 (4)	0.44 (6)	[1	1.5]	
28	96.194 (2)	0.92 (8)	0.44 (8)	0.29 (7)	[2	1.5]	
29	96.3457 (4)	14.6 (3)	0.56 (6)	0.58 (6)	1	[0.5]	
30	96.630 (1)	2.16 (8)	1.33 (12)	0.96 (13)	2	[1.5]	
31	102.698 (1)	27.9 (3)	0.65 (6)	0.33 (3)	1	1.5	

Table 2. Continued

	E_0 (keV)	Γ_n (eV)	$g\Gamma_n\Gamma_\gamma/\Gamma^a$ (eV)	Γ_γ (eV)	ℓ^b	J^b	Notes
32	103.087 (2)	0.64 (12)	0.75 (6)	0.90 (30)	[1	1.5]	
33	105.942 (1)	3.46 (12)	1.34 (9)	0.83 (7)	2	[1.5]	
34	112.719 (1)	6.59 (18)	1.02 (7)	0.55 (4)	2	1.5	
35	121.02	0.034	0.032 (27)	0.45	[1	0.5]	3
36	122.60	0.073	0.126 (44)	0.45	[1	1.5]	3
37	122.801 (1)	61.9 (7)	0.59 (7)	0.30 (3)	1	1.5	
38	124.187 (2)	10.2 (5)	0.59 (5)	0.63 (6)	1	0.5	
39	125.175 (1)	12.9 (4)	1.16 (8)	0.61 (4)	2	1.5	
*40	129.861 (2)	588. (3)	0.57 (8)	0.57 (8)	0	0.5	
41	130.17	0.90	0.82 (12)	0.75	[2	1.5]	3
42	140.479 (4)	2735. (6)	1.58 (24)	1.58 (24)	0	0.5	
43	141.15	0.62	0.68 (17)	0.75	[2	1.5]	3
44	142.31	0.95	0.61 (11)	0.45	[1	1.5]	3
45	149.83	0.14	0.21 (3)	0.45	[1	1.5]	3
46	153.945 (4)	5.0 (5)	0.56 (5)	0.63 (6)	1	[0.5]	
47	161.778 (2)	6.7 (4)	1.13 (9)	0.62 (5)	2	[1.5]	
48	169.127 (2)	21.6 (8)	1.67 (25)	0.87 (13)	2	1.5	
*49	169.275 (2)	962. (3)	1.00 (14)	1.00 (14)	0	0.5	
50	173.19	2.0	0.22 (5)	0.25 (5)	[1	0.5]	
51	173.688 (1)	38.8 (7)	0.48 (7)	0.24 (3)	1	1.5	
52	175.89	0.08	0.13 (5)	0.45	[1	1.5]	3
53	179.766 (1)	16.9 (5)	0.49 (7)	0.25 (4)	1	1.5	
54	181.08	[6.4 (7)	[0.50 (25)	0.54 (25)	[1	0.5]	5
55	181.185 (1)	29.2 (5)]	2.36 (25)]	0.81 (8)	2	2.5	5
56	187.088 (4)	6.0 (4)	0.54 (13)	0.28 (7)	2	[1.5]	
*57	187.737 (4)	3620. (7)	1.02 (25)	1.02 (25)	0	0.5	
58	188.07	0.056	0.10 (5)	0.45	[1	1.5]	3
59	189.97	[24. (2)	[0.28 (10)	0.28 (10)	[1	0.5]	5
60	190.02 (1)	14.2 (18)]	0.61 (10)]	0.31 (5)	2	[1.5]	5
61	193.015 (2)	20.9 (7)	1.15 (10)	0.39 (4)	2	2.5	
62	195.747 (2)	72.7 (14)	0.54 (7)	0.54 (7)	1	0.5	
63	201.581 (1)	32.8 (7)	1.63 (14)	0.84 (7)	2	1.5	
64	203.80	0.042	0.079 (33)	0.75	[2	1.5]	3
65	205.95	1.41 (11)	1.05 (10)	0.47 (6)	2	[2.5]	
66	207.997 (2)	12.5 (5)	0.68 (8)	0.35 (4)	1	1.5	
67	208.83	0.15	0.22 (7)	0.45	[1	1.5]	3
68	209.72	0.06	0.11 (4)	0.75	[2	1.5]	3
69	210.699 (3)	5.9 (3)	1.16 (12)	0.41 (4)	2	2.5	
70	215.98	0.26	0.33 (6)	0.45	[1	1.5]	3
*71	220.586 (2)	1267. (4)	1.68 (21)	1.68 (21)	0	0.5	
72	221.844 (5)	8.7 (6)	0.43 (9)	0.22 (5)	1	[1.5]	
73	223.69	1.3 (6)[c]	1.02 (10)	0.84 (28)	[2	1.5]	
74	225.855 (2)	56.2 (12)	0.89 (11)	0.90 (11)	1	[0.5]	

Table 2. Continued

	E_0 (keV)	Γ_n (eV)	$g\Gamma_n\Gamma_\gamma/\Gamma^a$ (eV)	Γ_γ (eV)	ℓ^b	J^b	Notes
75	229.91	0.42	0.54 (8)	0.75	[2	1.5]	3
76	232.550 (2)	25.4 (6)	2.22 (19)	1.16 (10)	2	1.5	
77	234.893 (1)	31.7 (5)	2.38 (18)	0.81 (6)	2	2.5	
78	241.625 (2)	11.6 (4)	3.46 (26)	1.28 (11)	2	2.5	
79	243.41	0.11	0.18 (6)	0.45	[1	1.5]	3
*80	244.991 (1)	487. (3)	0.60 (10)	0.60 (10)	0	0.5	
81	246.34	0.16	0.12 (12)	0.45	[1	0.5]	3
82	252.49	0.25	0.16 (8)	0.45	[1	0.5]	3
83	253.556 (1)	42.1 (6)	1.74 (19)	0.59 (6)	2	2.5	
84	256.158 (5)	5.4 (4)	1.08 (12)	0.60 (7)	2	[1.5]	
85	259.902 (3)	13.1 (5)	0.68 (10)	0.35 (5)	1	1.5	
86	260.76	0.09	0.16 (7)	0.75	[2	1.5]	3
87	263.641 (1)	125.6 (14)	0.56 (11)	0.56 (11)	1	0.5	
88	264.34	1.0 (5)[c]	0.29 (12)	0.41 (25)	[1	0.5]	
89	267.044 (1)	78.7 (6)	0.98 (19)	0.33 (6)	2	2.5	
90	267.693 (8)	7.0 (5)	0.77 (30)	0.87 (38)	1	[0.5]	
91	269.772 (1)	158.3 (14)	0.41 (11)	0.41 (11)	1	0.5	
92	274.69	0.56	0.25 (14)	0.45	[1	0.5]	3
*93	276.336 (1)	228.8 (19)	0.52 (11)	0.26 (6)	1	1.5	
*94	277.206 (6)	3650. (9)	0.80 (19)	0.80 (19)	0	0.5	
95	280.986 (5)	8.9 (5)	1.70 (19)	0.94 (10)	2	[1.5]	
96	283.05	4.8 (4)	0.64 (32)	0.74 (43)	1	[0.5]	
97	283.985 (3)	9.3 (4)	1.40 (19)	0.49 (7)	2	2.5	
98	285.550 (2)	17.7 (5)	2.15 (21)	0.75 (7)	2	2.5	
99	288.765 (2)	31.5 (8)	1.38 (17)	0.71 (9)	2	1.5	
100	290.415 (2)	33.9 (7)	[0.75 (17)	0.38 (9)	1	1.5	5
101	290.74	3.6 (3)	0.80 (17)]	0.45 (9)	[2	1.5]	5
102	293.225 (2)	197.6 (20)	0.69 (11)	0.69 (11)	1	0.5	
103	295.88	0.33	0.38 (11)	0.45	[1	1.5]	3
104	299.974 (2)	28.1 (6)	1.51 (18)	0.78 (9)	2	1.5	
105	302.99	0.15	0.22 (11)	0.45	[1	1.5]	3
106	304.493 (3)	18.3 (6)	0.81 (14)	0.41 (7)	1	1.5	
107	306.32	0.33	0.19 (12)	0.45	[1	0.5]	3
108	306.99	1.0 (5)[c]	0.71 (30)	0.55 (39)	[1	1.5]	
109	310.980 (1)	144.5 (15)	1.18 (16)	1.19 (16)	1	0.5	
110	312.84	1.7 (8)[c]	0.41 (13)	0.54 (24)	[1	0.5]	
111	314.744 (1)	52.9 (6)	3.36 (29)	1.14 (10)	2	2.5	
*112	317.909 (6)	7118. (12)			0	0.5	6
113	321.779 (7)	9.9 (6)	1.23 (22)	0.66 (13)	2	[1.5]	
114	324.013 (10)	10.5 (8)	0.32 (16)	0.33 (17)	1	[0.5]	
*115	331.447 (2)	[327.6 (25)	[0.60 (20)	0.60 (20)	0	0.5	5
*116	331.510	27.0 (13)]	0.83 (20)]	0.42 (10)	2	1.5	5
117	334.417 (2)	4.2 (4)	1.77 (20)	0.69 (9)	2	[2.5]	

Table 2. Continued

	E_0 (keV)	Γ_n (eV)	$g\Gamma_n\Gamma_\gamma/\Gamma^a$ (eV)	Γ_γ (eV)	ℓ^b	J^b	Notes
*118	340.770 (1)	[132.8 (10)	[0.90 (27)	0.45 (14)	1	1.5	5
119	341.059 (3)	30.5 (11)]	0.95 (27)]	0.48 (14)	2	[1.5]	5
120	341.766 (12)	3.8 (3)	1.24 (22)	0.74 (16)	[1	1.5]	
121	344.753 (2)	45.2 (8)	1.63 (22)	0.83 (11)	2	1.5	
*122	348.904 (1)	256.2 (13)	1.23 (19)	0.62 (10)	1	1.5	
123	350.322 (1)	93.1 (9)	1.96 (25)	0.99 (13)	2	1.5	
124	353.768 (2)	34.6 (7)			[2	1.5]	7
125	356.705 (7)	8.4 (6)			2	[1.5]	
*126	357.263 (3)	2205. (11)			0	0.5	
*127	361.078 (6)	7775. (16)			0	0.5	
128	362.716 (2)	93.6 (15)			1	1.5	
129	366.797 (5)	13.6 (7)			2	2.5	
130	373.747 (4)	5.4 (10)			2	[1.5]	
131	377.247 (11)	5.1 (8)			[1	1.5]	
132	379.184 (2)	47.6 (9)			2	1.5	
*133	381.360 (9)	12.33E+3 (2)			0	0.5	
134	385.93	2.0			[2	2.5]	
135	386.849 (3)	89.9 (16)			1	1.5	
136	393.523 (5)	54.6 (21)			1	0.5	
137	401.787 (2)	148.2 (14)			2	1.5	
138	403.134 (2)	621.0 (24)			1	1.5	
*139	405.408 (4)	2329. (9)			0	0.5	
*140	418.183 (2)	[748. (4)			1	1.5	
141	419.118	53.8 (12)]			2	2.5	
142	428.604 (9)	22.4 (17)			1	[0.5]	
143	431.001 (16)	5.8 (7)			2	[1.5]	
144	434.777 (2)	140.6 (14)			2	1.5	
*145	438.296 (4)	[1918. (8)			0	0.5	
146	438.687	13.7 (11)]			2	[1.5]	
147	439.517	10.3 (17)			1	[0.5]	
148	448.217	[251. (5)			1	0.5	
149	448.811 (2)	236.3 (21)]			2	2.5	
150	451.288 (2)	93.5 (14)			1	1.5	
151	455.170 (15)	7.7 (9)			2	[1.5]	
152	457.040 (4)	97.0 (23)			1	0.5	
153	458.045 (2)	145.0 (15)			1	1.5	
154	460.275 (16)	6.9 (7)			2	[1.5]	
155	464.379 (2)	72.3 (9)			2	2.5	
156	468.656	11.4 (13)			[1	0.5]	
*157	469.934 (4)	2566. (9)			0	0.5	
158	481.158 (2)	133.1 (12)			2	2.5	
159	485.330 (8)	41.4 (20)			1	0.5	
160	487.560 (14)	9.7 (14)			2	[1.5]	

Table 2. Continued

	E_0 (keV)	Γ_n (eV)	$g\Gamma_n\Gamma_\gamma/\Gamma^a$ (eV)	Γ_γ (eV)	ℓ^b	J^b	Notes
161	489.815	179.0 (24)			1	1.5	
162	490.568 (2)	418.1 (31)			2	1.5	
163	493.824 (5)	42.8 (13)			[2	1.5]	
*164	499.316 (2)	110.3 (12)			2	1.5	
*165	500.194 (4)	1726. (8)			0	0.5	
*166	503.405 (2)	147.5 (14)			2	2.5	
167	508.268 (13)	24.7 (19)			1	0.5	
*168	511.675 (2)	512.1 (28)			1	1.5	
*169	513.201 (4)	310. (6)			1	[0.5]	
170	513.385	52.3 (20)			[3	2.5]	
171	514.705 (8)	20.8 (12)			2	[1.5]	
172	523.042 (22)	6.5 (8)			[2	1.5]	
173	527.396 (2)	90.0 (12)			2	2.5	
174	531.855 (2)	98.5 (11)			2	2.5	
175	533.558 (4)	72.5 (14)			1	1.5	
*176	535.921 (3)	255.5 (35)			0	0.5	
*177	538.737 (2)	459.6 (27)			1	1.5	
178	543.98	21.3 (19)			[1	0.5]	
179	544.413 (3)	131.8 (17)			1	1.5	
180	545.653	308.8 (18)			[2	2.5]	
181	545.773	268. (4)			[0	0.5]	
182	552.500 (3)	61.0 (11)			2	2.5	
183	556.76	12.0			2	[1.5]	
184	558.783	149.7 (16)			2	2.5	
*185	558.854 (4)	854. (6)			1	0.5	
*186	561.015 (8)	1500. (10)			0	0.5	
*187	561.394 (4)	376. (4)			1	1.5	
188	565.497 (4)	49.8 (12)			2	[2.5]	
189	567.350 (20)	17.3 (19)			1	[0.5]	
190	569.399 (3)	86.6 (12)			2	2.5	
191	575.212	87.1 (27)			0	0.5	
*192	577.419 (3)	1456. (5)			1	1.5	
193	579.878 (2)	162.1 (15)			2	2.5	
194	581.068 (28)	12.9 (19)			[1	0.5]	
195	590.416 (4)	68.3 (12)			2	2.5	
196	591.424 (22)	8.2 (15)			[2	1.5]	
197	595.136 (4)	186. (4)			1	0.5	
198	595.894 (5)	65.2 (16)			2	1.5	
199	598.024 (23)	12.4 (22)			[1	0.5]	
200	603.591 (4)	83.4 (15)			1	1.5	
201	607.945 (32)	11.3 (16)			[1	0.5]	
202	610.150 (7)	24.9 (10)			2	[2.5]	
203	613.111	8.4 (10)			[2	1.5]	

Table 2. Continued

	E_0 (keV)	Γ_n (eV)	$g\Gamma_n\Gamma_\gamma/\Gamma^a$ (eV)	Γ_γ (eV)	ℓ^b	J^b	Notes
*204	613.936 (6)	2642. (14)			0	0.5	
205	614.141	82.2 (18)			2	[1.5]	
*206	614.873 (5)	300. (5)			1	0.5	
207	615.971	19.9 (15)			2	[1.5]	
208	623.441	14.9 (22)			[1	0.5]	
209	623.892 (10)	20.5 (11)			2	2.5	
210	626.694 (8)	36.3 (15)			1	1.5	
211	629.044 (30)	14.6 (28)			1	[0.5]	
212	631.138 (3)	137.9 (18)			2	1.5	
213	633.473 (5)	160.7 (33)			1	0.5	
214	636.495 (9)	35.3 (15)			[2	1.5]	
215	637.491 (2)	163.7 (14)			2	2.5	
216	641.535 (10)	58.1 (27)			1	0.5	
217	644.187 (7)	43.5 (15)			1	1.5	
218	645.98	58.9 (18)			[1	1.5]	
*219	646.665 (2)	667.3 (24)			2	2.5	
220	653.540 (2)	259.4 (22)			1	1.5	
221	654.900	21.6 (24)			[1	0.5]	
222	655.640	169.8 (24)			2	[2.5]	
223	655.830	165. (8)			1	0.5	
224	656.230	22.6 (20)			[1	1.5]	
225	657.826 (3)	487. (5)			1	1.5	
226	658.559	202. (4)			2	1.5	
227	663.406 (28)	9.0 (12)			[2	1.5]	
228	665.597 (4)	121.9 (20)			1	1.5	
*229	665.655 (22)	27.96E+3 (7)			0	0.5	
230	668.058 (24)	11.8 (14)			[2	1.5]	
231	671.281 (3)	212.1 (25)			2	1.5	
232	672.961 (9)	51.7 (20)			2	[1.5]	
233	680.675 (9)	35.1 (14)			2	[2.5]	
234	681.473 (11)	75.5 (35)			1	[0.5]	
235	683.944 (16)	21.9 (16)			2	[1.5]	
236	685.192 (3)	204.4 (18)			2	2.5	
237	688.658	9.7 (18)			[1	0.5]	
238	689.605 (3)	240.0 (24)			1	1.5	
239	691.108 (3)	133.2 (15)			[2	2.5]	7
*240	693.506 (5)	1727. (19)			0	0.5	
*241	695.628	496. (6)			2	1.5	
*242	696.188	599. (6)			1	1.5	
243	702.345 (14)	24.3 (15)			2	[1.5]	
244	705.197 (11)	16. (4)			[1	0.5]	
245	708.155 (11)	5.6 (13)			[1	1.5]	
*246	710.659 (20)	20.94E+3 (7)			0	0.5	
247	714.345 (8)	61.7 (20)			2	1.5	

Table 2. Continued

	E_0 (keV)	Γ_n (eV)	$g\Gamma_n\Gamma_\gamma/\Gamma^a$ (eV)	Γ_γ (eV)	ℓ^b	J^b	Notes
248	715.727 (8)	63.1 (21)			1	1.5	
*249	717.008 (5)	708. (9)			1	0.5	
250	721.336	148.2 (30)			2	[1.5]	
251	721.877 (5)	155.8 (28)			1	1.5	
*252	727.834 (3)	671. (4)			2	2.5	7
253	731.818 (5)	90.3 (17)			2	2.5	
*254	737.726	646. (11)			1	1.5	
*255	737.856	329. (7)			2	2.5	
256	739.534 (9)	52.6 (19)			2	[1.5]	
*257	741.680 (10)	5719. (27)			0	0.5	
258	744.98	44. (4)			[1	0.5]	
259	745.685 (4)	220.6 (31)			1	1.5	
*260	750.192 (3)	690. (7)			1	1.5	
*261	752.706 (7)	2462. (24)			0	0.5	
*262	756.281 (3)	1039. (5)			2	2.5	7
263	759.175 (9)	74.6 (24)			1	1.5	
264	765.013 (5)	132.5 (24)			2	[1.5]	
265	765.725	38.9 (33)			[1	0.5]	
*266	766.724 (3)	835. (5)			1	1.5	7
*267	769.537 (9)	3957. (23)			0	0.5	
268	770.225	35.6 (35)			[1	0.5]	
269	770.916 (4)	351.1 (33)			1	1.5	
270	772.311 (13)	52.0 (26)			2	[1.5]	
271	778.081 (6)	162.0 (29)			2	1.5	
272	779.435	34. (4)			[1	0.5]	
273	780.456 (4)	489. (4)			2	1.5	
274	782.84	250. (8)			2	[1.5]	
275	782.85	87. (7)			[2	2.5]	
276	785.27	166. (8)			[1	0.5]	
277	785.60	134.4 (29)			[1	1.5]	
*278	786.27	1629. (27)			1	0.5	
279	786.52	113. (4)			[2	1.5]	
280	786.97	98.0 (34)			[2	1.5]	
*281	787.27	1384. (16)			0	0.5	
*282	788.974 (3)	997. (7)			2	2.5	
283	794.020 (5)	185.9 (30)			2	[1.5]	
284	795.394	89. (5)			1	[0.5]	
285	795.944	40.2 (27)			2	[1.5]	
286	798.19 (4)	11.3 (23)			[2	1.5]	
287	801.419 (22)	52. (4)			1	[0.5]	
*288	804.532 (3)	681. (5)			2	1.5	
289	806.575 (5)	204.2 (30)			1	1.5	
290	814.464 (6)	453. (8)			1	0.5	

Table 2. Continued

	E_0 (keV)	Γ_n (eV)	$g\Gamma_n\Gamma_\gamma/\Gamma^a$ (eV)	Γ_γ (eV)	ℓ^b	J^b	Notes
291	816.33	[182. (4)			2	1.5	
292	816.858 (5)	314. (4)]			1	1.5	
293	818.54	[29. (4)			[1	0.5]	
294	819.14	63. (5)			[1	0.5]	
295	820.144 (4)	170.4 (23)]			2	2.5	
296	821.504 (26)	42. (4)			1	[0.5]	
*297	825.678 (9)	[263. (10)			0	0.5	
*298	825.86	229. (6)]			1	1.5	
*299	828.632 (3)	679. (4)			2	2.5	
300	833.762 (8)	245. (6)			1	0.5	
*301	835.798 (3)	536.4 (32)			2	2.5	
302	838.340 (12)	44.5 (18)			[2	2.5]	
*303	839.308 (6)	2411. (25)			0	0.5	
*304	845.452 (3)	883. (5)			2	2.5	
305	850.377 (9)	63.4 (20)			[2	2.5]	
306	851.92	121.8			2	2.5	1
*307	856.2	3.47E+3 (32)			0	0.5	1
308	865.4	802.			2	2.5	1
*309	883.	2.87E+3 (42)			0	0.5	1
*310	893. (4)	28.2E+3 (32)			0	0.5	1
*311	1283. (19)	740.E+3 (24)			0	0.5	1

*Denotes that parameters E_0 and Γ_n for this resonance were adjusted during the final fit to the transmission data with the code SAMMY. The covariance matrix associated with the uncertainties on these adjusted parameters is available from the authors.

[a]The capture kernels and their uncertainties were taken from the Geel capture measurements and analysis (COR84).

[b]Square brackets are used to indicate that the assignment is uncertain.

[c]Parameter adjusted by trial and error. A 50% uncertainty was estimated.

Note 1. Fictitious resonance outside the range of our analysis.

Note 2. These parameters and their uncertainties are from Ref. PER86.

Note 3. Resonance seen in Geel capture data (COR84) but not in our transmission data. The radiation width, Γ_γ, was set equal to 0.45 eV for $\ell = 1$ resonance and to 0.75 eV for $\ell = 2$ resonances. The corresponding value of the neutron width, Γ_n, was checked to be consistent with our transmission data.

Note 4. The neutron width, Γ_n, and the radiation width, Γ_γ, were both determined by the fit to the transmission data. The capture kernel is in good agreement with the value obtained from the Geel capture data (COR84).

Note 5. Unresolved resonance in the capture data. See Sect. 4.1 for the determination of the capture kernels.

Note 6. This s-wave resonance was not analyzed by Corvi et al. (COR84).

Note 7. Probably a multiplet.

Table 3. Resonance parameters of the large s-wave resonances for the minor iron isotopes and for the ^{55}Mn impurity, used in the analysis of the natural iron transmission data from 5 to 120 keV. The combined parameters of this table with those of Table 2 were used to generate the fits to the total cross section shown in Figs. 1 to 5. Channel radii used in the calculation were 4.0 fm for the ^{54}Fe isotope, 5.3 fm for the ^{57}Fe isotope, and 5.2 fm for the ^{58}Fe and ^{55}Mn isotopes.

E_o (keV)	Γ_n (eV)[a]	Γ_γ (eV)	ℓ	J	Isotope	Notes
−40.30	18377.	2.00	0	0.5	^{54}Fe	1
3.954	224.	1.14	0	0.0	^{57}Fe	1
6.266	441.	1.32	0	1.0	^{57}Fe	
7.786	1166.	2.10	0	0.5	^{54}Fe	
10.433	340.	1.60	0	0.5	^{58}Fe	
20.90	934.	0.75	0	2.0	^{55}Mn	2
27.10	420.	0.75	0	3.0	^{55}Mn	2
29.10	3482.	4750.	0	1.0	^{57}Fe	3
[35.40	1370.	0.75	0	3.0	^{55}Mn	2
35.60	1320.	0.75	0	2.0	^{55}Mn	2
[41.05	454.	0.75	0	3.0	^{55}Mn	2
41.52	762.	2000.	0	1.0	^{57}Fe	3
43.70	6447.	2.20	0	0.5	^{58}Fe	
47.124	426.	2.00	0	1.0	^{57}Fe	
52.950	2173.	2.00	0	0.5	^{54}Fe	
53.57	3.4	0.50	1	1.5	^{54}Fe	
56.01	8194.	2.00	0	0.0	^{57}Fe	
[57.55	557.	0.75	0	3.0	^{55}Mn	2
57.70	518.	0.75	0	2.0	^{55}Mn	2
60.00	624.	0.75	0	2.0	^{55}Mn	2
61.33	3995.	300.	0	1.0	^{57}Fe	3
64.55	926.	0.75	0	3.0	^{55}Mn	2
66.85	219.	0.75	0	3.0	^{55}Mn	2
67.01	2104.	1.00	0	0.5	^{58}Fe	
70.10	864.	0.75	0	2.0	^{55}Mn	2
71.91	1720.	2.00	0	0.5	^{54}Fe	
77.50	1997.	1000.	0	1.0	^{57}Fe	4
81.73	396.	0.75	0	2.0	^{55}Mn	2
[93.84	203.	2.00	0	1.0	^{57}Fe	
94.20	12625.	7.70	0	0.5	^{58}Fe	
97.05	240.	0.75	0	2.0	^{55}Mn	2
[98.799	544.	2.00	0	0.5	^{54}Fe	
98.85	1500.	0.75	0	3.0	^{55}Mn	
105.70	2196.	0.75	0	2.0	^{55}Mn	2
[109.50	2765.	1.30	0	1.0	^{57}Fe	
110.20	1127.	1550.	0	1.0	^{57}Fe	3
111.65	3600.	0.75	0	3.0	^{55}Mn	2
125.00	1514.	2.00	0	1.0	^{57}Fe	1
126.00	3073.	2.00	0	0.0	^{57}Fe	1
129.50	4260.	4000.	0	1.0	^{57}Fe	1
130.20	1892.	2.00	0	0.5	^{54}Fe	1
147.60	1892.	2.00	0	0.5	^{54}Fe	1
189.50	35212.	2.00	0	0.5	^{54}Fe	1
244.68	17357.	2.00	0	0.5	^{54}Fe	1

[a] These parameters were adjusted by the code except for resonances with Note 2.

See Notes on next page.

Table 3. Continued

Note 1. Fictitious resonances outside the energy range of the natural iron analysis. These resonances are needed to describe the smooth cross section in the region analyzed; they are therefore an integral part of the parameter file.

Note 2. Neutron widths, Γ_n, and average radiation widths, Γ_γ, from Mughabghab et al. (MUG81).

Note 3. The values for the radiation widths, Γ_γ, are from the natural iron analysis of M. C. Moxon (MOX88). These large values are necessary to simulate inelastic scattering. The neutron widths were readjusted to fit our data but do not differ significantly from Moxon's values.

Note 4. The radiation width, Γ_γ, was adjusted, starting from the value of 750 eV given by M. C. Moxon (MOX88). Note 3 also applies.

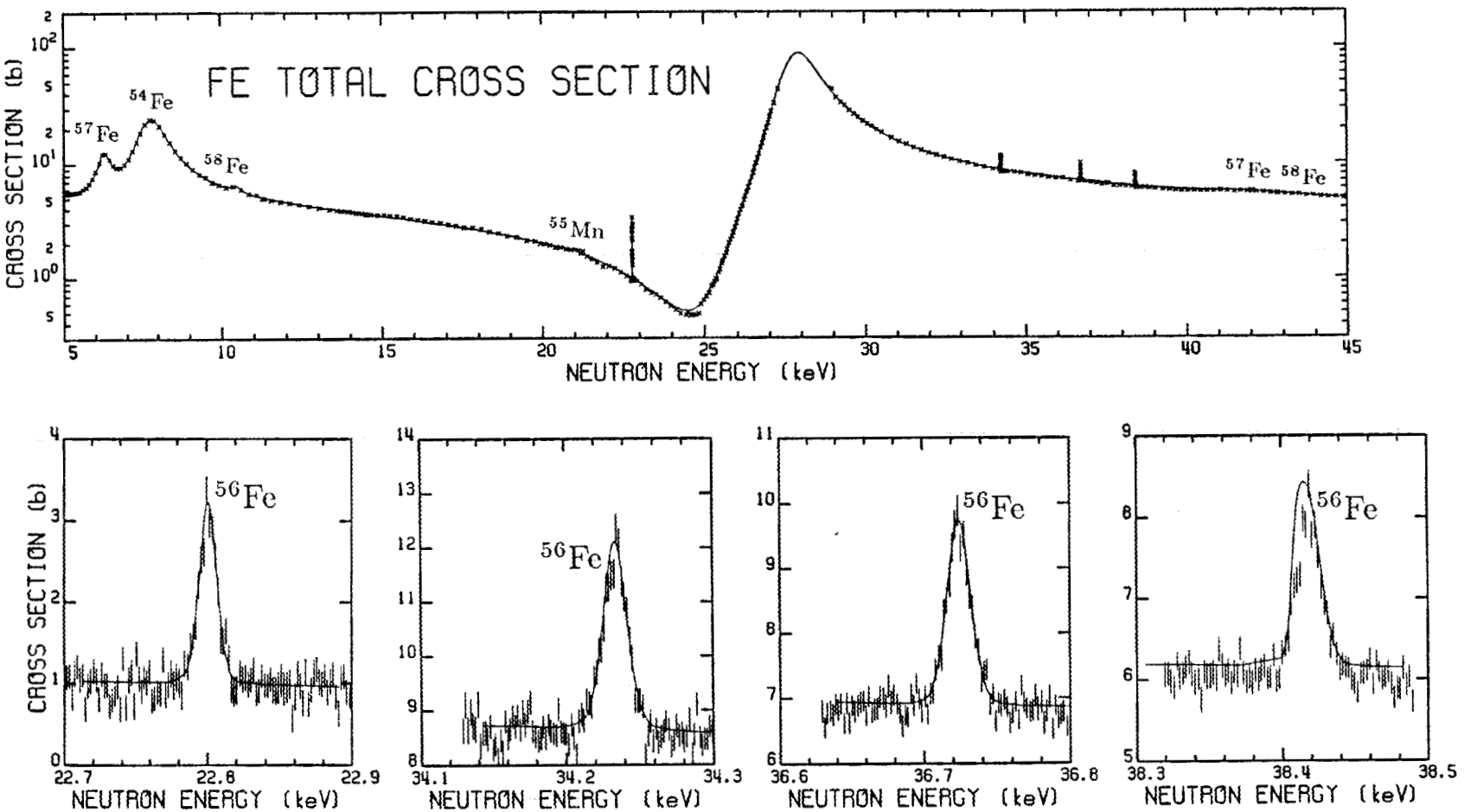

Fig. 2. Top: Natural iron theoretical total cross section calculated with combined parameters of Tables 2 and 3, compared with the total cross-section data from 5 to 45 keV. For the minor iron isotopes and the ^{55}Mn impurity only the total cross section of the large resonances were calculated. Bottom: The four ^{56}Fe narrow resonances from the upper plot were enlarged to show in detail the comparison of the calculated cross section with the data.

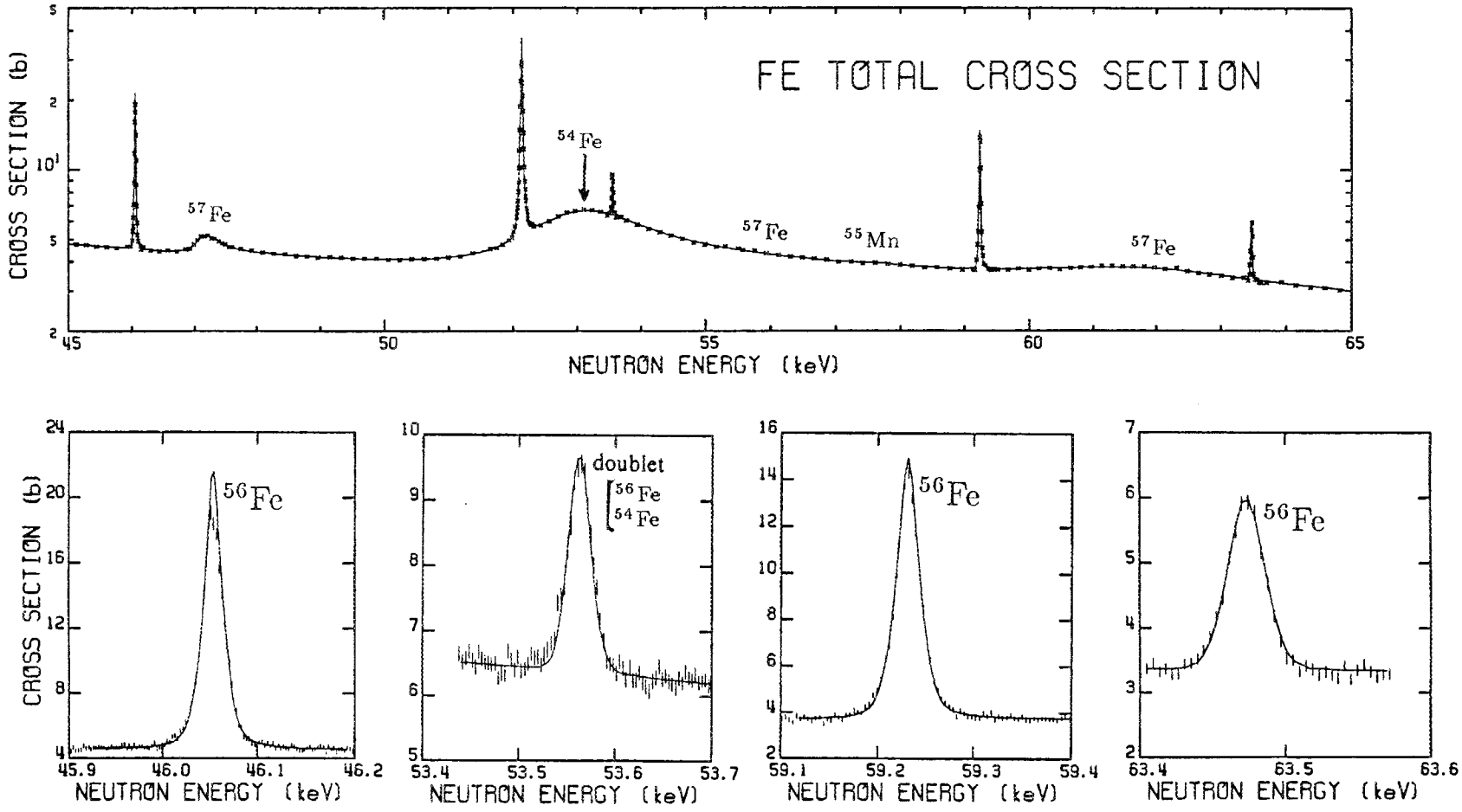

Fig. 3. Top: Same as Fig. 2 (top) except from 45 to 65 keV. Bottom: Four of the five ^{56}Fe narrow resonances from the upper plot were enlarged to show in detail comparison of the calculated cross section with the data.

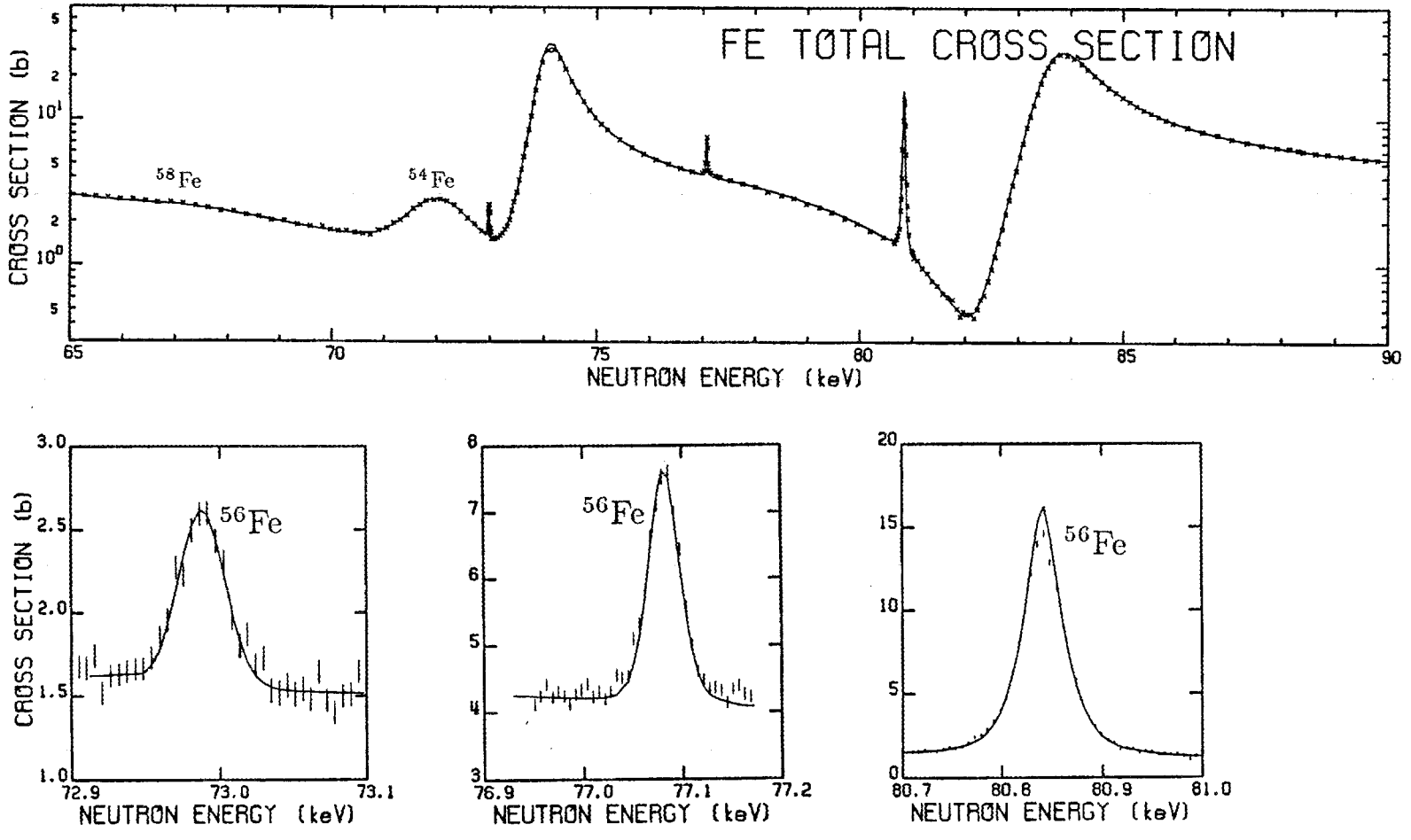

Fig. 4. Top: Same as Fig. 2 (top) except from 65 to 90 keV. Bottom: The three ^{56}Fe narrow resonances from the upper plot were enlarged to show in detail comparison of the calculated cross section with the data.

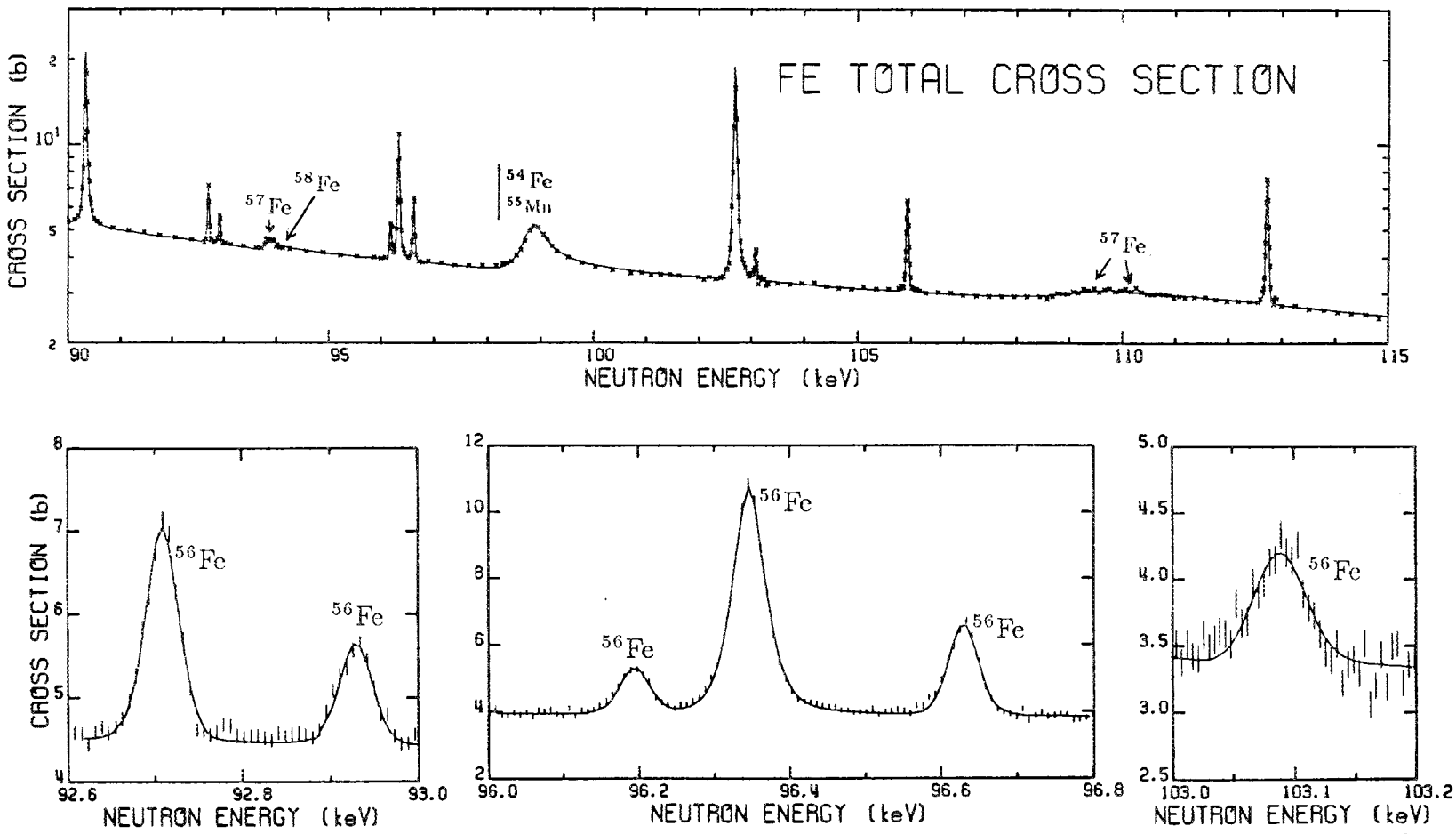

Fig. 5. Top: Same as Fig. 2 (top) except from 90 to 115 keV. Bottom: The two groups of ^{56}Fe narrow resonances around 92.8 and 96.4 keV, and the narrow resonance at 103.1 keV, were enlarged from the upper plot to show in detail comparison of the calculated cross section with the data.

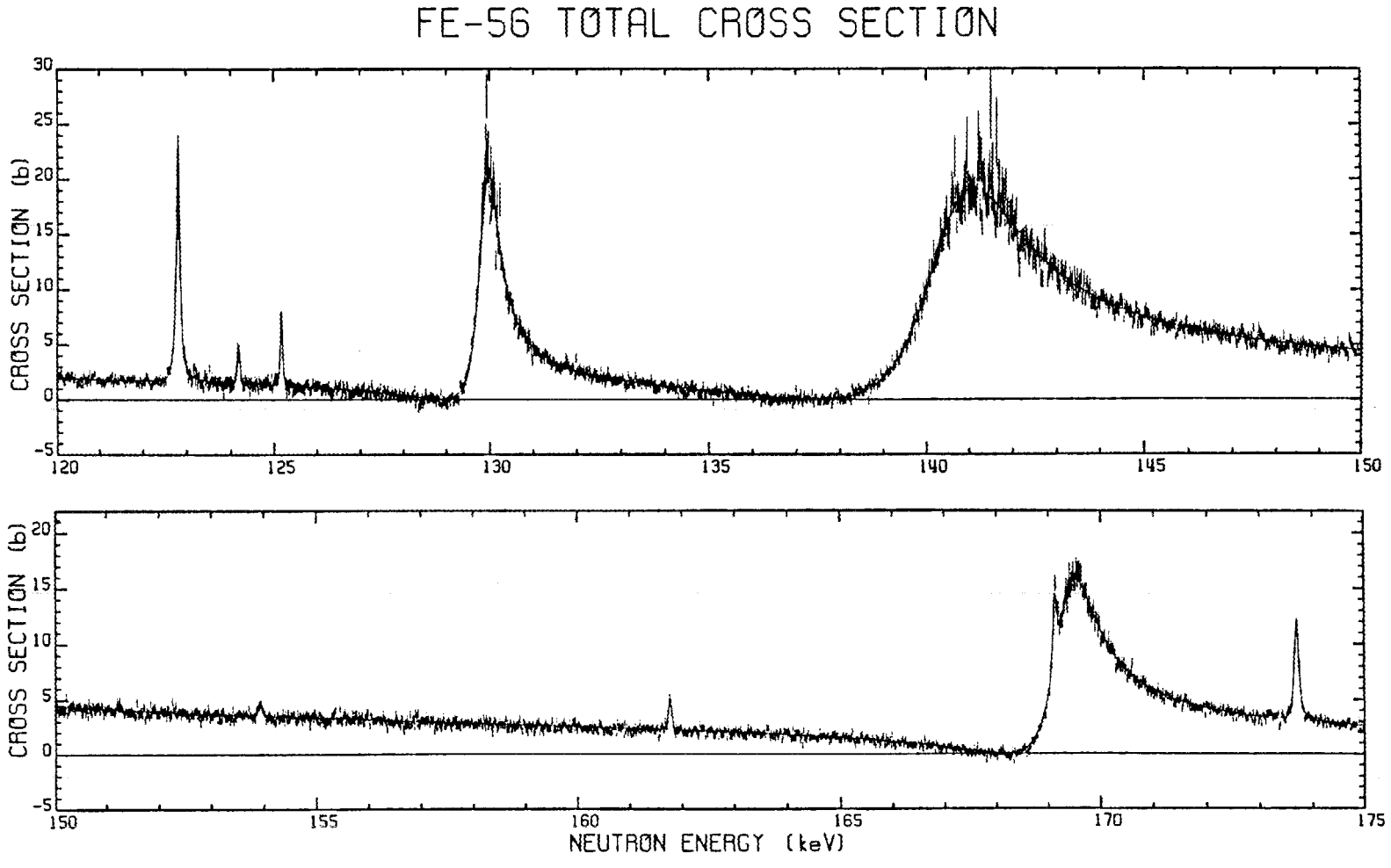

Fig. 6. ^{56}Fe theoretical cross section calculated with parameters of Table 2, compared with the total cross-section data from 120 to 175 keV.

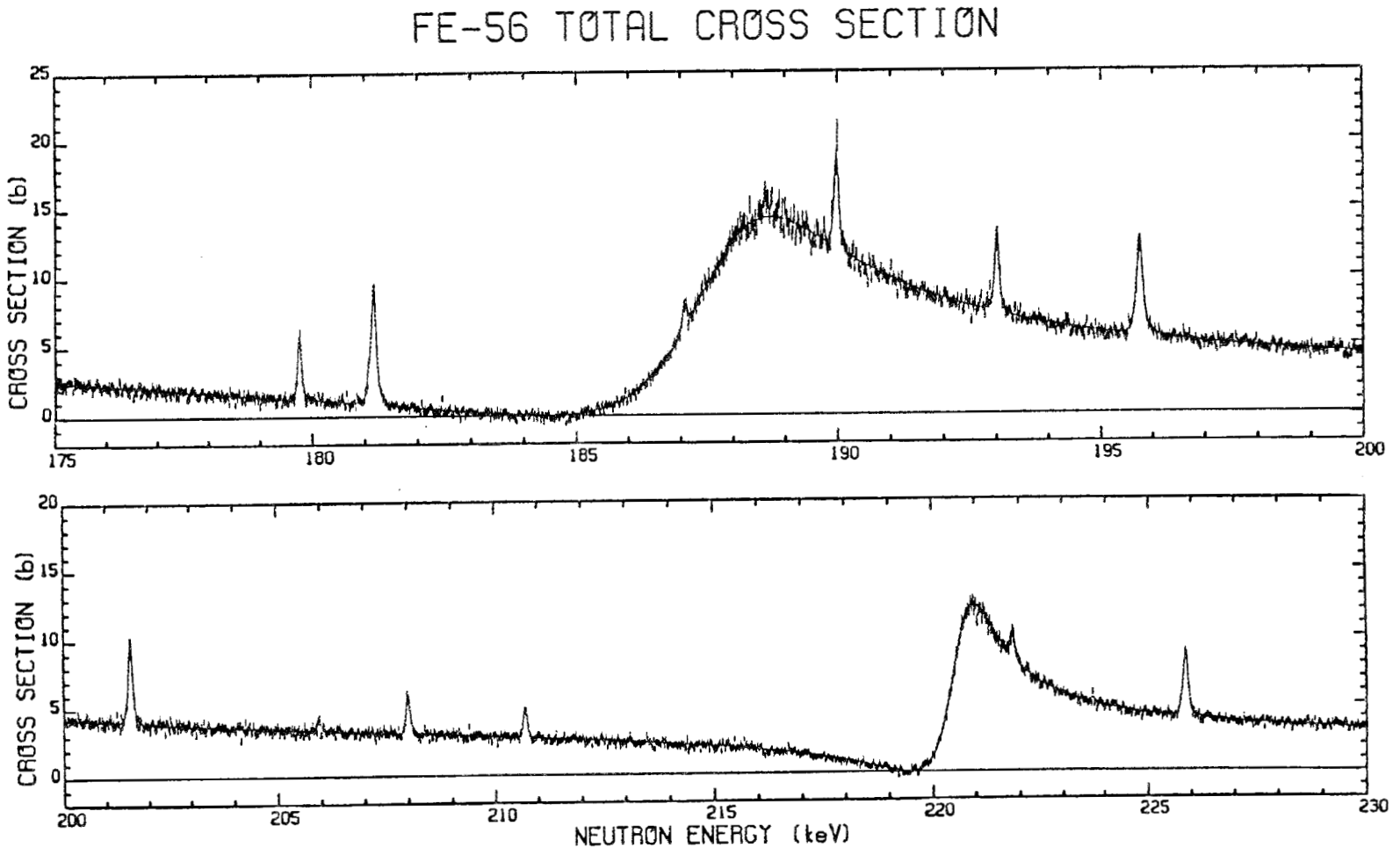

Fig. 7. Same as Fig. 6 except from 175 to 230 keV.

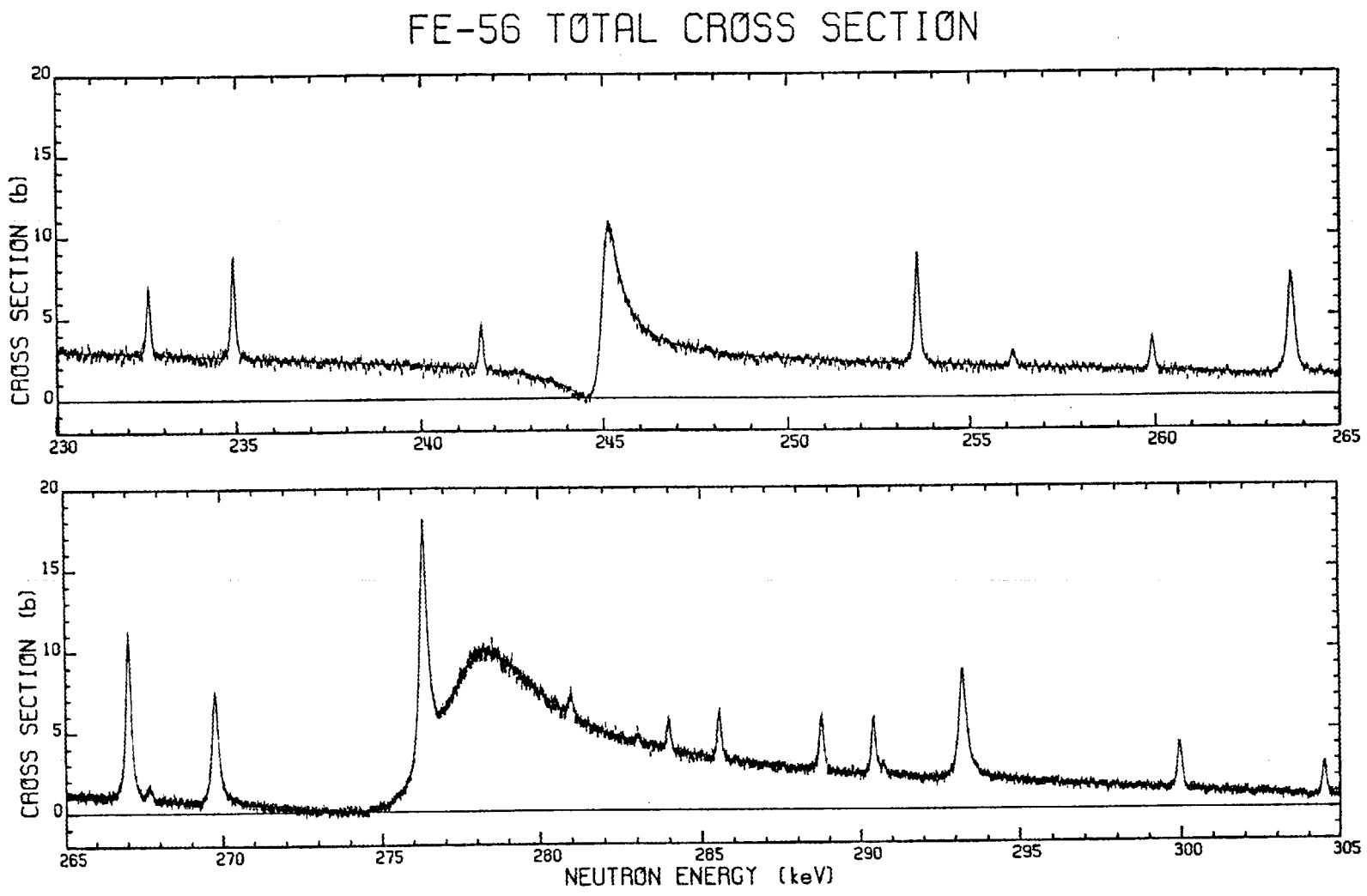

Fig. 8. Same as Fig. 6 except from 230 to 305 keV.

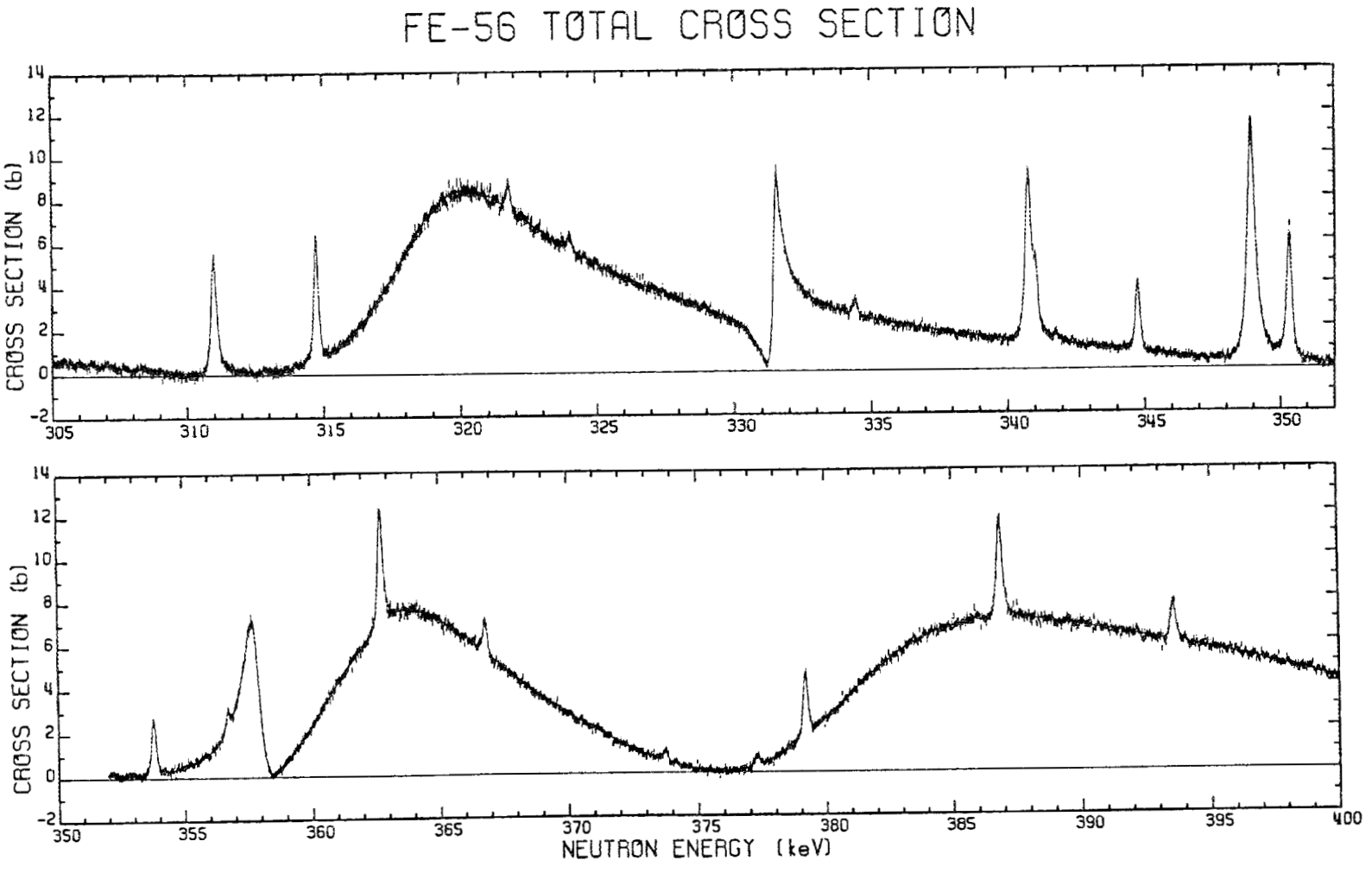

Fig. 9. Same as Fig. 6 except from 305 to 400 keV.

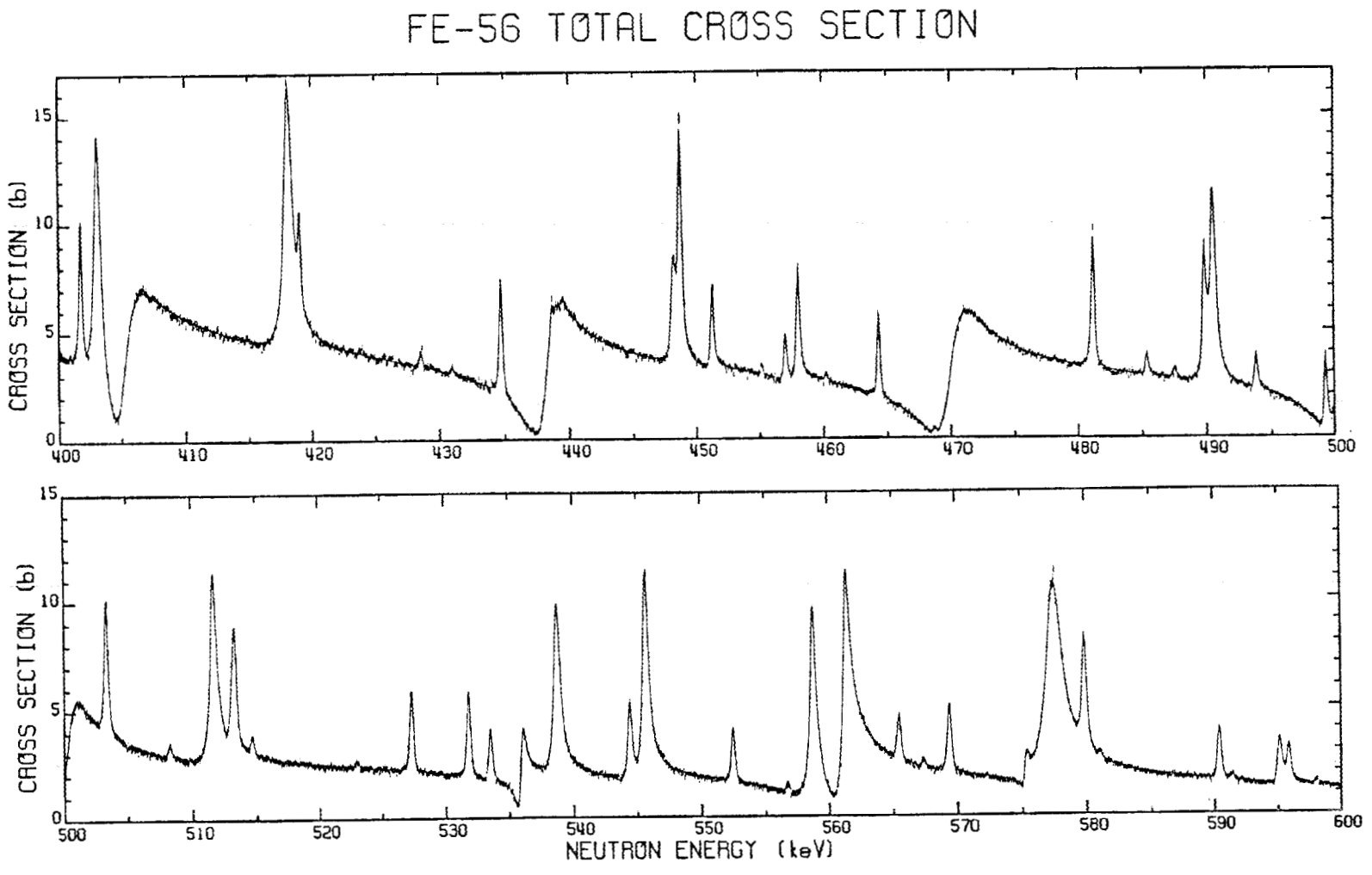

Fig. 10. Same as Fig. 6 except from 400 to 600 keV.

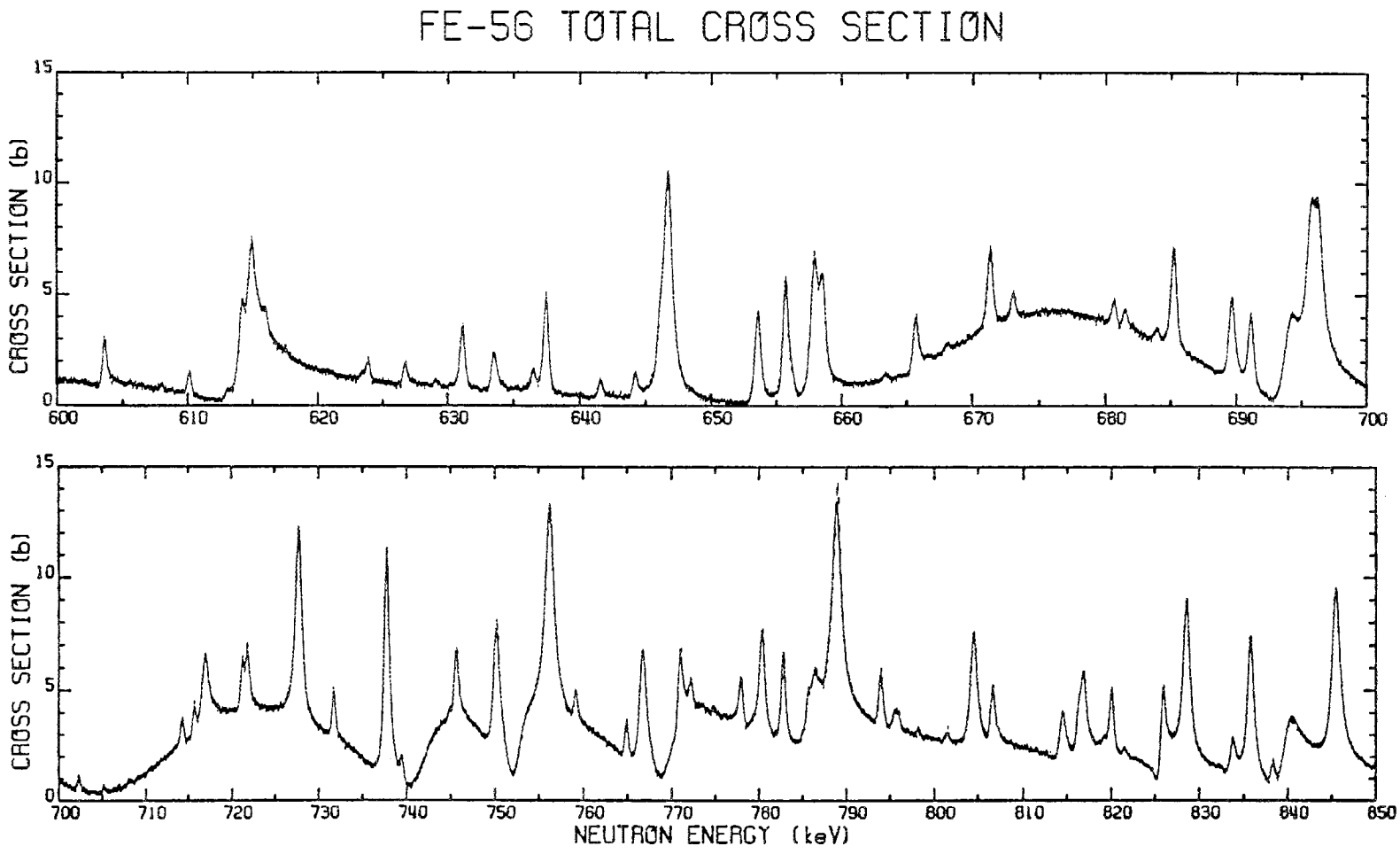

Fig. 11. Same as Fig. 6 except from 600 to 850 keV.

Table 4. Comparison of resonance energies and neutron widths, times the statistical weight g, for $\ell > 0$ resonances observed in our transmission data and in the 200-m Geel transmission data, between 40 and 240 keV. Uncertainties are given in parentheses. The notation is such that 10.4 (12) means 10.4 ± 1.2.

Present Work				Cornelis et al. (COR85)			
E_o (keV)	$g\Gamma_n$ (eV)[a]	ℓ^b	J^b	E_o (keV)	$g\Gamma_n$ (eV)[a]	ℓ^b	J^b
46.0535	10.28 (16)	1	1.5	46.089	10.4 (12)	$\ell > 0$	
52.1397	34.58 (26)	1	1.5	52.172	25.2 (6)	[1	1.5]
53.561	2.24 (10)	[1	0.5]				
59.2318	9.62 (16)	1	1.5	59.259	7.8 (6)	$\ell > 0$	
63.474	1.60 (6)	[1	1.5]				
72.988	0.84 (6)	[2	2.5]				
77.082	3.52 (12)	1	0.5				
80.8419	35.34 (33)	2	2.5	80.879	25.9 (4)	$\ell > 0$	
90.3379	44.0 (6)	1	[1.5]	90.374	34.5 (7)	$\ell > 0$	
92.708	3.60 (16)	2	[1.5]				
92.928	1.52 (22)	[1	1.5]				
96.194	1.84 (16)	[2	1.5]				
96.3457	14.6 (3)	1	[0.5]	96.385	12.6 (3)	$\ell > 0$	
96.630	4.32 (16)	2	[1.5]	96.655	7.0 (10)	$\ell > 0$	
102.698	55.8 (6)	1	1.5	102.74	44.8 (7)	[1	0.5]
103.087	1.28 (24)	[1	1.5]				
105.942	6.92 (24)	2	[1.5]				
112.719	13.2 (4)	2	1.5	112.75	11.0 (10)	$\ell > 0$	
122.801[c]	123.8 (14)	1	1.5	122.82	103.4 (11)	1	0.5
124.187[c]	10.2 (5)	1	0.5	124.20	5.0 (13)	$\ell > 0$	
125.175[c]	25.8 (8)	2	1.5	125.19	17.0 (7)	$\ell > 0$	
153.945	5.0 (5)	1	[0.5]				
161.778	13.4 (8)	2	[1.5]	161.84	10. (5)	$\ell > 0$	
169.127	43.2 (16)	2	1.5				
173.19	2.0	[1	0.5]				
173.688	77.6 (14)	1	1.5	173.69	62.1 (11)	$\ell > 0$	
179.766	33.8 (10)	1	1.5	179.79	17.8 (16)	$\ell > 0$	
181.08	6.4 (7)	[1	0.5]				
181.185	87.6 (15)	2	2.5	181.17	70.3 (11)	$\ell > 0$	
187.088	12.0 (8)	2	[1.5]				
189.97	24. (2)	[1	0.5]				
190.02	28. (4)	2	[1.5]	190.00	50.9 (11)	$\ell > 0$	
193.015	62.7 (21)	2	2.5	192.98	37.2 (8)	$\ell > 0$	
195.747	72.7 (14)	1	0.5	195.76	71.5 (13)	$\ell > 0$	

Table 4. Continued

Present Work				Cornelis et al. (COR85)			
E_o (keV)	$g\Gamma_n$ (eV)[a]	ℓ^b	J^b	E_o (keV)	$g\Gamma_n$ (eV)[a]	ℓ^b	J^b
201.581	65.6 (14)	2	1.5	201.56	48.4 (2)	$\ell > 0$	
205.95	4.2 (3)	2	[2.5]				
207.997	25.0 (10)	1	1.5	208.03	17. (4)	$\ell > 0$	
210.699	17.7 (9)	2	2.5	210.63	13. (3)	$\ell > 0$	
221.844	17.4 (12)	1	[1.5]				
223.69	2.6 (12)	[2	1.5]				
225.855	56.2 (12)	1	[0.5]	225.84	58. (10)	$\ell > 0$	
232.550	50.8 (12)	2	1.5	232.52	30. (10)	$\ell > 0$	
234.893	95.1 (15)	2	2.5	234.87	70. (5)	$\ell > 0$	

[a]Statistical uncertainties are given in parentheses.

[b]Square brackets are used to indicate that the assignment is uncertain.

[c]Spin and parity assignments are discussed in Sect. 3.2. Theoretical calculations are compared with the differential elastic scattering data in Fig. 12.

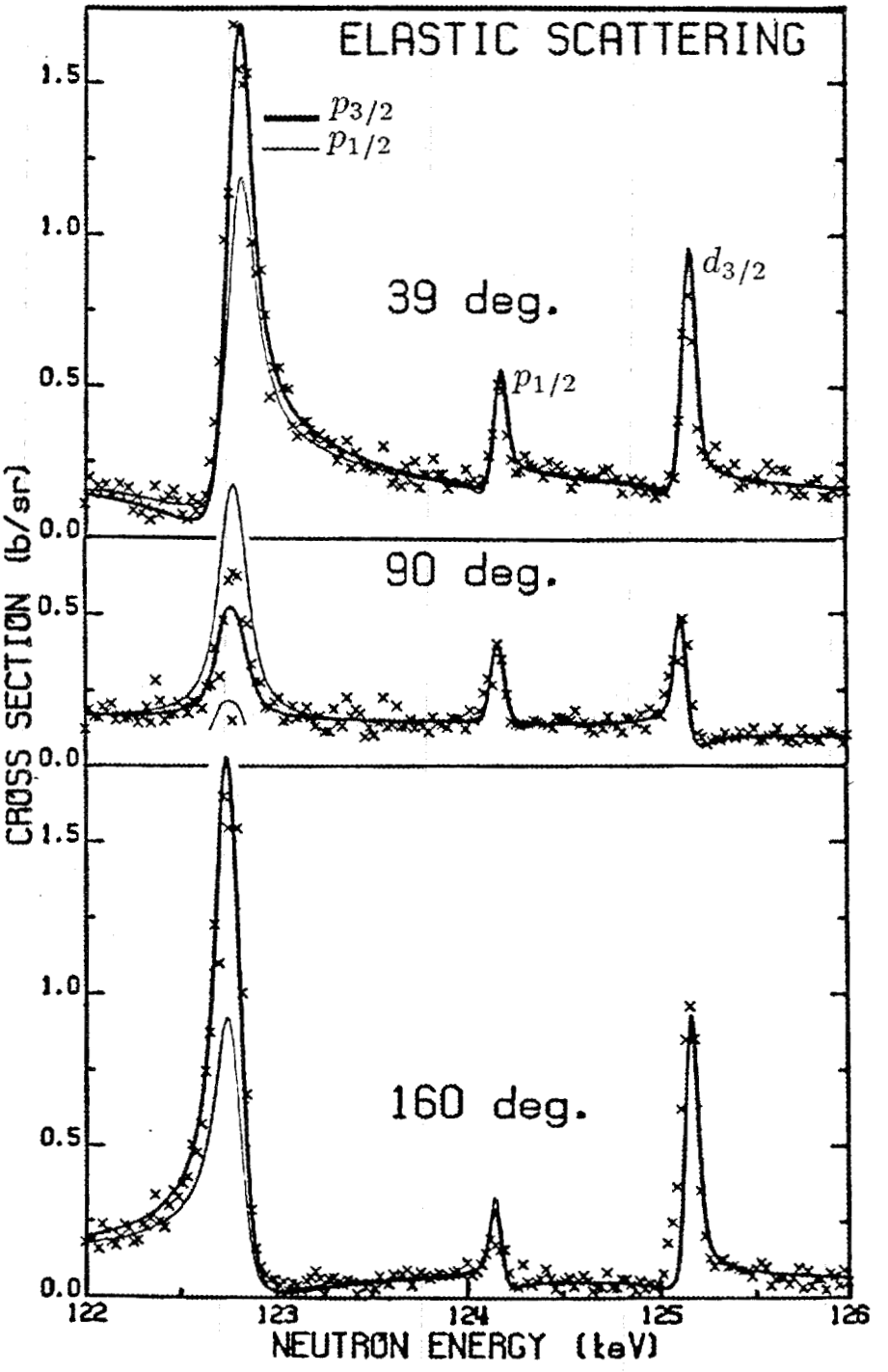

Fig. 12. Theoretical differential elastic-scattering cross sections calculated with the ℓ and J values assigned in this work (thick line) and with those assigned in Ref. COR85 (thin line) compared with data for three scattering angles. Transmission data are equally well fitted when the 122.8-keV resonance is either a $p_{1/2}$ or a $p_{3/2}$ resonance; however, the elastic-scattering data clearly favor the $p_{3/2}$ assignment.

Table 5. Comparison of resonance energies and neutron widths, times the statistical weight g, for $\ell > 0$ resonances observed in our transmission data and in Geel and Karlsruhe data, between 500 and 600 keV.

Present work				Cornelis et al. (COR83)				Cierjacks et al. (CIE78)			
E_o (keV)	$g\Gamma_n$ (eV)	ℓ^a	J^a	E_o (keV)	$g\Gamma_n$ (eV)	ℓ	J	E_o (keV)	$g\Gamma_n$ (eV)	ℓ	J
503.405	443.	2	2.5	503.23	452.	2	1.5	502.84	1200.	1	1.5
508.268	24.7	1	0.5	508.08	20.	$\ell > 0$		507.78	<120.		[1.5]
511.675	1024.	1	1.5	511.55	1028.	1	1.5	511.24	840.	1	1.5
513.201	[310.	1	[0.5]	513.16	400.	2	1.5	512.72	260.	1	0.5
513.385	157.	[3	2.5]								
514.705	41.6	2	[1.5]	514.59	40.	$\ell > 0$		514.16	<60.	$\ell > 0$	
523.042	13.0	[2	1.5]								
527.396	270.	2	2.5	527.24	266.	2	1.5	526.99	150.	1	0.5
531.855	296.	2	2.5	531.73	256.	2	1.5	531.45	320.	1	1.5
533.558	145.0	1	1.5	533.39	156.	1	0.5	533.17	120.	2	1.5
538.737	919.	1	1.5	538.61	800.	1	1.5	538.28	920.	2	1.5
543.98	[21.3	[1	0.5]								
544.413	263.6	1	1.5	544.30	236.	$\ell > 0$		544.02	190.	1	0.5
545.653	[926.	[2	2.5]	545.54	1038.	1	1.5	545.27	920.	2	1.5
545.773	268.	[0	0.5]								
				547.02	12.	$\ell > 0$					
552.500	183.0	2	2.5	552.33	166.	$\ell > 0$		552.06	200.	1	0.5
556.76	24.0	2	[1.5]					556.20	<60.	$\ell > 0$	
558.783	[449.	2	2.5								
558.854	854.	1	0.5	558.62	1018.	1	1.5	558.41	940.	1	1.5
561.394[b]	752.	1	1.5	561.41[b]	922.	2	1.5	561.01	400.	1	1.5
565.497	149.	2	[2.5]	565.29	100.	$\ell > 0$		565.02	120.	1	0.5
567.350	17.3	1	[0.5]	567.17	30.	$\ell > 0$					
569.399[b]	260.	2	2.5	569.30[b]	192.	2	1.5	568.94	300.	2	1.5
								571.35	<60.	$\ell > 0$	
								574.98	260.	1	0.5
577.419	2912.	1	1.5	577.27	2940.	1	1.5	576.79	1400.	2	1.5
								577.37	200.	1	0.5
579.878[b]	486.	2	2.5	579.79[b]	410.	2	1.5	579.12	340.	1	0.5
581.068	12.9	[1	0.5]								
								587.94	<70.	$\ell > 0$	
590.416[b]	205.	2	2.5	590.24[b]	220.	1	0.5	589.93	200.	1	0.5
591.424	16.4	[2	1.5]	591.30	15.	$\ell > 0$		590.95	<70.	$\ell > 0$	
595.136	186.	1	0.5	594.96	170.	1	0.5	594.72	150.	1	0.5
595.894	130.4	2	1.5	595.64	120.	$\ell > 0$		595.40	130.	0	0.5
598.024	12.4	[1	0.5]	597.80	8.	$\ell > 0$		598.74	<70.	$\ell > 0$	

[a] Square brackets are used to indicate that the assignment is uncertain.
[b] Spin and parity assignments are discussed in Sect. 3.2.

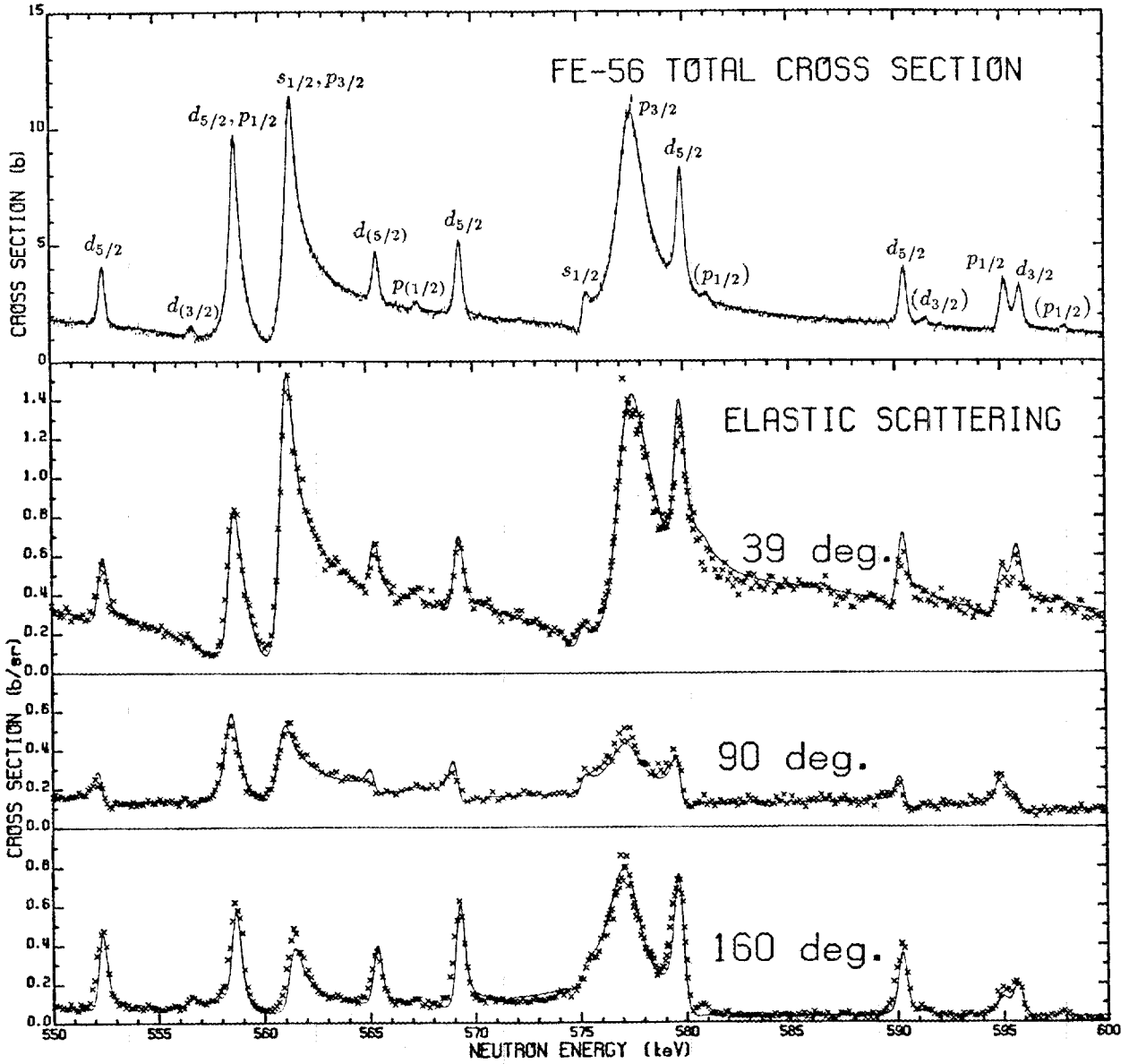

Fig. 13. In the upper plot the theoretical total cross section, calculated with parameters in Table 2, is compared with the data. Parentheses are used to indicate uncertain ℓ and J assignments. These assignments were made using the differential elastic-scattering data shown in the three lower plots.

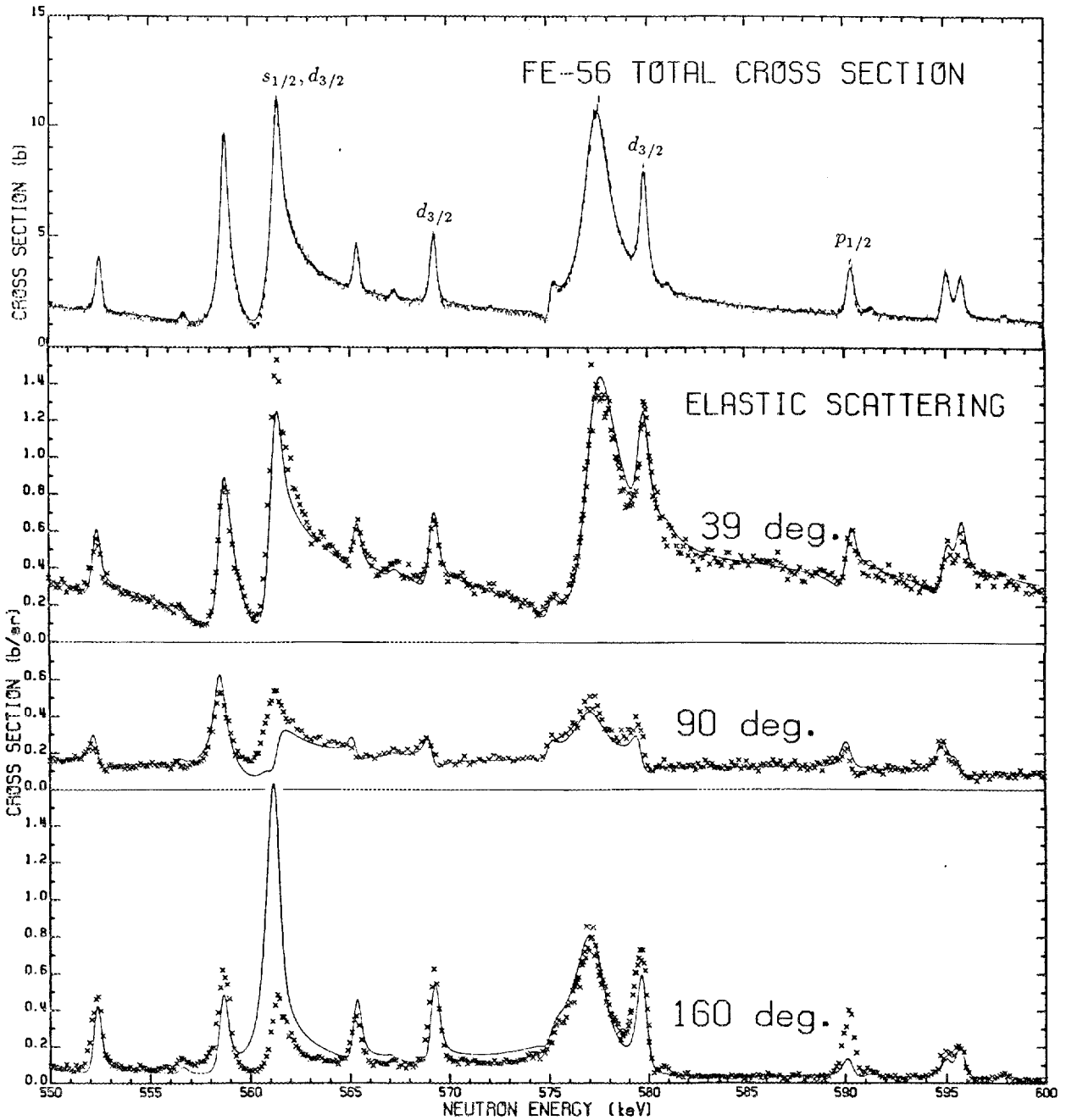

Fig. 14. This figure is the same as Fig. 13 except that the ℓ and J assignments of four $\ell > 0$ resonances were set to the values assigned in Ref. COR83 (see Table 5). The assignments for the other resonances, not specified here, were kept the same as in Fig. 13. The ORELA transmission data were fitted using this new set of assignments and the total cross section calculated with the resulting parameters is compared with the data in the upper plot. The theoretical differential elastic-scattering cross sections are compared with the data, at three different angles, in the lower part of the figure. The agreement with the differential elastic-scattering data is now clearly unsatisfactory, especially at 90° and 160° scattering angles, for three of the four resonances.

4. RESULTS

Results of the simultaneous analyses of the transmission and differential elastic-scattering data, described in Sect. 3, were combined with the results of the ^{56}Fe capture data analysis of Corvi et al. (COR84) which extends to 350 keV. The resonance parameters obtained from our analyses, the capture kernels from Ref. COR84 and the parameters of the 1.15-keV resonance from Ref. PER86 are given in Table 2. The parameters of the large resonances of the minor iron isotopes and of a small ^{55}Mn impurity present in the natural iron sample (used in obtaining the transmission data analyzed below 120 keV) are given in Table 3.

In Table 2 parameters for 302 resonances are reported in the 1- to 850.4-keV energy range and for 9 fictitious resonances given outside that energy range. The groups of resonances corresponding to each figure, Figs. 2 to 11, are separated by a blank line. The resonance number is in the first column. A star next to the resonance number indicates that the parameters of this resonance were among the 139 parameters that were adjusted in the last fit to the transmission data with the code SAMMY. The covariance matrix associated with these 139 adjusted parameters is available from the authors. The next four columns show the energies of the resonances, the neutron widths, the capture kernels from Ref. COR84 (except for 3 resonances as discussed below) and the radiation widths. Each parameter is followed by its uncertainty in parentheses.

The orbital angular momentum, ℓ, and the spin, J, for each resonance are given in columns 6 and 7. Square brackets indicate uncertain assignments. The numbers in the last column correspond to notes found at the end of the table. Brackets in columns 3 and 4 are used to indicate multiplets in transmission or capture data.

In Table 3 the energy parameters, the neutron widths, and the radiation widths of the resonances of the minor iron isotopes and of the ^{55}Mn impurity, present in the natural iron sample, are given in the first 3 columns. The orbital angular momentum and the spin for each resonance are in columns 4 and 5. The isotopes are identified in column 6 and notes are given in the last column.

Note 1, in both Tables 2 and 3, is used to indicate fictitious resonances outside the range of our analysis. These resonances are an integral part of our parameter set since they simulate the smooth cross section generated by all the resonances external to the energy region analyzed, but whose tails extend into the energy region of interest.

The resonance at 1.15 keV was the subject of a special NEANDC task force. The parameters given in Table 2 for this resonance result from the work of this task force. See Ref. PER86 for details.

4.1 CAPTURE KERNELS AND RADIATION WIDTHS

The main characteristics of the Geel capture experiment are given in Table 1. Experimental details and data reduction techniques are given in Refs. COR82 and COR84. We used the capture kernels from the most recent analysis of these data, which were normalized to the capture area in the 1.15-keV resonance as determined from the transmission measurements (COR84). In this experiment an improper weighting function was used (COR88) and to normalize the data to the capture

area of the 1.15-keV resonance does not necessarily give the exact correction for this improper weighting function. Therefore, these data are being reanalyzed with the appropriate weighting function (COR89).

For resonances with large neutron widths the capture kernels are essentially given by the product of the radiation widths, Γ_γ, and the weighting factors, g. Therefore, unless we use different spin and parity assignments, our radiation widths are the same as in Ref. COR84. For most other well-defined resonances the radiation widths could be slightly different, even when the same assignment was used, due to small differences in the values of the neutron widths.

Twenty-six of the resonances reported in Table 2, below 350 keV, were seen in the capture data but were undetected in our transmission or differential elastic-scattering data due to their very small neutron widths. The energy parameters of these 26 resonances were slightly readjusted from the values given in Ref. COR84 to be consistent with our energy scale. These resonances are indicated by note 3. The capture kernels for these resonances are well defined by the capture data analysis but the radiation widths, and the spin and parity assignments, are arbitrary provided the corresponding neutron widths are sufficiently small that no resonance dips are observed in the transmission data for these resonances. The radiation widths reported in Table 2 for these resonances are the average values of 0.45 eV or 0.75 eV determined from the isolated and well-defined p- and d-wave resonances respectively, as explained in Sect. 6.5.

As previously mentioned, for 3 narrow resonances (Nos. 9, 11 and 20) the capture kernels are not from Ref. COR84 but were obtained from our transmission data analysis (Note 4 in Table 2). Both neutron and radiation widths were adjusted to fit the data. For these resonances the neutron widths are about 10 times smaller than the radiation widths so the capture kernels are well determined by the values of Γ_n. The capture kernels values obtained from our transmission data are in good agreement with those obtained by Corvi et al. from their capture experiment.

Five resonances which were analyzed as singlets in the capture data were found to be doublets in transmission. In only one instance were the two resonances fully resolved (Nos. 100 and 101). Note 5 in Table 2, which is always found on two consecutive lines, indicates that the capture kernels assigned to the members of the doublet add up to the value found in the capture data analysis. The division was not entirely arbitrary in the sense that we assigned a larger portion of the kernel to a d-wave than to a p-wave level so that the radiation widths, whenever possible, are close to the average values of Γ_γ.

An example is the doublet around 180 keV (resonances No. 54 and 55). Around that energy only one resonance was identified by Corvi et al., for which a capture kernel of 2.86 ± 0.25 eV was given. If 0.50 eV is assigned to the first resonance and 2.36 eV to the second one, the radiations widths are 0.54 ± 0.25 eV for the $p_{1/2}$ resonance and 0.81 ± 0.08 eV for the $d_{5/2}$ resonance, which are in good agreement with the average radiation widths. In view of the weak criteria used to divide the capture kernel we assign to each part of the kernel the same uncertainty of 0.25 eV which was assigned to the total value.

4.2 DISCUSSION OF THE UNCERTAINTIES

The uncertainties given in Table 2 for the energy parameters and the neutron widths are from the output of the code SAMMY except for the four narrow resonances (Nos. 73, 88, 108 and 110) for which the neutron widths were adjusted by trial and error and a 50% uncertainty assigned. In this analysis all uncertainties calculated by the code SAMMY are statistical uncertainties and do not include estimates of systematic uncertainties.

As mentioned earlier, a star (*) at the beginning of a line indicates that the energy and the neutron width of this resonance were adjusted in the last run of SAMMY. The full covariance matrix for these adjusted parameters is available from the authors. The uncertainties reported on the energy parameters and neutron widths of the other resonances were obtained with the code SAMMY during preliminary analyses.

The systematic uncertainty of $\approx$0.01% on the absolute energy scale is not included in the standard deviation associated with the energy prameters given in the first column of Table 2.

The uncertainties on the radiation widths given in Table 2 were propagated from the uncorrelated uncertainties on the capture kernels, given in Ref. COR84, and the uncertainties on the neutron widths.

Background and normalization parameters were adjusted in the fitting process. Residual backgrounds were found to be negligible: $(-1.8\pm0.2)\times10^{-4}$ for the natural iron transmission data and $(-2.3\pm0.1)\times10^{-3}$ for the ^{56}Fe transmission data. While renormalization of the natural iron data was not required (1.0012 ± 0.0008), in the case of the ^{56}Fe data a renormalization larger than expected (1.0225 ± 0.0005) was necessary and is not presently understood.

4.3 SPIN AND PARITY ASSIGNMENTS

In the transmission data analysis from 5 to 850.4 keV, 32 resonances show the characteristic potential interference pattern of s-waves and were assigned as s-wave resonances. One assigned s-wave resonance, at 545.77 keV, which is part of a doublet, does not clearly show this characteristic potential interference pattern and therefore has an uncertain s-wave assignment. This leaves 242 resonances with an angular orbital momentum larger than zero.

When the differential elastic-scattering data are compared to the theoretical calculations, as explained in Sect. 3.2, spin and parity assignments for many of the 242 $\ell > 0$ resonances can be made. The orbital angular momentum L can definitely be assigned to 184 resonances, i.e., to 76% of the $\ell > 0$ resonances analyzed in the transmission data: 85 are p-wave and 99 are d-wave resonances. The 58 resonances which cannot be given a definite ℓ-assignment are either narrow resonances or part of a multiplet. Resonances with a neutron width too small to produce unambiguous characteristic patterns in differential scattering cross-section plots (and the resonances seen only in the capture data) are given a $p_{1/2}$ assignment by default, except if, below 350 keV, a higher spin is required to accommodate a particularly large capture area.

The spin J of 81% of the 85 p-wave resonances can be assigned with some degree of confidence (23 resonances have a spin of 1/2 and 46 a spin of 3/2). A smaller proportion (63%) of the 99 d-wave resonances could be given a definite spin assignment (25 have a spin of 3/2 and 37 a spin of 5/2). It is interesting to note that for each orbital angular momentum the number of resonances with a definite J-assignment is in agreement with the $(2J+1)$ rule. However the number of p- or d-wave levels, with definite J assignments, is much less than predicted by the $(2J+1)$ rule, based on the assigned 33 $\ell = 0$ resonances. This was expected since the total number of $\ell > 0$ resonances with a definite spin and parity assignment is only 54% of the $\ell > 0$ resonances analyzed in transmission data. In addition, in the 2 to 350-keV energy interval alone 26 narrow resonances, of which none of the spin and parity assignments could be certain, were observed in the capture data and not in the transmission data. This leads us to conclude that many more narrow resonances were not seen in our transmission data above 350 keV where no capture data were analyzed.

Considering all the $\ell > 0$ resonances given in Table 2 we find 140 assigned p-wave resonances and only 128 d-wave resonances whereas according to the $(2J+1)$ rule, starting from 33 s-wave resonances we should have 99 p-wave and 165 d-wave levels. The larger than predicted fraction of p-wave resonances assigned in Table 2 is a consequence of the fact that many narrow resonances were assigned as p-wave by default.

4.4 THERMAL CROSS SECTIONS

The thermal capture cross section reported by Mughabghab et al. (MUG81) for ^{56}Fe is 2.59 ± 0.14 b. The first s-wave resonance at 27.8 keV contributes only 0.04 b to the thermal capture cross section and the other observed s-wave resonances contribute less than 0.01 b. The difference of 2.54 b should be attributed to bound levels. The radiation widths of the three s-wave bound levels were chosen so that they generate the missing 2.54 b and are consistent with the average value of 0.92 eV, with a standard deviation of 0.41 eV, found for unbound levels (see Sect. 6.5).

The final ^{56}Fe resonance parameters of Table 2 also correctly predict the thermal total cross section as recommended in Ref. MUG81 (see Sect. 3.1).

5. COMPARISON WITH RESULTS FROM PREVIOUS ANALYSES

The resonance parameters from our analysis will first be compared with those obtained at Geel from two transmission data analyses, performed by Cornelis from Antwerp and Mewissen and Poortmans from Mol, which cover the energy range from 40 to 850 keV (COR83 and COR85). We will also compare our parameters with earlier ORELA results that had been extensively used in the ENDF/B-V evaluation (PER80): a 200-m transmission data analysis up to 500 keV (PAN75) and an analysis of 40-m differential elastic-scattering data up to 400 keV (PER77). Finally we will compare some of our s-wave resonance parameters and spin and parity assignments with those given in the total and differential elastic-scattering data analysis performed by Cierjacks and Schouky (CIE78) at Karlsruhe. Their analysis overlaps the present work only in the 450- to 850-keV energy region.

5.1 COMPARISON WITH GEEL RESULTS

The Geel transmission data are the results of two experiments. The first experiment was performed with a 400-m flight path and a neutron burst width of 4.5 ns. It covered the energy range from 240 keV to 19 MeV. Details of the experimental setup and of the data analysis from 240 to 850 keV are given in Ref. COR83. Characteristics of the second experiment and results of the analysis, which covers the energy range from 40 to 240 keV, are not yet published and were the subject of a private communication (COR85). This experiment was performed with a 200-m flight path and a burst width of 14.5 ns. These two sets of data were analyzed with the R-matrix multi-level code MULTI using a single channel radius of 5.0 f.

In Table 6 our s-wave resonance parameters are compared with those from the Geel analyses. Below 240 keV their energy parameters are systematically higher than ours by as much as 0.04% but generally lower above 240 keV by up to 0.14% for the large s-wave resonance at 665.65 keV. As shown in the last column of Table 6, the neutron widths are in good agreement below 240 keV (less than 4% discrepancy) but some large discrepancies, between 20% and 40%, are observed for five of the 23 s-wave resonances reported in both analyses above 240 keV.

In our analysis the transmission data for the resonance around 545.7 keV is well fitted as a doublet composed of an s-wave resonance and a d-wave resonance (see Fig. 10), but this doublet fails to reproduce the differential elastic-scattering data. Therefore, the assignments for both resonances are uncertain. In the Cornelis et al. analysis this resonance is fitted as a single large resonance with a definite $p_{3/2}$ assignment (see Table 5) but the minimum in their data around 545 keV is not well fitted. From our differential elastic scattering data this resonance is definitely not a single $p_{3/2}$ resonance.

The s-wave resonance reported by Cornelis et al. at 737.11 keV is, in our analysis, a $p_{3/2}$ resonance as required by the elastic-scattering data. In the 4 keV energy interval from 785 to 789 keV, a seven-resonance multiplet which includes an s-wave resonance at 787.27 keV was required to describe the data. Cornelis et al. do not include a s-wave resonance in their analysis of this energy interval and fail to reproduce the two minima in the data around 782 and 785 keV.

Table 6. Parameters for s-wave resonances from Table 2 compared with results of Geel analyses. Uncertainties are given in parentheses. The notation is such that 1.409 (1) means 1.409 ± 0.001.

Present Work		Cornelis et al. (COR85 and COR83)		
E_o (keV)	Γ_n (keV)[a]	E_o (keV)	Γ_n (keV)[b]	$\frac{\Gamma_n \text{ (ORNL)}}{\Gamma_n \text{ (Geel)}}$
27.791	1.409 (1)			
74.029	0.6115 (8)	74.055	0.6317 (28)	0.97
83.628	1.215 (1)	83.665	1.243 (4)	0.98
129.861	0.588 (3)	129.89	0.583 (3)	1.01
140.479	2.735 (6)	140.52	2.691 (7)	1.02
169.275	0.962 (3)	169.26	0.968 (4)	0.99
187.737	3.620 (7)	187.79	3.525 (9)	1.03
220.586	1.267 (4)	220.58	1.214 (5)	1.04
244.991	0.487 (3)	244.92	0.435 (60)	1.12
277.206	3.650 (9)	277.15	3.55 (30)	1.03
317.909	7.118 (12)	318.20	7.00 (70)	1.02
331.447	0.328 (3)	331.38	0.30 (30)	1.09
357.263	2.205 (11)	357.32	1.80 (18)	1.23
361.078	7.775 (16)	361.33	8.60 (80)	0.90
381.360	12.33 (2)	381.79	12.6 (12)	0.98
405.408	2.329 (9)	405.37	2.63 (26)	0.89
438.296	1.918 (8)	438.20	1.52 (15)	1.26
469.934	2.566 (9)	469.70	3.09 (30)	0.83
500.194	1.726 (8)	500.15	1.58 (16)	1.09
535.921	0.256 (4)	535.77	0.259 (26)	0.99
545.773[c]	0.268 (4)			
561.015	1.500 (10)	561.22	1.36 (20)	1.10
575.212	0.087 (3)	575.08	0.069 (7)	1.26
613.936	2.642 (14)	613.70	2.49 (50)	1.06
665.655	27.96 (3)	664.74	28.6 (25)	0.98
693.506	1.727 (19)	693.30	1.79 (18)	0.96
710.659	20.94 (7)	709.91	21.0 (20)	1.00
		737.11	0.48 (6)	
741.680	5.719 (27)	741.58	5.72 (60)	1.00
752.706	2.462 (24)	752.40	1.74 (18)	1.41
769.537	3.957 (23)	769.06	4.70 (50)	0.84
787.27	1.384 (16)			
825.678	0.263 (10)	825.41	0.42 (6)	0.63
839.308	2.411 (25)	838.99	2.20 (22)	1.10

[a]Statistical uncertainties are given in parentheses.

[b]Above 240 keV, uncertainties seem to include a systematic contribution.

[c]Uncertain s-wave assignment

Comparison of some of the parameters for the non s-wave resonances is shown in Tables 4 and 5 given earlier in Sect. 3.2 (see pages 31 and 34). The $\ell > 0$ resonances from the Geel 200-m data analysis are compared with our $\ell > 0$ resonances between 40 and 240 keV in Table 4. In this energy interval we find 16 more isolated $\ell > 0$ resonances than Cornelis et al. (39 versus 23) and we also find it necessary to replace two of their resonances by doublets in order to obtain a good fit to our transmission data. Below 120 keV where our transmission measurements were done with a natural iron sample, it is possible that the nine resonances seen in our data, but not reported by Cornelis et al., are from minor iron isotopes. However, all of these resonances were also clearly observed in the ^{56}Fe capture data analyzed by Corvi et al., thus confirming that they are ^{56}Fe resonances. For most of the resonances our values of $g\Gamma_n$ are significantly larger than in the Geel analysis. The spin and parity assignments in this energy region were discussed earlier in Sect. 3.2.

Roughly 20% more $\ell > 0$ resonances were observed in our 200-m transmission data between 240 and 850 keV than in the Geel 400-m data. A sample of resonance parameters in a 100-keV region, from 500 and 600 keV, is given in Table 5. Three of the six resonances reported in our analysis, but not in the Geel analysis, are part of doublets. However, the three small isolated resonances at 523.02, 556.76 and 581.07 keV, even though clearly seen in our data (see Fig. 10), were not reported by Cornelis et al. Comparison of the J^π assignments is meaningful for resonances with unambiguous assignments in both analyses. This is the case for 72 $\ell > 0$ resonances between 240 and 850 keV. Among those 72 assignments we agree with 45 of the Geel assignments and disagree with 27. The J^π assignments for the resonances in the 550- to 600-keV region were discussed in detail in Sect. 3.2 where it was shown that Geel assignments that differ from ours are inconsistent with our differential elastic-scattering data.

5.2 COMPARISON WITH PREVIOUS ORELA RESULTS

5.2.1 Transmission

A natural iron transmission experiment previously performed at ORELA (PAN75) also used the 200-m flight path. The data were analyzed from 20 to 500 keV with an R-matrix multi-level code for the s-wave resonances and interfering $\ell > 0$ resonances, and with a Harvey-Atta area analysis code for the $\ell > 0$ non-interfering resonances.

Our s-wave resonance parameters are compared with those of Pandey et al. in Table 7. In general their energy parameters are lower than ours and their neutron widths are systematically larger with the exception of four resonances. For the resonances around 405 and 438 keV the neutron widths reported by Pandey et al. are more than twice as large as the values obtained in our analysis. Above 350 keV, where there is strong interference between large s-wave resonances, their fit to the transmission data is very poor.

Pandey et al. reported 80 $\ell > 0$ resonances in the 20 to 500 keV energy range whereas, in that same energy range, we analyzed 126 $\ell > 0$ resonances.

Table 7. Parameters for s-wave resonances from Table 2 compared with earlier results. Uncertainties are given in parentheses. The notation is such that 1.409 (1) means 1.409 ± 0.001.

Present work		Pandey et al. (PAN75)		Cierjacks et al. (CIE78)	
E_o (keV)	Γ_n (keV)[a]	E_o (keV)	Γ_n (keV)	E_o (keV)	Γ_n (keV)
27.791	1.409 (1)	27.66	1.50 (5)		
74.029	0.6115 (8)	73.98	0.53 (2)		
83.628	1.215 (1)	83.65	1.30 (5)		
129.861	0.588 (3)	129.8	0.60 (5)		
140.479	2.735 (6)	140.4	2.80 (5)		
169.275	0.962 (3)	169.2	1.0 (1)		
187.737	3.620 (7)	187.6	3.7 (1)		
220.586	1.267 (4)	220.5	0.99 (5)		
244.991	0.487 (3)	245.0	0.59 (2)		
277.206	3.650 (9)	276.6	4.3 (1)		
317.909	7.118 (12)	317.0	8.8 (5)		
331.447	0.328 (3)	331.2	0.32 (5)		
357.263	2.205 (11)	356.9	3.60 (30)		
361.078	7.775 (16)	362.0	6.7 (5)		
381.360	12.33 (2)	380.9	13.8 (14)		
405.408	2.329 (9)	403.5	7.7 (7)		
438.296	1.918 (8)	437.0	4.7 (4)		
469.934	2.566 (9)	469.2	3.2 (3)	469.46	1.76
500.194	1.726 (8)			499.96	1.12
535.921	0.256 (4)			535.52	0.18
545.773[b]	0.268 (4)				
561.015	1.500 (10)			560.51	1.96
575.212	0.087 (3)			575.50	0.55
				595.40[c]	0.13
				602.87[c]	0.15
				609.55[b,c]	0.10
613.936	2.642 (14)			613.38	2.47
665.655	27.96 (3)			665.36	24.3
693.506	1.727 (19)			692.84	1.94
710.659	20.94 (7)			716.4	27.8
741.680	5.719 (27)			741.62	8.9
752.706	2.462 (24)			752.61	9.6
769.537	3.957 (23)			769.30	6.66
787.27	1.384 (16)			784.59	1.42
				818.15[d]	0.90
825.678	0.263 (10)			824.77	0.35
839.308	2.411 (25)			839.86	1.90

[a]Statistical uncertainties are given in parentheses.
[b]Uncertain s-wave assignment.
[c]Resonance identified as a $\ell > 0$ resonance in the present work.
[d]Resonance identified as a multiplet of $\ell > 0$ resonances in the present work.

5.2.2 Differential Elastic Scattering

Elastic-scattering angular distributions from natural iron were measured from 20 to 500 keV by W. E. Kinney and F. G. Perey (KIN77) using a 40-m flight path. The data, which were reported as five Legendre coefficients as a function of energy, were analyzed between 40 and 400 keV using an R-function formalism (PER77). The spins and parities of 60 $\ell > 0$ resonances were assigned, of which 44 were confirmed by the present work but 15 were found to be different due likely in large part to higher resolution of the new data. A resonance at 182.25 keV, reported by Pandey et al. and also by Kinney and Perey, was not seen in our new data.

5.3 COMPARISON WITH KARLSRUHE RESULTS

Measurements of transmission and differential elastic-scattering cross sections for natural iron at ten scattering angles were reported between 450 keV and 3 MeV by Cierjacks and Schouky (CIE78). These data were analyzed up to 900 keV. Spins and parities for 117 resonances were assigned and then used by them in fitting their transmission data.

The s-wave resonance parameters from the present analysis and those of Cierjacks and Schouky are compared in Table 7 in the region from 450 to 850 keV, where the 2 analyses overlap. Four resonances identified as s-wave resonances in Ref. CIE78 are definitely $\ell > 0$, or multiplets of $\ell > 0$ resonances, in the present work. The resonance we report at 545.77 keV, which has an uncertain s-wave assignment, is not seen in the Karlsruhe data. Their energy parameters are lower than ours for 11 of the 15 s-wave resonances observed in both data sets, however the large resonance around 710 keV is almost 6 keV higher in energy in their analysis than in the present work. Eleven of the 15 neutron widths differ by more than 25% from our values and the neutron widths of the resonances at 575 and 752 keV are, respectively, six and four times larger than the values we obtained in our analysis. The fit to their transmission data is not shown; therefore, we are unable to compare their data and their fit with ours.

From 450 to 850 keV the Karlsruhe analysis specifies J^π assignments for 84 $\ell > 0$ resonances but above 770 keV we are unable to match their $\ell > 0$ resonances with ours. In the 450- to 770-keV energy interval where Cierjacks and Schouky claim to determine the J^π of 70 $\ell > 0$ resonances, 56 of them unambiguously, we agree with only 14 of their assignments and definitely disagree with 33. In Table 5 we compare parameters of the $\ell > 0$ resonances obtained in their analysis with our parameters, in a 100-keV region from 500 to 600 keV. In this small region we agree with only four of their assignments and definitely disagree with 12. Few details are available concerning the Karlsruhe data and analysis; therefore, reasons for these large discrepancies cannot be determined.

6. DISCUSSION AND EXTRACTION OF AVERAGE PARAMETERS

6.1 REDUCED NEUTRON WIDTH DISTRIBUTION

6.1.1 $\ell = 0$ Resonances

The distribution of the normalized reduced neutron widths of the 33 s-wave resonances observed in the transmission data analysis from 5 to 850 keV is represented by the histogram in Fig. 15a. Such data are usually assumed to follow a Porter-Thomas distribution (POR56).

The reduced neutron width at 1 eV for a s-wave resonance is given by

$$\Gamma_n^0 = \Gamma_n \sqrt{1 \text{ ev } / E_n} \ ,$$

where E_n is the neutron energy in eV.

The Porter-Thomas density function is:

$$P(x) = 2(\pi x)^{-1/2} \, e^{-x/2} \ ,$$

where $x = \Gamma_n^0 / < \Gamma_n^0 >$ and $< \Gamma_n^0 >$ is the average reduced neutron width.

The smooth curve in Fig. 15a is the Porter-Thomas density function normalized to give 28 levels under the curve above 0.1, equal to the observed number of levels above that value of $\Gamma_n^0 / < \Gamma_n^0 >$ where we assume that no s-wave resonance was missed. The total number of levels under the Porter-Thomas distribution curve when such a normalization factor is used is 37.3 levels. Since only 33 s-wave resonances were observed we conclude that up to four narrow s-wave resonances could have been missed.

Given the small number of observed levels it is difficult to ascertain if the reduced level widths follow a Porter-Thomas distribution. However, as a further test the average value of $(\Gamma_n^0 / < \Gamma_n^0 >)^2$ was calculated and found to be equal to 2.6 ± 1.2 which is consistent with the value of 3 obtained for a Porter-Thomas distribution.

The average reduced neutron width, $< \Gamma_n^0 >$, is equal to 5.9 eV with an uncertainty of 1.3 eV due to the finite sample of 33 levels.

6.1.2 $\ell > 0$ Resonances

As noted previously in Sect. 4.3, 140 resonances in Table 2 were given a p-wave assignment whereas only 128 were assigned as d-waves. Since many narrow resonances were given a p-wave assignment by default we suspect that too many resonances were assigned as p-wave and that most of those mistakenly assigned are narrow resonances. However in the case of the 29 narrow resonances with uncertain d-wave assignments, these assignments were chosen as most probable on the basis of the elastic-scattering data or because of large capture areas; this leads to an underestimation of d-wave levels.

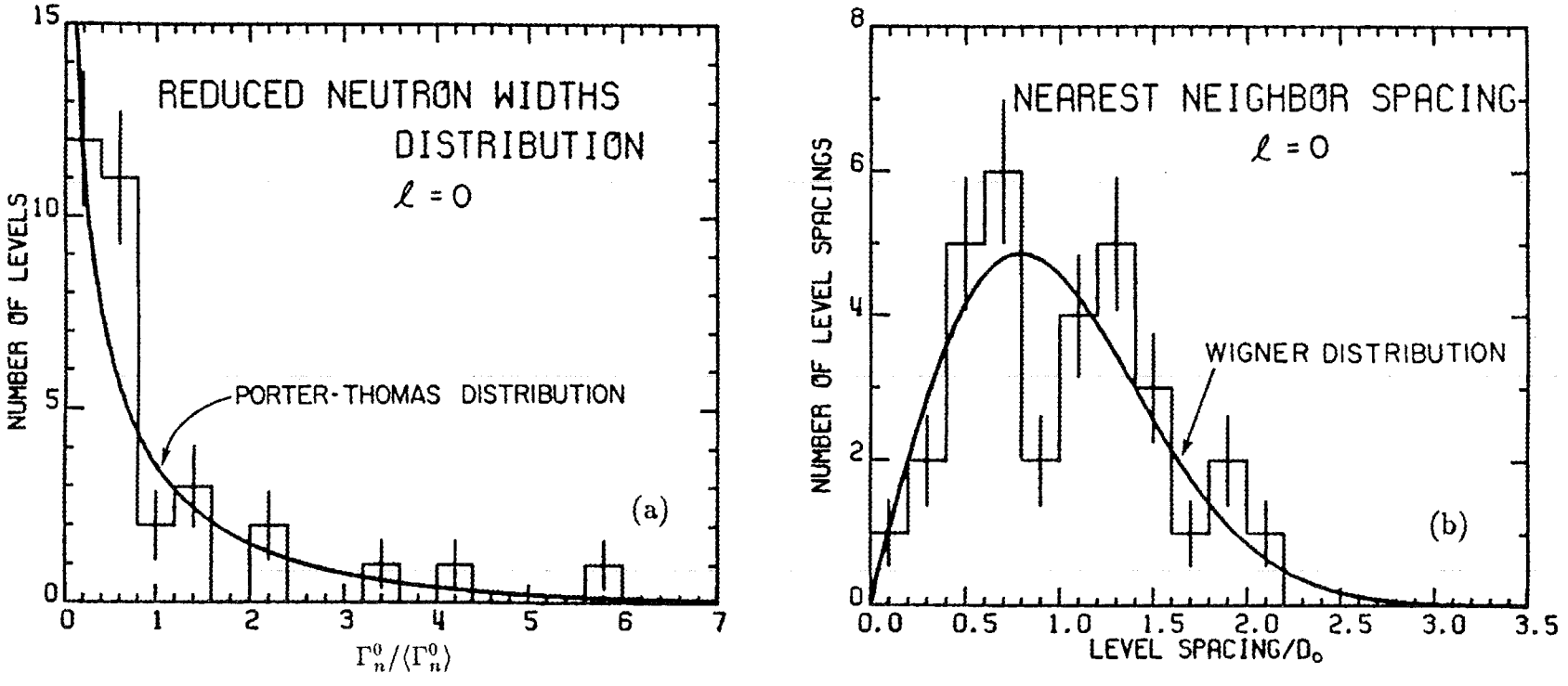

Fig. 15. (a) Distribution of normalized reduced neutron widths for the 33 observed s-wave resonances in Table 2. The smooth curve is the Porter-Thomas distribution normalized to the area under the histogram corresponding to values of $\Gamma_n^o/<\Gamma_n^o>$ larger than 0.1. **(b) Distribution of nearest level spacings for the 33 observed s-wave resonances.** The smooth curve is the Wigner distribution normalized to the area under the histogram.

Comparison of the reduced neutron width distribution for all the assigned p- or d-wave levels with a Porter-Thomas distribution provides information on how much we over- or underestimated the number of levels.

The reduced neutron widths at 1 eV for the p- and d-wave levels are given by:

$$\Gamma_n^1 = \Gamma_n\sqrt{1 \text{ eV } / E_n}[1 + (1/k^2R^2)] \quad \text{for } \ell = 1$$

$$\text{and } \Gamma_n^2 = \Gamma_n\sqrt{1 \text{ eV } / E_n}[1 + (3/k^2R^2) + (9/k^4R^4)] \quad \text{for } \ell = 2$$

where E_n is the neutron energy in eV, k is the wave number and R the channel radius.

When the normalized distribution for the 140 assigned p-wave levels, calculated with an average reduced neutron width of 0.53 eV, was compared to a Porter-Thomas distribution normalized to the number of p-wave levels corresponding to values of $\Gamma_n^1 / < \Gamma_n^1 >$ larger than 0.2, we arrive at an overestimation of at least 15 levels. Assuming that these 15 levels are narrow resonances, having values of $\Gamma_n^1 / < \Gamma_n^1 >$ smaller than 0.2, we can evaluate a more realistic average reduced width and generate a new histogram for the distribution of the 140 p-wave reduced widths normalized to this new average value. This histogram was again compared to a Porter-Thomas distribution to obtain a better estimate of the expected number of p-wave levels. Through such successive approximations we came to the conclusion that we had assigned approximately 21 too many narrow levels as p-wave. The new average reduced width calculated with 119 p-wave levels is 0.61 eV.

Using successive approximations for the d-wave levels, as described above for the p-wave levels, we determined that 20 d-wave levels could have been missed. That the number of possibly missed d-wave levels is close to the number of p-wave levels found in excess is purely coincidental. However, the fact that they are so close indicates that the distribution of the reduced widths for the $\ell = 1$ and $\ell = 2$ resonances agree with Porter-Thomas distributions.

The histograms of the assigned levels normalized to the corrected average reduced width of 0.61 eV for the p-wave levels and 3.0 eV for the d-wave levels are shown in Fig. 16. The Porter-Thomas distributions are normalized to the number of assigned levels corresponding to values of $\Gamma_n^\ell / < \Gamma_n^\ell >$ larger than 0.2. The integrals under the Porter-Thomas distribution curves, from 0 to ∞, are 119 levels for $\ell = 1$ and 148 levels for $\ell = 2$. The corresponding total strengths are 72.7 eV and 448 eV respectively.

6.2 S-WAVE LEVEL SPACINGS

The average level spacing for the s-wave resonances, D_0, obtained from the 33 s-wave resonances reported in Table 2 is 25.4 keV with an uncertainty of 2.2 keV due to the finite sample of 32 spacings. In Table 8 our estimated average level spacing is compared with values obtained from earlier analyses and from the BNL evaluation of neutron resonance parameters by Mughabghab et al. (MUG81).

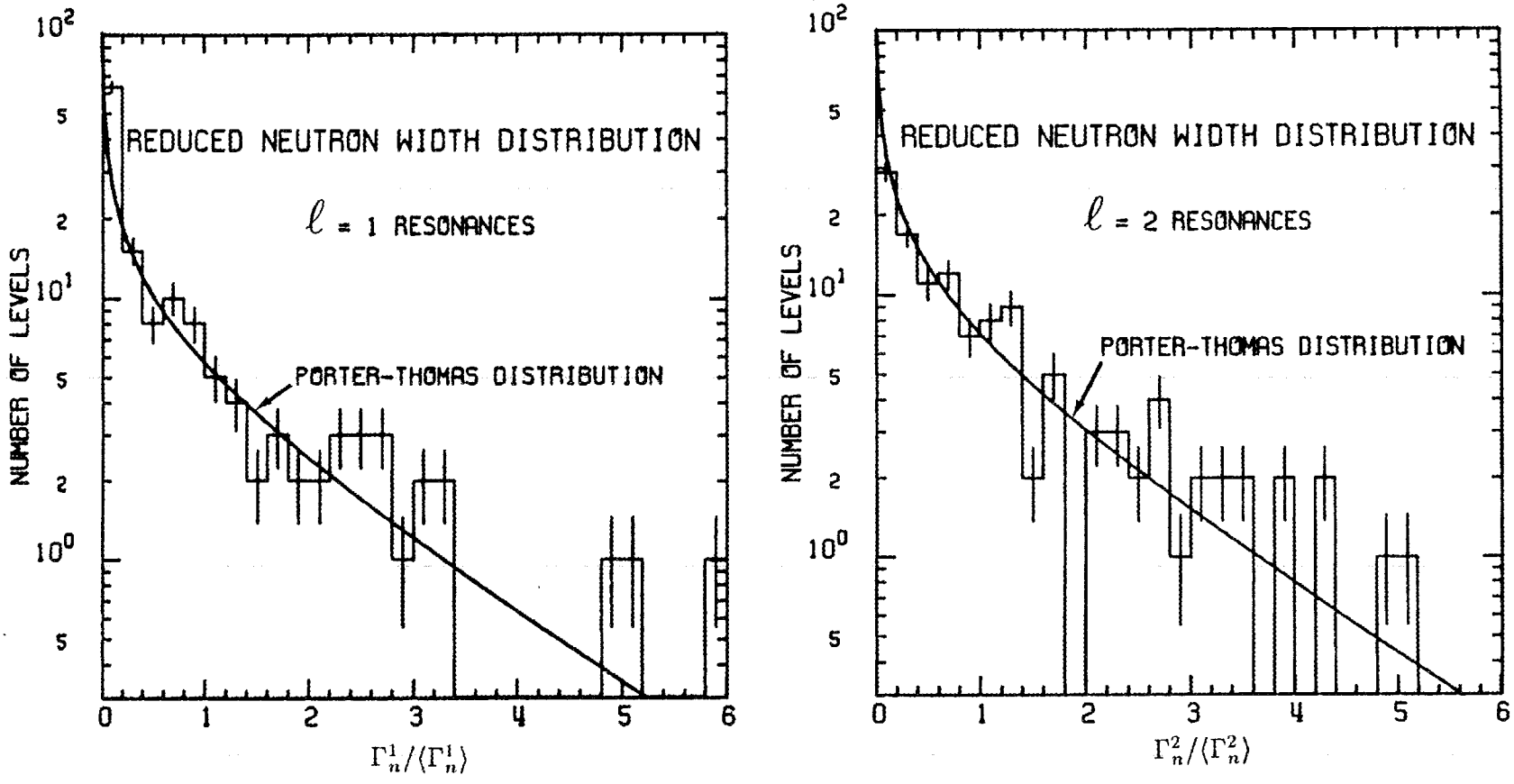

Fig. 16. Distributions of normalized reduced neutron widths for $\ell = 1$ and $\ell = 2$ resonances. All assigned $\ell = 1$ and $\ell = 2$ resonances were used to generate the histograms. The smooth curves are Porter-Thomas distributions normalized to the areas under the histograms corresponding to values of $\Gamma_n^\ell / < \Gamma_n^\ell >$ larger than 0.2.

Table 8. Resonance parameter statistics for s-wave resonances compared with results of three earlier analyses and with recommended values of Mughabghab et al.

Source	Energy range (keV)	D_o (keV)	S_o (10^4)
Present work	5–850	25.4 ± 2.2	2.3 ± 0.6
Present work	5–360		1.7 ± 0.7
Cornelis et al. (COR83 and COR85)	40–850	25.5[a]	
Cornelis et al. (COR83)	240–850		2.6 ± 0.8
Cierjacks et al. (CIE78)	450–900	19.6 ± 1.8	2.6 ± 0.8
Pandey et al. (PAN75)	10–500	$25. \pm 5.$	2.6 ± 0.9
Pandey et al. (PAN75)	10–200		1.9 ± 0.9
Mughabghab et al. (MUG81)	1–900	$17. \pm 2.$	2.6 ± 0.6

[a]Not reported by Cornelis et al. This value was calculated from their parameters reproduced in Table 6.

Average level spacings were not reported by Cornelis et al. (COR83 and COR85). The value of D_0 given in Table 8 was calculated from their resonance parameters reproduced in Table 6. This value of D_0 and the one reported by Pandey et al. (PAN75) are in good agreement with our result. No correction was applied to any of these values of D_0 for possibly missed levels. The value of D_0 reported by Cierjacks et al. (CIE78), 19.6 ± 1.8 keV, is noticeably smaller than our value, due to the misassignment of 4 s-wave resonances as shown in Table 7, where their parameters are compared to ours from 450 to 850 keV. The even smaller value of 17 ± 2 keV recommended by Mughabghab et al. (MUG81) is inconsistent with the 39 s-wave resonances they report in the 1- to 900-keV energy region. Such a small value for D_0 would assume that 15 s-wave levels were missed. This assumption was confirmed neither by our analysis nor by the Cornelis et al. analysis of high resolution transmission data.

The normalized distribution of the s-wave nearest neighbor spacings is compared to the Wigner distribution (WIG57) in Fig. 15b. The Wigner density function is expressed as:

$$P(x) = \frac{1}{2}\pi x e^{-\frac{1}{4}\pi x^2}$$

where $x = d_0/D_0$. d_0 is the spacing between neighboring s-wave levels and D_0 is the s-wave average level spacing . The Wigner distribution was normalized to the area under the histogram.

The normalized distribution of the s-wave level spacings shown by the histogram in Fig. 15b is in good agreement with the Wigner distribution as confirmed by the values of their second moments. The average value of $(d_0/D_0)^2$ for the observed

resonances was found to be equal to 1.23 ± 0.19 which is consistent with the value of 1.27 for a Wigner distribution.

6.3 LEVEL DENSITIES

The results of our transmission and differential elastic-scattering data analysis are compared with the prediction of the Gilbert and Cameron level density model (GIL65).

Gilbert and Cameron started from a Fermi-gas model of the nucleus which was modified to take into account the pairing energy and possible shell model effects, using an effective excitation energy U instead of the actual excitation energy E. The density of levels of total angular momentum J at an excitation energy U is given by

$$\rho(U,J) = \frac{\exp[2\sqrt{aU}]}{12a^{1/4}U^{5/4}} \frac{(2J+1)}{2\sqrt{2}} \times \frac{\exp[-(J+1/2)^2/2\sigma^2]}{\sigma^3} ,$$

where a is the Fermi-gas constant and σ^2 is the spin cutoff parameter. The effective excitation energy U is related to the actual excitation energy E above the ground state by the relation $U = E - \Delta$ where Δ is a pairing correction inferred from odd-even mass differences.

In the Fermi-gas model the spin cutoff parameter σ^2 is given by:

$$\sigma^2 \simeq q^2 A^{2/3}\sqrt{aU} .$$

where q^2 is related to the mean square of the projection of the total angular momentum of the states around the Fermi level. Following Facchini and Saetta-Menichella (FAC68) we adopt the value of 0.146 for q^2. The value of 1.54 MeV for Δ was taken from Gilbert and Cameron.

The Fermi-gas constant a was obtained using the computer code LEVDEN (LAR88) based upon the number of s-wave resonances observed in a given energy interval. If we assume that no s-wave levels were missed in the 0- to 850-keV energy interval then the 33 observed levels result in a value of a equal to 7.66 MeV^{-1} and the model predicts that only 229 p- and d-wave levels should have been observed. This value is much smaller than the 267 observed levels. In fact we would expect the model to predict more levels than we observed since levels must have been missed, in particular above 350 keV where capture data were not available. We are assuming that, due to penetrabilities, very few f-wave levels could be observed. From the Porter-Thomas distribution of reduced level widths (Sect. 6.1) we estimate that there are possibly four missing s-wave levels. With 37 ± 4 s-wave levels the value of a increases to 7.80 ± 0.14 MeV^{-1} and the number of p- and d-wave levels predicted rises to 257 ± 28. The cumulative number of observed levels is compared to this prediction in Fig. 17 (full line). Due to missed levels, the level density model curve should be above the data points. The dashed line was obtained assuming 41 s-wave levels. It is unlikely that 20% of s-wave levels were missed.

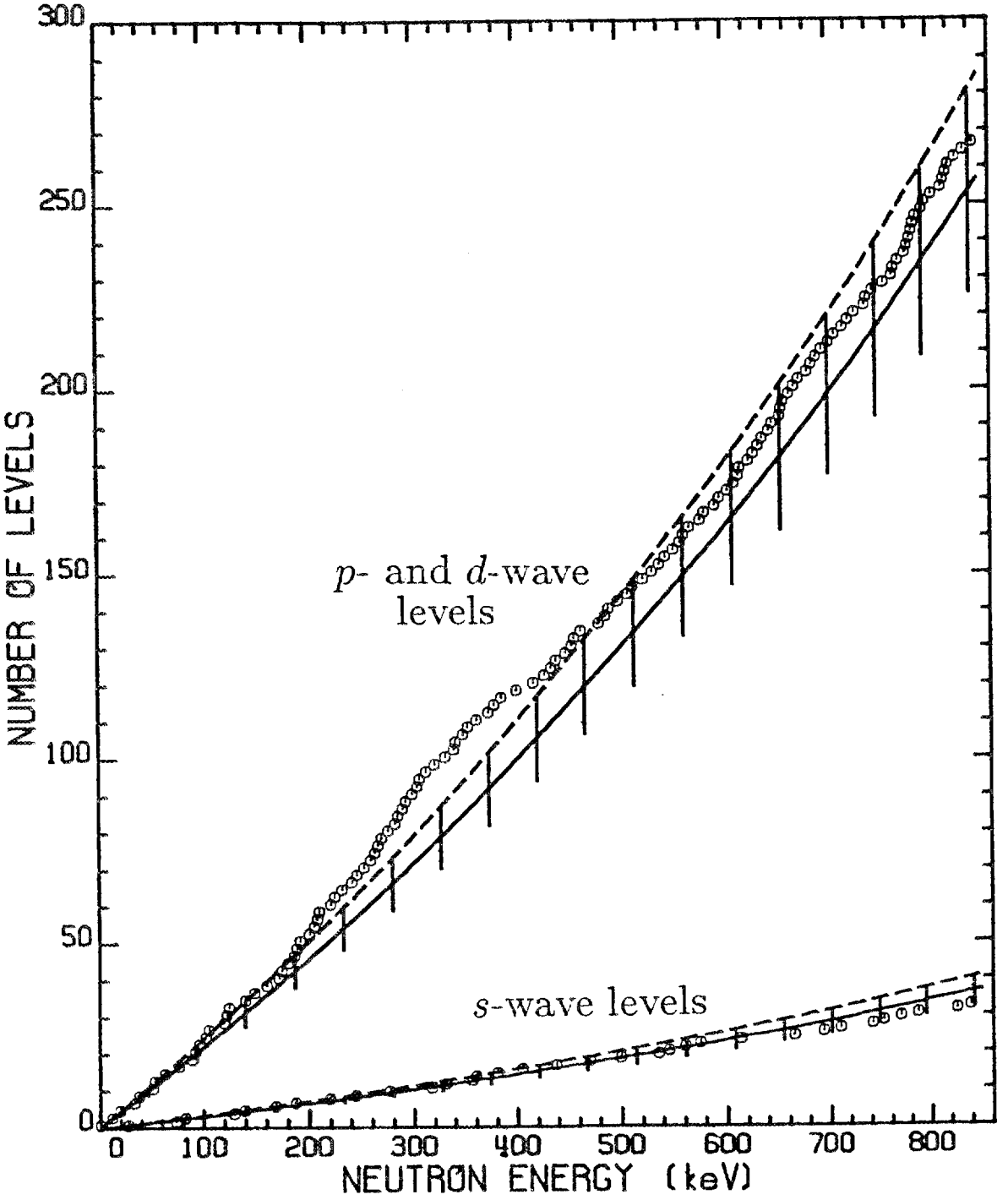

Fig. 17. Cumulative number of s-wave levels, and p- and d-wave levels as a function of incident neutron energy. Circles represent the number of observed levels. Lines represent the numbers of levels predicted by the Fermi-gas model (Gilbert and Cameron formula). Full lines are obtained assuming four missing s-wave levels and dashed lines assuming eight missing s-wave levels.

The Porter-Thomas distribution (Sect. 6.1) and the Fermi-gas model suggest that several s-wave levels may have been missed. The Dyson-Metha Δ_3 statistics test (DYS63) is often used to test for missing levels. When applied to our data in the range 0 to 850 keV the measured value of Δ_3 is 0.299 compared with a predicted value of 0.347 ± 0.110. Therefore, this test fails to indicate that any s-wave levels were missed. In fact the angular momentum of the resonance at 545.77 keV is questionable and if a $\ell > 0$ rather than a $\ell = 0$ assignment is given to this resonance the value of Δ_3 calculated with the 32 remaining s-wave resonances increases to 0.332 compared with a predicted value of 0.344 ± 0.110. The difference between the calculated and the predicted values of Δ_3 is, in this case, only 10% of the standard deviation whereas it was 40% when the 33 resonances were used. Therefore, the statistics test provides a weak indication that this resonance could possibly be a $\ell > 0$ resonance.

In Fig. 18 the histogram shows the cumulative number of the observed s-wave levels, the full line is the linear approximation corresponding to the Δ_3 statistics and the dashed line represents the fit to the same data using the Fermi-gas model. In both calculations the 33 observed s-wave levels were used in the fitting process. Note that the curvature occurring in the Fermi-gas model does not follow the data trend as well as the straight line corresponding to the Δ_3 statistics.

It would seem that the observed number of levels of various angular momenta are not consistent with the Gilbert and Cameron level density model.

Blokhin and Ignatyuk have reported (BLO76) that under certain conditions the level density could be parity-dependent. Let us assume that below 350 keV we have missed only a few levels and that most spins and parities were correctly assigned, even though some p-assignments are arbitrary as discussed in Sect. 4.3. Given that there are 12 s-wave levels below 350 keV, the number of d-wave levels predicted by the Gilbert and Cameron formula agrees with the number of observed d-wave levels (48 vs 45) whereas about twice as many p-wave levels are observed than predicted (63 vs 32). If such an enhancement of negative-parity levels is applied to the full energy range of the analysis the model would predict 52 more p- and d-wave levels than observed. It is reasonable to assume that most of these 52 levels were missed in the 350- to 850-keV energy region where no capture data were available. This would imply that above 350 keV 22% of the levels were missed which is consistent with what was observed below 350 keV where 24% of the levels seen in the capture data were too narrow to be detected in the transmission data.

It would be interesting to investigate if the Blokhin and Ignatyuk model would justify such a parity-dependence for ^{56}Fe.

6.4 STRENGTH FUNCTION

6.4.1 $\ell = 0$ Resonances

A plot of the cumulative sum of reduced neutron widths of observed s-wave resonances as a function of energy is given Fig. 19. It reveals that almost 50% of the observed strength lies in two small energy intervals that span less than 10% of the energy range analyzed. Consequently, the s-wave strength function based upon the total strength observed up to 850 keV, $(2.3 \pm 0.6) \times 10^{-4}$, is considerably larger than the one based upon the strength observed only up to 360 keV, $(1.7 \pm 0.7) \times 10^{-4}$.

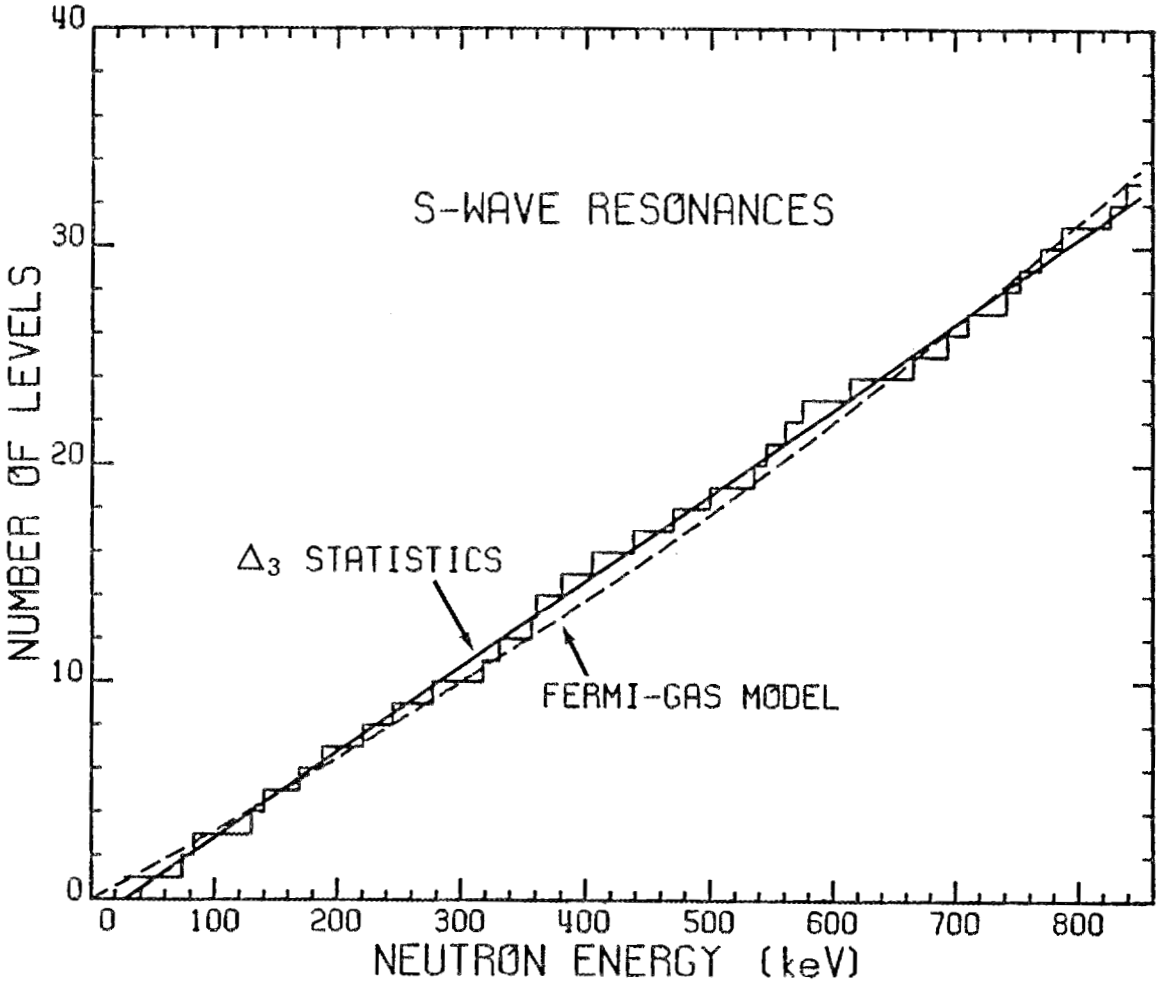

Fig. 18. Cumulative number of *s*-wave resonances as a function of incident neutron energy. The histogram represents the number of observed resonances. The full line is the fit to the data using the Δ_3-statistics test of Dyson and Metha. The dashed line is the fit to the data using the Fermi-gas model. Thirty-three *s*-wave resonances, as observed between 0 and 850 keV, were used in both calculations.

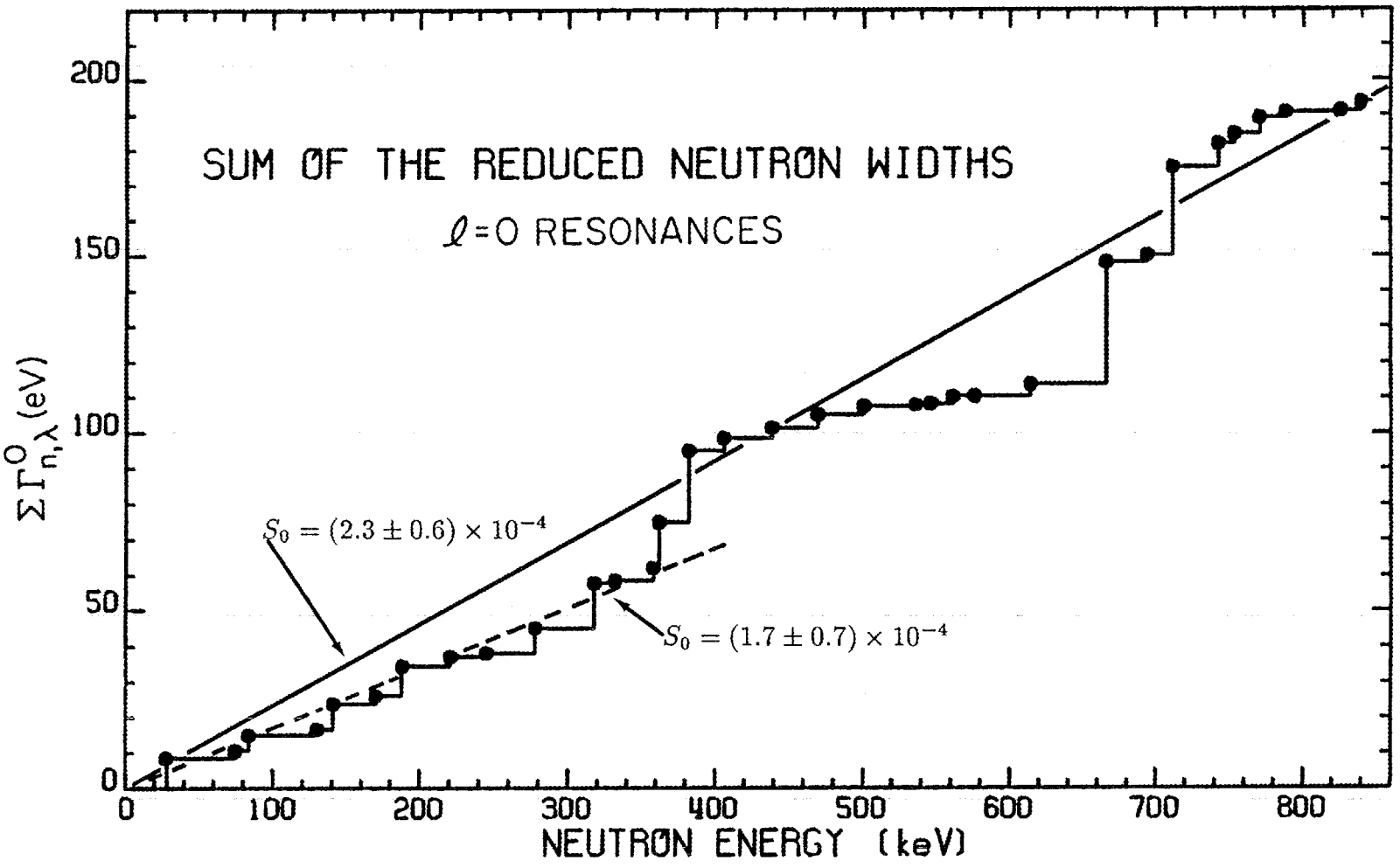

Fig. 19. Sum of reduced neutron widths for s-wave resonances as function of incident neutron energy. The strength function for the entire range of the analysis is given by the slope of the full line. The slope of the dashed line gives the strength function below 360 keV.

A comparison of the average level spacing and strength function from this work with previously published results is given in Table 8. The two conspicuous large steps in the staircase plot could indicate the presence of particle vibration doorway states.

If one is interested in studying modulations of the strength function in terms of doorway states, it is convenient to average the reduced R function with a Lorentzian weighting function (MAC80 and references herein). The poles of the Teichman-Wigner reduced R function (TEI52) are necessarily below the energy axis, and we have

$$R(E) = \sum_{\lambda} \frac{\gamma_{n,\lambda}^2}{E_\lambda - E - i\gamma_{e,\lambda}^2/2} ,$$

where in our case $\gamma_{e,\lambda}^2$'s are the effective reduced level widths for the eliminated channels; i.e., the capture channels. It should be noted that the sum is to be carried over all the poles of the R function, that is to say, it should include the poles outside the energy region analyzed. Because the poles of the reduced R function are below the real axis, if one calculates the R function at an energy $E + iI$, where I is a positive number, one is calculating an average value of the R function at the energy E. The amount of averaging that one performs is controlled by the size of I. In the statistical model, one makes I very large compared to the average level spacing in order to completely average over the statistical fluctuations. If the level widths have a Porter-Thomas distribution, I must also be very large in order to effectively average over the fluctuations. The value of the R function at a complex energy $E + iI$ where $I >> \gamma_{e,\lambda}^2$ is usually denoted by

$$R(E + iI) = \bar{R}(E, I) + i\pi S(E, I) ,$$

where

$$\bar{R}(E, I) = \sum_{\lambda} \frac{\gamma_{n,\lambda}^2 (E_\lambda - E)}{(E_\lambda - E)^2 + I^2}$$

and

$$S(E, I) = \frac{I}{\pi} \sum_{\lambda} \frac{\gamma_{n,\lambda}^2}{(E_\lambda - E)^2 + I^2} .$$

Because of the factor $E_\lambda - E$ in the numerator, $\bar{R}(E, I)$ is often identified with the contribution of the distant levels, away from the value of E, to the average. The absence of such a factor in the numerator of $S(E, I)$ means that its value at energy E is more strongly dominated by levels near energy E. $S(E, I)$ is often called the Lorentzian averaged strength function.

The Lorentzian average of the reduced neutron widths for ^{56}Fe calculated with a value of I equal to 50 keV is shown in Fig. 20. A similar modulation of the Lorentz-weighted s-wave strength function of the reduced level widths was observed for ^{60}Ni (PER83). Two large oscillations are clearly displayed for both nuclides. However, because so few levels are involved in these modulations of the strength function, it is possible that these modulations have a purely statistical origin rather than being an indicator of doorway states.

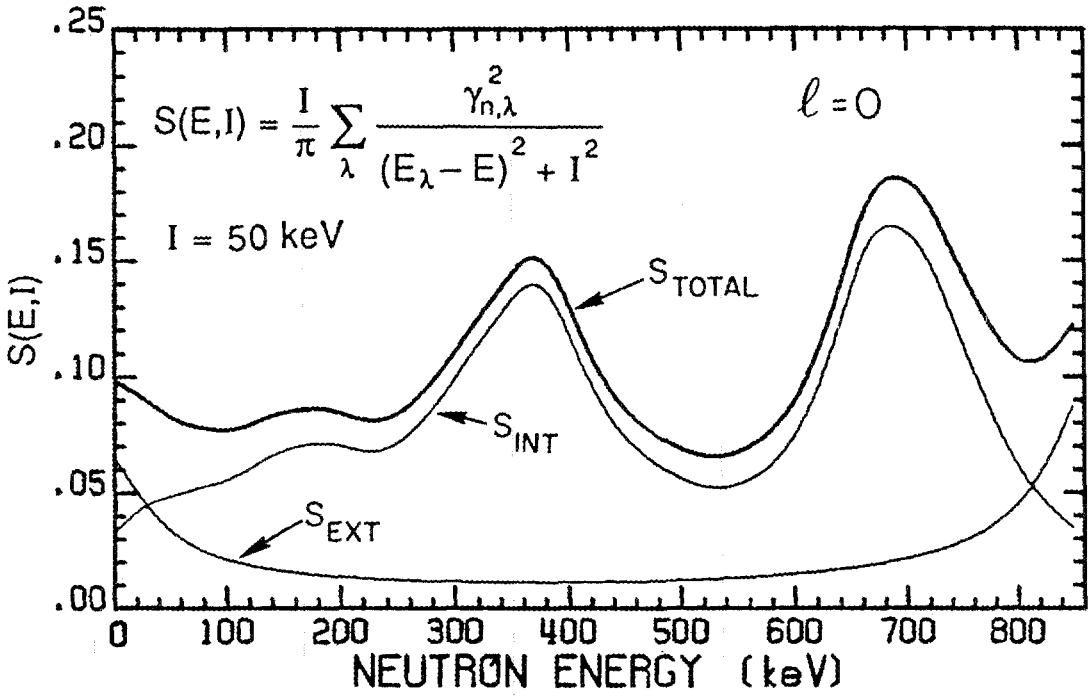

Fig. 20. Lorentz-weighted s-wave strength function for reduced neutron widths averaged with $I = 50$ keV between 0 and 850 keV. S_{INT} is the contribution of the 33 observed s-wave resonances inside the 0- to 850-keV region. S_{EXT} is the contribution of the seven fictitious resonances outside the range of the analysis. S_{TOTAL} is the sum of S_{INT} and S_{EXT}.

6.4.2 $\ell > 0$ Resonances

Since the differential elastic-scattering data allowed us to assign a definite orbital angular momentum to most of the large non-s-wave resonances it is meaningful to determine the p- and d-wave strength functions for those large resonances. Even though these resonances represent only about 60% of the total number of the $\ell > 0$ resonances, they contribute most of the strength.

For the 86 resonances having a definite p-wave assignment the cumulative plot of the reduced neutron widths is not a linear function of neutron energy, as shown in Fig. 21a. The value of the strength function for the energy region from 400 to 850 keV, $(1.1 \pm 0.2) \times 10^{-4}$, is roughly twice the value of $(0.51 \pm 0.12) \times 10^{-4}$ obtained for the energy region from 1 to 400 keV. The sum of the reduced widths is equal to 72 eV which is in good agreement with the total strength of 73 eV predicted for the p-wave levels in the Porter-Thomas distribution, as discussed in Sect. 6.1.2.

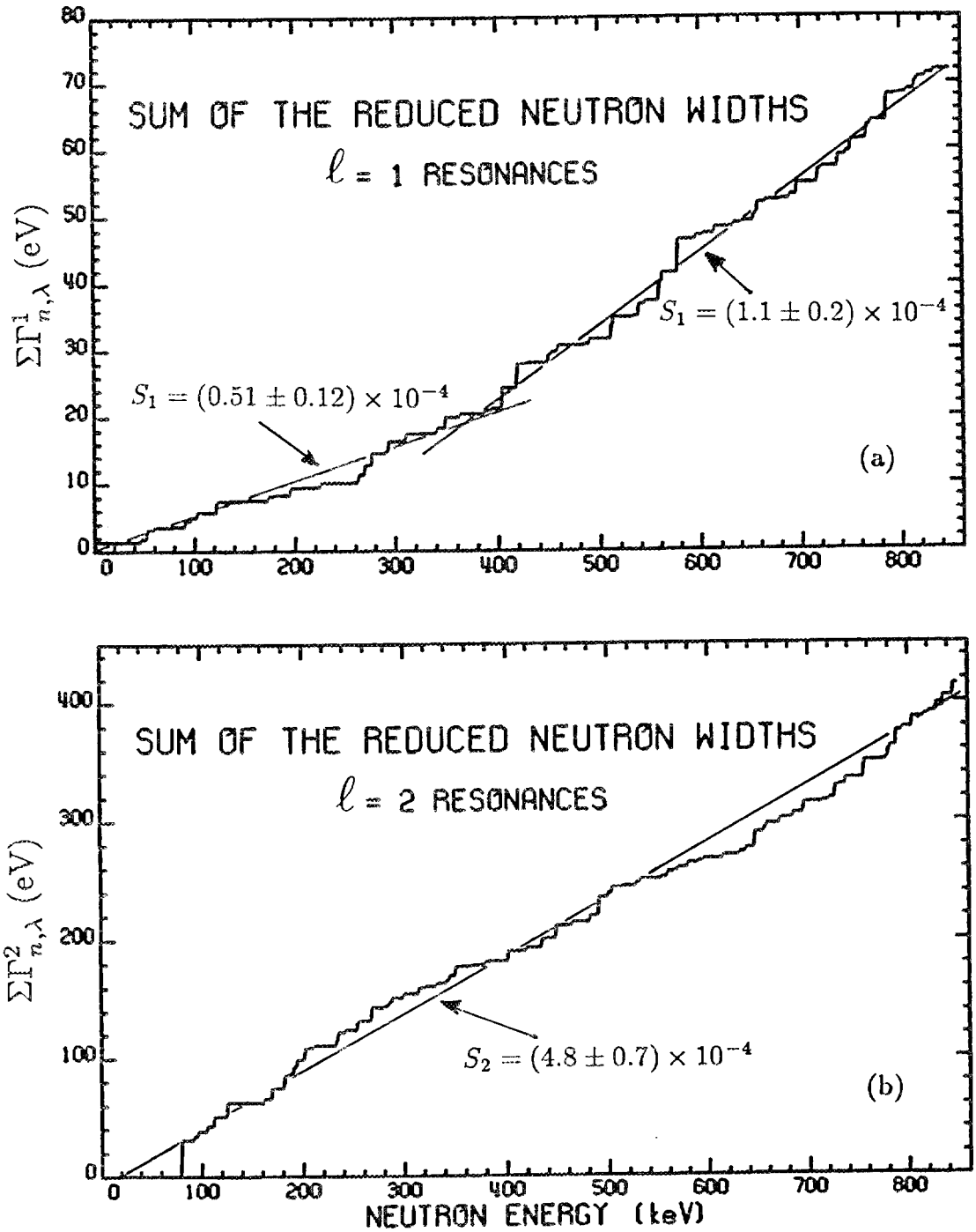

Fig. 21. Sum of reduced neutron widths for $\ell = 1$ and $\ell = 2$ resonances as a function of incident neutron energy. Only resonances with definite ℓ-assignment were used to generate the histograms. Slopes of the straight lines are the strength functions S_1 and S_2.

Figure 21b shows the sum of the reduced neutron widths as a function of incident energy for the 99 d-wave resonances having a definite ℓ-assignment. It is well represented by a straight line. The strength function is equal to $(4.8 \pm 0.7) \times 10^{-4}$ and the total strength of 418 eV is only 7% lower than the value obtained for the 148 d-wave resonances predicted by the Porter-Thomas distribution.

6.5 AVERAGE RADIATION WIDTHS

6.5.1 $\ell = 0$ Resonances

The average radiation width of 0.97 eV for the s-wave resonances reported by Corvi et al. (COR84) was calculated from 11 of the 12 s-wave resonances observed in the 20- to 350-keV energy range. The standard deviation of the distribution is 0.42 eV. As explained in Sect. 3.3, the resonance at 318 keV is a large resonance which was practically indistinguishable from the capture background and was not analyzed by Corvi et al.

In Ref. COR84 the resonance seen in capture around 331.4 keV was analyzed as a single s-wave resonance whereas in our transmission and differential elastic-scattering data analyses it was identified as a doublet composed of an s- and a d-wave resonance. The capture area of 1.43 eV reported by Corvi et al. for the single s-wave resonance was split arbitrarily between the two resonances seen in our data. Therefore, the 0.60 eV which we assign to the s-wave resonance cannot meaningfully be used in calculating the average radiation width. The new average of 0.92 eV, with a standard deviation of 0.41 eV, was calculated using the ten s-wave resonances below 300 keV.

The value of 1.46 eV reported in the earlier Fe evaluation (PER80) was based upon the analysis of the ORELA capture data by Allen et al. (ALL76) up to 400 keV. In this analysis the neutron sensitivity effects were greatly underestimated.

6.5.2 $\ell > 0$ Resonances

Only the resonances whose angular momentum and spin were determined through analysis of the differential elastic-scattering data were used in the computation of the average radiation widths for the $\ell = 1$ and $\ell = 2$ resonances. Of these resonances we eliminated the ones which were part of a multiplet not resolved in the capture data since, for these resonances, only the sum of the capture areas is well determined, and not the capture area of each individual resonance in the multiplet. The mean value of the distribution of the radiation widths of the p-wave resonances, calculated from the parameters of 19 resonances, is 0.45 eV and the standard deviation is 0.23 eV. For the d-wave resonances the mean value was also calculated from 19 resonances and is 0.75 eV with a standard deviation of 0.27 eV.

Comparing the numbers given in Table 9 for each ℓ-value is not straightforward since the criteria for inclusion of resonances in the average calculations were not the same in all three works. Corvi et al. used the spin and parity assignments from Ref. PER80 but included in their average calculations all the resonances seen in capture and transmission data even if the spin and parity assignments were uncertain. Both transmission and differential elastic-scattering data analyzed in the present work have better energy resolution than the data used in the earlier iron evaluation

(PER80); therefore, some spin and parity assignments were revised. Most of the changes in the assignments were for higher spin values. This has the effect of decreasing the radiation widths as shown in Table 9, where the new $< \Gamma_\gamma >$'s are 17% smaller for p-wave resonances and 11% smaller for d-wave resonances than the values reported earlier in Ref. PER80.

The large standard deviations of the distributions are in keeping with the fact that there are very few primary transitions in neutron capture by ^{56}Fe.

Table 9. Average radiation widths, $< \Gamma_\gamma >$, and their standard deviations, from this work and from two earlier publications. N represents the number of resonances used to calculate the average radiation width.

ℓ	This work		Corvi et al. (COR84)		Fe evaluation (PER80)	
	N	$< \Gamma_\gamma >$ (eV)	N	$< \Gamma_\gamma >$ (eV)	N	$< \Gamma_\gamma >$ (eV)
0	10	0.92 ± 0.41	11	0.97 ± 0.42	15	1.46 ± 0.60
1	19	0.45 ± 0.23	35	0.55 ± 0.20	27	0.54 ± 0.16
2	19	0.75 ± 0.27	31	0.77 ± 0.24	23	0.84 ± 0.25

6.6 CORRELATION BETWEEN Γ_n^0 AND Γ_γ FOR S-WAVE RESONANCES

Because a correlation between the reduced neutron widths and the radiation widths of the s-wave resonances might indicate some nonstatistical effect, for example valence neutron capture, such correlation coefficients are frequently calculated.

From the analyses of high-resolution ORELA data for medium weight nuclides the correlation coefficients between Γ_n^0 and Γ_γ for nine nuclides in the mass region $54 \leq A \leq 68$ were reported in previous publications (Refs. PER83 and PER88). The correlations coefficients were all positive and ranged from 0.33 for ^{59}Co to 0.94 for ^{54}Fe. In contradistinction Corvi et al. (COR84) fail to observe any correlations for ^{56}Fe; the correlation coefficient based on the 11 s-wave resonances observed in their capture data up to 350 keV being equal to 0.08 ± 0.34.

However, as discussed earlier, our transmission and differential elastic-scattering data analyses indicate that the s-wave resonance at 331 keV is a doublet unresolved by Corvi et al. Consequently, the value of Γ_γ for this resonance is smaller than the value used by Corvi et al. in calculating their correlation coefficient. If one calculates the correlation coefficient based upon the ten s-wave resonances below 300 keV one obtains a value of 0.29 ± 0.15 (if the neutron widths of Ref. COR84 are used instead of those determined in this work the value is 0.25 ± 0.14). This relatively low value for the correlation coefficient, compared to those for other nuclides in this mass region, may be due to the small number of resonances upon which it is based and is consistent with the lack of structure in the strength function below 300 keV, as evident from Fig. 19.

7. CONCLUSIONS

In the ENDF/B-V evaluation the resonance parameters for neutron interactions with ^{56}Fe covered the energy region below 400 keV. The purpose of this work was to extend the resolved resonance energy region for the ENDF/B-VI evaluation. This report gives resonance parameters for an energy range twice as large as the one covered in the previous evaluation. These resonance parameters provide a complete and accurate description of the scattering cross section from thermal to 850 keV and are consistent with the accepted values for the thermal total and capture cross sections. Our parameters were compared with those obtained at other laboratories.

Good agreement was found between our parameters for s-wave resonances and those of Geel (COR83 and COR85) except for the neutron widths of five of the resonances above 400 keV where the discrepancies are larger than 20%. However, as reported in Sect. 5.3, the agreement is very poor with the Karlsruhe parameters (CIE78): 11 of the 15 neutron widths of the s-wave resonances analyzed above 450 keV where our two analyses overlap, differ by more than 25%; for two of those resonances the neutron widths differ by more than 100%.

It is not clear why Cornelis and al. missed 40% of the $\ell > 0$ resonances we observed below 240 keV and 20% above that energy. However the neutron widths for the $\ell > 0$ resonances reported in both analyses are generally in good agreement.

The differential cross section data allowed us to make definite ℓ assignments for 69% of the 267 $\ell > 0$ resonances reported between 5 and 850 keV, but a definite J assignment could be made only for 49% of these 267 resonances. Only one-third of our definite spin and parity assignments agree with definite assignments given by Cornelis et al. based solely on their transmission data. Even though Cierjacks et al. analyzed differential elastic-scattering data in addition to their transmission data, we disagree with most of their spin and parity assignments. We also disagree with most of their reported neutron widths for $\ell > 0$ resonances.

The $\ell > 0$ resonances with uncertain J assignments are mostly narrow resonances or resonances which are part of a multiplet and were given a $p_{1/2}$ assignment by default (if such an assignment did not conflict with our differential elastic-scattering data). No attempt was made to assign spins and parities to achieve the proportion of p- and d-wave resonances required by the $(2J+1)$ rule, however the number of resonances assigned as p- or d-wave were compared to the number of resonances predicted by the $(2J+1)$ rule. As expected, because of the $p_{1/2}$ assignment given by default to many narrow resonances, more resonances have a p assignment than predicted and fewer have a d assignment.

Our average level spacing for s-wave resonances is in good agreement with those of Cornelis et al. and of Pandey et al. (PAN75) but not with the value of 19.6 ± 1.8 keV reported by Cierjacks et al., nor with the value of 17 ± 2 keV recommended by Mughabghab et al. (MUG81). Both values are markedly lower than our value of 25.4 ± 2.2 keV. The s-wave strength function for the entire range of this analysis, from 5 to 850 keV, is $(2.3 \pm 0.6) \times 10^{-4}$, and agrees with the value of $(2.6 \pm 0.8) \times 10^{-4}$ reported in earlier publications.

The results from the analysis of Geel capture data by Corvi et al. (COR84) below 350 keV were used even though their capture data are subject to revision for

reasons given in Sect. 4.1. Radiation widths of resonances analyzed in transmission, capture and differential elastic-scattering data were determined up to 350 keV and the average radiation widths were compared with those reported by Corvi et al. and by Perey and Perey (PER80). Due to the small number of resonances used to calculate the $< \Gamma_\gamma >$'s the standard deviations are large. The only significant difference is in the $< \Gamma_\gamma >$ of the s-wave resonances which is 1.5 eV in Ref. PER80 and was found to be 0.92 eV in the present work. However, this large discrepancy is still within the standard deviations.

Our improved knowledge of the resonance parameters for neutron interaction with ^{56}Fe and the extension of the energy region described by those parameters are of significant importance in reactor calculations since it eliminates the need to deal with a very approximate unresolved resonance formalism.

REFERENCES

ALL76 B. J. Allen, A. R. de L. Musgrove, J. W. Boldeman, M. J. Kenny, and R. L. Macklin, *Nucl. Phys.* **A269**, 408 (1976).

BET69 N. A. Betz, J. W. Reynolds, and G. G. Slaughter, *Proc. Conf. on Computer Systems in Experimental Nuclear Physics, Skytop, Pennsylvania*, 1969, Columbia University Report No. CONF-690301, p. 218.

BLA52 J. M. Blatt and L. C. Biedenharn, *Rev. Mod. Phys.* **24**, 258 (1952).

BLO76 A. I. Blokhin and A. V. Ignatyuk, *Sov. J. Nucl. Phys.* **23**, 31 (1976).

CIE78 S. Cierjacks and I. Schouky, *Proc. Intern. Conf. on Neutron Physics and Nuclear Data for Reactors*, Harwell, 1978 (OECD, Paris, 1978) p. 187.

COR82 F. Corvi, A. Brusegan, R. Buyl, G. Rohr, R. Shelley, and T. van der Veen, *Proc. Intern. Conf. on Nuclear Data for Science and Technology, Antwerp*, p. 131 (1983).

COR83 E. M. Cornelis, L. Mewissen, and F. Poortmans, *Proc. Intern. Conf. on Nuclear Data for Science and Technology, Antwerp*, p. 135 (1983).

COR84 F. Corvi, A. Brusegan, R. Buyl, and G. Rohr, *Proc. Consultants Meeting on Nuclear Data for Structural Materials, Vienna, Austria* 1983, International Nuclear Data Committee Report INDC(NDS)-152 L, 1984.

COR85 E. M. Cornelis, L. Mewissen, and F. Poortmans, private communication (1985).

COR88 F. Corvi, A. Prevignano, H. Liskien, and P. B. Smith, *Nucl. Instr. and Meth.* **A265**, 475 (1988).

COR89 F. Corvi, private communication (1989).

DYS63 F. G. Dyson and M. L. Metha, *J. Math. Phys.* **4**, 701 (1963).

FAC68 U. Facchini and E. Saetta-Menichella, *Energia Nucleare*, vol. 15, n.1, 54, Gennalo 1968.

GAR71 J. Garg, J. Rainwater, and W. W. Havens, Jr., *Phys. Rev. C* **3**, 2447 (1971).

GIL65 A. Gilbert and A. G. W. Cameron, *Can. J. Phys.* **43**, 1446 (1965).

HAR88 J. A. Harvey, N. W. Hill, F. G. Perey, G. L. Tweed, and L. Leal, *Proc. Intern. Conf. on Nuclear Data for Science and Technology, Mito, Japan*, p. 115 (1988).

HOR86 D. J. Horen, C. H. Johnson, J. L. Fowler, A. D. MacKellar, and B. Castel, *Phys. Rev. C* **34**, 429 (1986).

KIN77 W. E. Kinney and F. G. Perey, *Nucl. Sci. Eng.* **63**, 418 (1977).

LA80-90 N. M. Larson and F. G. Perey, *Users Guide for SAMMY: A Computer Model for Multilevel R-Matrix Fits to Neutron Data Using Bayes' Equations*, ORNL/TM-7485, Oak Ridge National Laboratory, 1980; *Updated Users'Guide for SAMMY*, ORNL/TM-9179, Oak Ridge National Laboratory, 1984, ORNL/TM-9179/R1, 1985, and ORNL/TM-9179/R2, 1990.

LAR83 D. C. Larson, N. M. Larson, J. A. Harvey, N. W. Hill, and C. H. Johnson, *Application of New Techniques to ORELA Neutron Transmission Measurements and Their Uncertainty Analysis: The Case of Natural Nickel from 2 keV to 20 MeV*, Oak Ridge National Laboratory Report, ORNL/TM-8203, 1983.

LAR88 N. M. Larson, D. C. Larson, C. M. Perey, and F. G. Perey, *LEVDEN; A Level Density Code Using the Fermi-gas Model*, ORNL/TM-10843 (in progress).

MAC80 W. M. MacDonald, *Ann. Phys.* **125**, 253 (1980).

MOX88 M. C. Moxon, private communication.

MUG81 S. F. Mughabghab, M. Divadeenam, and N. E. Holden, *Neutron Cross Sections*, Vol. 1: ""Neutron Resonance Parameters and Thermal Cross Sections" (Academic Press, New York, 1981).

PAN75 M. S. Pandey, J. B. Garg, J. A. Harvey, and W. M. Good, *Proc. Intern. Conf. on Nuclear Cross Sections and Technology*, NBS Special Publication 425 (1975) vol. II, p. 748.

PER77 F. G. Perey, G. T. Chapman, W. E. Kinney, and C. M. Perey, in *Proc. Intern. Conf. on Neutron Data of Structural Materials for Fast Reactors, Geel, Belgium*, p. 530 (1979).

PER80 C. M. Perey and F. G. Perey, *Evaluation of Resonance Parameters for Neutron Interaction with Iron Isotopes for Energies up to 400 keV*, ORNL/TM-6405, Oak Ridge National Laboratory, 1980.

PER83 C. M. Perey, J. A. Harvey, R. L. Macklin, F. G. Perey, and R. R. Winters, *Phys. Rev. C* **27**, 2556 (1983).

PER86 F. G. Perey, *Proc. Intern. Conf. on Nuclear Data for Basic and Applied Science, Santa Fe, New Mexico*, p. 1523 (1986).

PER88 C. M. Perey, F. G. Perey, J. A. Harvey, N. W. Hill, N. M. Larson, and R. L. Macklin, *$^{58}Ni + n$ Transmission, Differential Elastic Scattering, and Capture Measurements and Analysis from 5 to 813 keV*, ORNL/TM-10841, Oak Ridge National Laboratory, 1988.

PER89 F. G. Perey, *RFUNC - A Code to Analyze Differential Elastic- Scattering Data*, ORNL/TM-1112, Oak Ridge National Laboratory, 1989.

PER90 F. G. Perey and S. N. Cramer, to be published.

POR56 C. E. Porter and R. G. Thomas, *Phys. Rev.* **104**, 483 (1956).

REI58 C. W. Reich and M. S. Moore, *Phys. Rev.* **111**, 929 (1958).

TEI52 T. Teichmann and E. P. Wigner, *Phys. Rev.* **87**, 123 (1952).

WIG57 E. P. Wigner, *Proc. Intern. Conf. on Neutron Time-of-Flight Methods, Gatlinburg*, Oak Ridge National Laboratory Report ORNL-2309 (1957), p. 57.

INTERNAL DISTRIBUTION

1. B. R. Appleton
2. G. de Saussure
3. J. K. Dickens
4. C. Y. Fu
5–9. J. A. Harvey
10. D. M. Hetrick
11. N. W. Hill
12. D. C. Larson
13–17. N. M. Larson
18. R. W. Peelle
19–23. C. M. Perey
24. F. G. Perey
25. S. A. Raby
26. S. Raman
27. R. W. Roussin
28. R. R. Spencer
29. R. C. Ward
30. L. W. Weston
31. J. J. Dorning (consultant)
32. R. M. Haralick (consultant)
33. J. E. Leiss (consultant)
34. N. Moray (consultant)
35. M. F. Wheeler (consultant)
36–37. Laboratory Records Department
38. Laboratory Records, ORNL–RC
39. Document Reference Section
40. Central Research Library
41. ORNL Patent Section

EXTERNAL DISTRIBUTION

42. James R. Reafsnyder, Deputy Assistant Manager, Energy Research and Development, U.S. Department of Energy, Oak Ridge Operations, Post Office Box 2008, Oak Ridge, Tennessee 37831-6269
43. G. F. Auchampaugh, Los Alamos National Laboratory, MS 442, P-3, Los Alamos, NM 87545
44. H. Beer, Kernforschungszentrum Karlsruhe, Institut für Angewandte Kernphysik, D7500 Karlsruhe 1, Germany
45. M. R. Bhat, Building 197D, National Nuclear Data Center, Brookhaven National Laboratory, Upton, NY 11973
46. R. C. Block, Department of Nuclear Engineering, Rensselaer Polytechnic Institute, Troy, NY 12181
47. A. Brusegan, Bureau Central de Mesures Nucleaires, Steenweg Naar Retie, B-2440 Geel, Belgium
48. R. F. Carlton, Middle Tennessee State University, Physics Department, Box 407, Murfreesboro, TN 37132
49. S. W. Cierjacks, Kernforschungszentrum Karlsruhe, Institut für Angewandte Kernphysik, Postfach 3640, D-7500 Karlsruhe, Germany
50. C. Coceva, ENEA Comitato Nazionale, C.R.E., Ezio Clemental, via G. Mazzini, 2, 40138, Bologna, Italy
51. E. M. Cornelis, University of Antwerp, RUCA, B-2000 Antwerp, Belgium
52. F. Corvi, CEC, Joint Research Centre, Geel Establishment, Central Bureau for Nuclear Measurements, B-2440 Geel, Belgium
53. C. L. Dunford, National Nuclear Data Center, Bldg. 197-D, Brookhaven National Laboratory, Upton, NY 11973
54. F. H. Fröhner, Institut für Neutronenphysikund Reaktortechnik, Kernforschungszentrum Karlsruhe, Postfach 3640, 7500 Karlsruhe, Germany

55. P. B. Hemmig, Physics Branch, Reactor Research and Technology, Office of Energy Technology, U.S. Department of Energy, Washington, DC 20585
56. R. N. Hwang, Argonne National Laboratory, Engineering Physics Division, Argonne, IL 60439
57. A. V. Ignatyuk, Physics and Power Engineering Institute, Obninsk, Kaluga Region, USSR
58. S. Iijama, Naig Nuclear Research Laboratory, Naig Co., LTD, 4-1 Ukishima-Cho, Kawasaki-Ku, Kawasaki-Shi 210, Japan
59. Y. Kikuchi, Nuclear Data Center, Department of Physics, Tokai-mura, Ibaraki-ken 31911, Japan
60. L. C. Leal, Argonne National Laboratory, 9700 South Cass Avenue, Building 208, Rm E143, Argonne, IL 60439
61. R. E. MacFarlane, Los Alamos National Laboratory, P. O. Box 1663, Los Alamos, NM 87545
62. C. Mahaux, Institut de Physique, Sart Tilman, 4000 Liege 1, Belgium
63. M. C. Moxon, Nuclear Physics Division, Atomic Energy Research Establishment, Harwell, Didcot, Oxon, OX11 ORA, United Kingdom
64. C. Nordborg, NEA Data Bank, Bat. 445, 91191 Gif-sur-Yvette CEDEX, France
65. S. Pearlstein, National Nuclear Data Center, Brookhaven National Laboratory, Building 197D, Upton, NY 11973
66. W. P. Poenitz, Argonne National Laboratory-West, P. O. Box 2528, Idaho Falls, ID 83403
67. F. Poortmans, Centre d'Etude de l'Energie Nucleaire, C.E.N./S.C.K., B-2400 Mol, Belgium
68. V. G. Pronyaev, Physics and Power Engineering Institute, Obninsk, Kaluga Region, USSR
69. G. Rohr, CEC, Joint Research Centre, Geel Establishment, Central Bureau for Nuclear Measurements, B-2440 Geel, Belgium
70. M. Salvatores, Commissariat a l'Energie Atomique, Centre d'Etudes Nucleaires de Cadarache, Boite Postale No. 1, 13115 Saint-Paul-Lez-Durance, France
71. D. L. Smith, Building 314, Engineering Physics Division, Argonne National Laboratory, 9700 South Cass Ave., Argonne, IL 60439
72. M. G. Sowerby, Nuclear Physics Division, Building 418, Atomic Energy Research Establishment, Harwell, Didcot, Oxon, OX11 ORA, United Kingdom
73. D. B. Syme, Nuclear Physics Division, Atomic Energy Research Establishment, Harwell, Didcot, Oxon, OX11 ORA, United Kingdom
74. H. Weigmann, Bureau Central de Mesures Nucleaires, Steenweg Naar Retie, B-2440 Geel, Belgium
75. S. L. Whetstone, Division of Nuclear Physics, ER 23/GTN, U.S. Department of Energy, Washington, DC 20585
76. R. M. White, Physics Department, MS L-298, Lawrence Livermore National Laboratory, P. O. Box 808, Livermore, CA 94550
77. Dr. R. R. Winters, Denison University, Department of Physics, Granville, OH 43023
78. K. Wisshak, Kernforschungszentrum Karlsruhe GmbH, Postfach 3640, 7500, Karlsruhe 1, Germany

79. P. G. Young, Los Alamos National Laboratory, T-2, MS B243, Los Alamos, NM 87545

80–149. National Nuclear Data Center, ENDF Distribution, Brookhaven National Laboratory, Upton, Long Island, NY 11973

150–159. Office of Scientific and Technical Information, P. O. Box 62, Oak Ridge, TN 37831